An Analysis of the Effects of Digital Phase Errors on the Performance of a FMCW-Doppler Radar

by

Kurt Peek

Picture: www.thalesgroup.com

A thesis submitted in partial fulfillment

Of the requirements for the degree of

MASTER OF SCIENCE in APPLIED PHYSICS

at

The University of Twente

Under the supervision of prof. dr. A.P. Mosk, prof. dr. W. Vos, and ir. R. Vinke

September 2011

Abstract

In modern frequency-modulated continuous-wave (FMCW) radars, the transmitter is increasingly being implemented using direct digital chirp synthesis (DDCS), which provides improvements in sweep linearity, stability, precision, agility, and versatility over analog techniques. Its main limitations are errors due to sampling of the modulating signal, phase truncation, and digital-to-analog converter (DAC) quantization, which produce spurious signals due to their deterministic nature. This thesis presents an analysis and simulation of the effect of two sources of digital phase errors – namely, the 'staircase' approximation of the linear frequency sweep and phase truncation – on the performance of a FMCW-Doppler transceiver which employs a DDCS in its transmitter. An upper bound for the amplitude of spurious targets resulting from these digital phase errors is established. Further, it is shown that provided the phase errors are periodic with the sweep period, the spurious targets are not offset from the target in Doppler. An algorithm for selecting the digital chirp parameters of a DDCS so as to ensure periodic and phase-continuous sweep transitions is devised. Finally, we investigate parallels of FMCW radar in the optical domain, and consider the fundamental question whether range resolution is fundamentally limited by the bandwidth of a transmitted signal, or its carrier frequency.

Table of Contents

1 Introduction 4
1.1 Linear frequency-modulated continuous-wave radar 5
1.2 Frequency sweep linearity 9
1.3 Digital chirp synthesis 11
1.4 This thesis 14
2 Theory of operation of a model FMCW-Doppler transceiver 15
2.1 Description of the model system 15
2.2 FMCW Doppler signal processing 17
2.3 Direct digital synthesis 33
2.4 Statement of the problem 41
3 An analysis of the effect of digital phase errors in the transmit signal on the beat signal spectrum 42
3.1 Mathematical model of a FMCW transceiver 42
3.2 Model of the phase errors in the digital samples generated by a DDS 53
3.3 The effect of periodic digital phase errors on the FMCW transceiver 56
3.4 Form of the digital phase error 68
3.5 An upper bound for the effect of digital phase errors on the beat signal spectrum 72
4 The effect of phase errors on Doppler processing 74
4.1 The effect of sinusoidal phase errors in the beat signal 74
4.2 The effect of sinusoidal phase errors in the transmitted signal 75
4.3 Verification by simulation 77
4.5 Conclusion 78
5 Implementing periodic and phase-continuous sweep transitions 79
5.1 Introduction 79
5.2 Chirp DDS discretization constraints 82
5.3 Selecting chirp parameters for CP frequency sweeping 85
5.4 Algorithm for selecting DDCS parameters 87
5.5 Concluding remarks 90
6 Conclusions and discussion 91
6.1 Summary of contributions to knowledge 91
6.2 Implications for technological development 92
6.3 Recommendations for further research 93
Appendix: FMCW-Doppler simulation 100

1 Introduction

"To see and not be seen" has been a cardinal principle of military commanders since the inception of warfare. Until the advent of World War II, the only means available to commanders from this point of view was espionage and intelligence gathering missions behind enemy lines. Just prior to World War II, the allies came up with a groundbreaking invention, the *pulsed radar*[1] which radically changed the equation and for the first time one could see without being seen in true sense of the term.

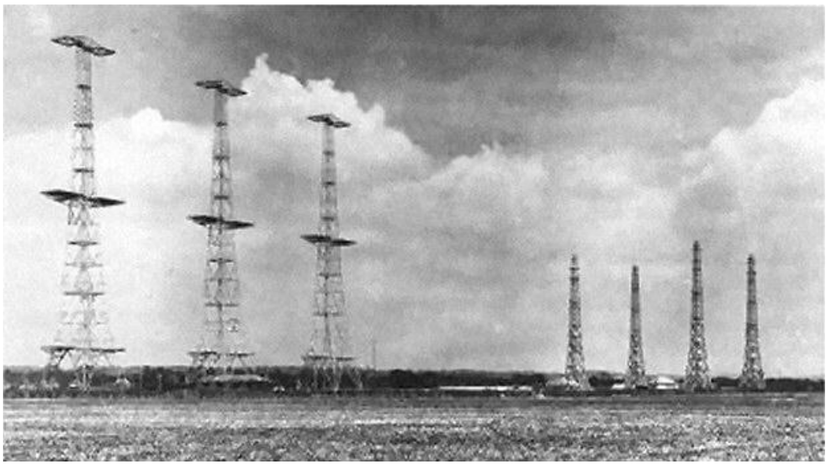

Figure 1 One of the 60 Chain Home radar sites employed by the Royal Air Force (RAF) during World War II. Three of the four transmitter aerials are visible to the left, while four receiver masts are grouped to the right. (Picture from http://spitfiresite.com/2010/04/early-radar-memories.html).

The pulsed radar estimates target range by transmitting a sequence of pulses of radio frequency (RF) energy and measuring the time for echoes scattered off the target to return to the radar. One of its earliest embodiments, the Chain Home coastal surveillance system (Figure 1), could sight German fighter formations well before they reached the English coast and could therefore concentrate allied fighter groups where they were most needed. The German fighters were not even aware that they were detected. In effect, the pulsed radar acted as a force multiplier and helped the allies defeat the vastly superior Luftwaffe in the Battle of Britain. The allies pressed home their advantage of having radar by going on the win the Battle of the Atlantic against German U-boats, catching them unawares on the surface at nighttime when they were charging their batteries. The German reaction to these events was slow and by the time they came up with their own radars and radar emission detectors (now called *intercept receivers*) it was too little, too late to influence the outcome of the war in their favor (Willis and Griffiths 2007).

After the war, understandably, radar engineers around the world concentrated on developing radar emission detectors (intercept receivers) during the Cold War that followed. This led to a "classic" situation in which intercept receivers had no difficulty detecting radar beams, and sometimes even their sidelobes, at long ranges. This is because the radar signals have to travel to the target and be partially reflected back to the radar, whereas the intercept receiver can intercept them after only a single trip. Since the 'reflection' of a radar signal generally involves the target intercepting only a small amount of the transmitted signal and scattering it over a wide volume, the effect is worse than

[1] The word "RADAR" is an acronym for **R**adio **D**etection **A**nd **R**anging, coined by the U.S. Navy in 1940.

just a doubling of the path length: it changes the fall-off in signal strength with range from a square-law process for an intercept receiver to one following a fourth-power law for a radar (Skolnik 2008).

The intercept receiver does not have things all its own way, however, because the radar has control of its own transmissions, and knows exactly what the received signals should look like, whereas the intercept receiver has only an approximate idea of the radar's characteristics, and must be general enough to be able to detect a wide variety of different radars. This means that whereas the radar receiver is optimally matched to receive its own transmissions, the ESM receiver is poorly matched to the radar (Fuller 1990).

Low probability of intercept (LPI) radars – which as their name suggests, can be intercepted, but with a low probability – attempt to exploit this advantage by resorting to *continuous-wave* (CW) transmissions instead of pulsed transmissions (Figure 2). CW transmissions employ low continuous power instead of the high peak power of pulsed radars, but achieve the same detection performance. This is possible because it is the *average* transmitted power that determines a radar's detection performance (Skolnik 2008).

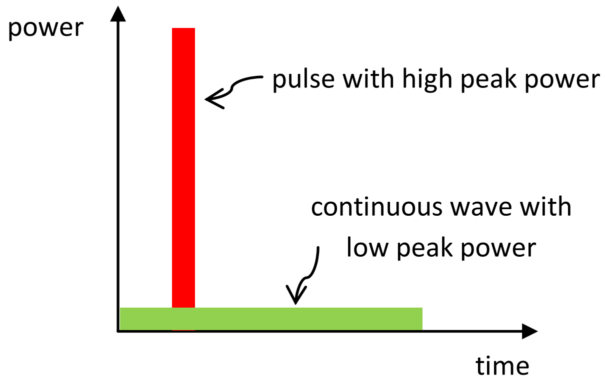

Figure 2 Illustration of a radar pulse (red) and a continuous-wave radar signal (green).

A "pure" CW radar transmitting continuous power at a single frequency, such as a traffic speed gauge, can only measure shifts in Doppler frequency, and cannot measure the range of targets. In order to measure range, the transmitted signal needs to be imparted a bandwidth – that is, the carrier wave must be *modulated*.

1.1 Linear frequency-modulated continuous-wave radar

One of the most popular forms of LPI modulation is *linear frequency modulation* (LFM), in which the instantaneous transmitted frequency is varied linearly with time. The linear variation of frequency with time is commonly referred to as a *chirp* or *frequency sweep*. Since the frequency cannot increase indefinitely, the time-frequency characteristic of the waveform is repeated periodically in a sawtooth or triangular fashion to generate a CW signal, as illustrated in Figure 3.

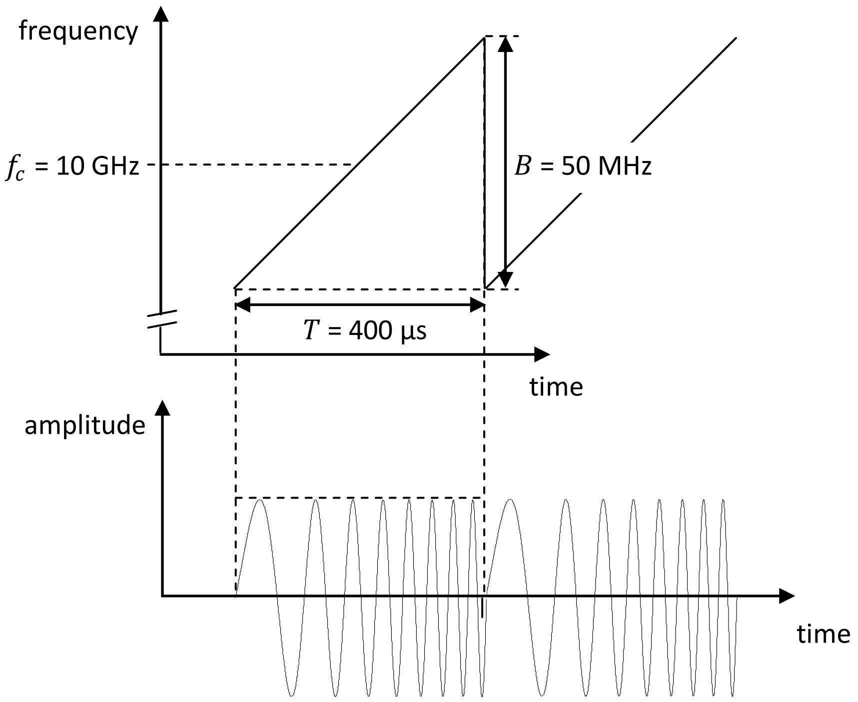

Figure 3 Schematic of a linear chirp ('up-chirp') with period T, frequency deviation B, and center frequency f_c.

The frequency sweep effectively places a 'time stamp' on the transmitted signal at every instant, and the frequency difference between the transmitted signal and the signal returned from the target (i.e. the reflected or received signal) can be used to provide a measurement of the target range, as illustrated in Figure 4.

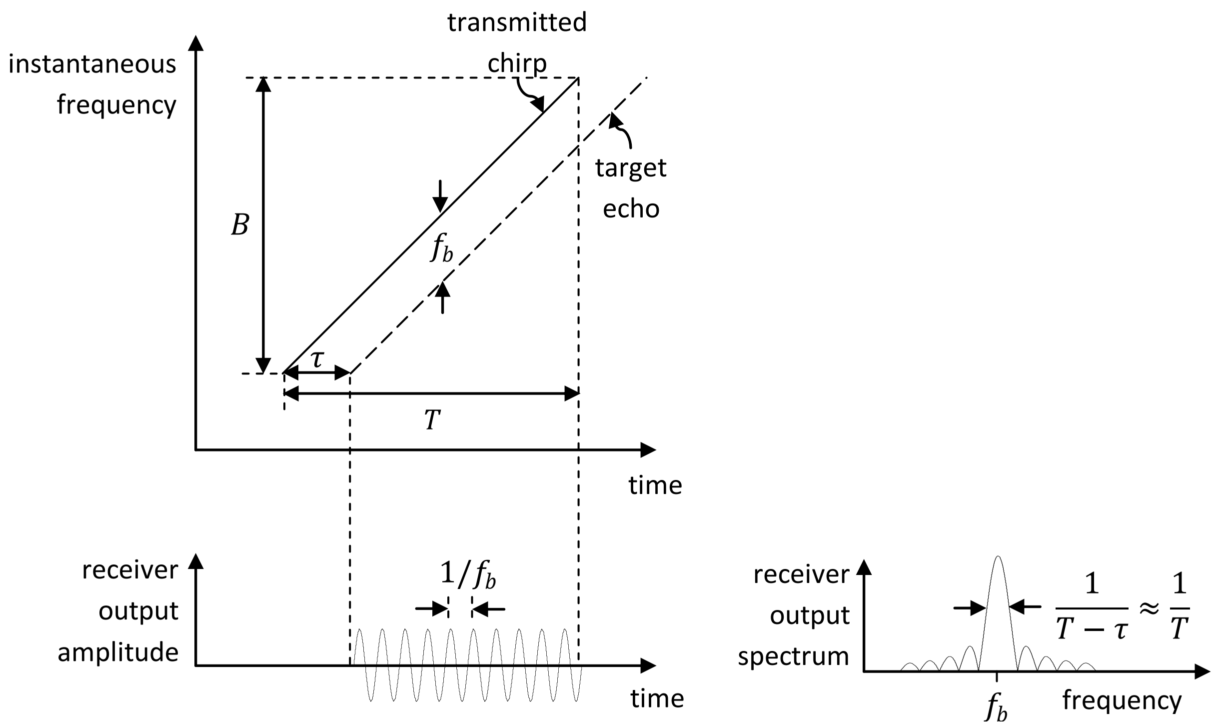

Figure 4 Basic principle of FMCW radar. Top left: time vs. instantaneous frequency plot of a transmitted linear chirp (solid line) with duration T and bandwidth B, and its echo from is a target (dashed line) is received τ seconds later. The difference or 'beat' frequency f_b between the transmitted and received signals is indicated. Bottom left: the amplitude of the beat signal with frequency f_b as a function of time. Bottom right: the spectrum of the beat signal is a 'sin(*x*)/*x*' or 'sinc' function centered at the beat frequency f_b, with a spectral width (strictly, width at -3.9 dB) of $1/(T-\tau)$, equal to the reciprocal of the period that the transmitted and received signals overlap in time. For $\tau \ll T$, the target spectral width is approximately $1/T$. (After (Willis and Griffiths 2007)).

As seen from Figure 4, the beat frequency f_b is proportional to the target transit time τ, and thus to the target range. More precisely, the proportionality constant between the two is the ratio of the chirp bandwidth B to the sweep period T, or *chirp rate*:

$$\frac{f_b}{\tau} = \frac{B}{T}. \tag{1.1}$$

For a stationary target, the two-way propagation delay to the target and back, τ, is given by

$$\tau = \frac{2R}{c}, \tag{1.2}$$

where R is the target range and c is the propagation velocity. Combining (1.1) and (1.2) and yields the *FMCW equation* relating range to beat frequency:

$$R = \frac{cT}{2B} f_b. \tag{1.3}$$

Thus, in FMCW radar, range is proportional to beat frequency[2]. Hence, by measuring the spectrum of the beat signal, a 1-D down-range map of target radar reflectivity vs. range, called the *range profile*, can be obtained.

The block diagram of a FMCW transceiver in Figure 5 shows how this is implemented. The beat signal is generated using a *mixer*[3]. The local oscillator (LO) port of the mixer is fed by a portion of the transmit signal, while the radio frequency (RF) port is fed by the target echo signal from the receive antenna. The ideal output of the mixer, called the intermediate frequency (IF) signal, is the product of the RF and LO signals, and consists of two components: one at the sum of the RF and LO frequencies, and one at their difference. The sum-frequency term is an oscillation at twice the carrier frequency of the transmitted chirp, and is filtered out either actively, or more usually because it is beyond the cut-off frequency of the mixer and subsequent receiver components (Brooker 2005). Thus, the signal passed to the spectrum analyzer is at the difference or 'beat' frequency as described above. The beat signal is passed to a spectrum analyzer, which is a bank of filters used to resolve targets in to range bins. Typically, the spectrum analyzer is implemented as an analog-to-digital converter (ADC) followed by a processor based on the fast Fourier transform (FFT).

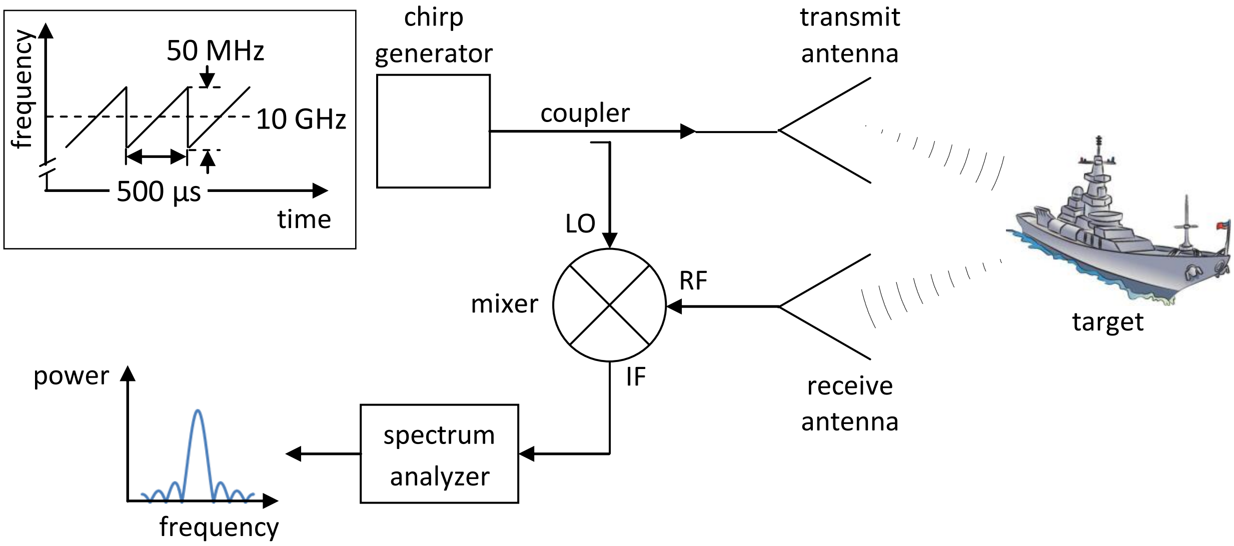

Figure 5 Simplified block diagram of a FMCW transceiver. A continuous-wave (CW) signal is modulated in frequency to produce a series of linear chirps (upper inset), which is radiated towards a target through an antenna. Typical parameters of the transmitted chirps are a carrier frequency of f_c = 10 GHz, a sweep period of T = 500 µs, and a chirp bandwidth of B = 50 MHz. The target echo received τ seconds later is mixed (multiplied) with a portion of the transmitted signal, obtained from the transmit path through a directional coupler, and the result is passed to a spectrum analyzer. For a single target, the power spectrum is a sharply peaked 'sinc' function (lower inset).

[2] Equation (1.3) holds for stationary targets. In the presence of (radial) target motion, the beat frequency f_b will be perturbed by a Doppler shift f_d which, if not compensated, will change the apparent range of the target. This phenomenon is called *range-Doppler coupling* and is discussed in Chapter 2.

[3] A *mixer* is a three-port device that uses a nonlinear or time-varying element to achieve frequency conversion (Pozar 2005). In its down-conversion configuration, it has two inputs, the *radio frequency* (RF) signal and the *local oscillator* (LO) signal. The output, or *intermediate frequency* (IF) signal, of an idealized mixer is given by the product of RF and LO signals.

The 100% duty cycle of a FMCW radar means that the transmit energy is spread over the whole duration T, and whole bandwidth B, of the sweep. However, the beat frequency energy is 'focused' into an equivalent bandwidth of $1/T$. This allows the FMCW receiver to narrow its noise bandwidth by a factor BT, the *time-bandwidth product* of the radar, and thus increase its sensitivity. This in turn allows the transmitted power to be reduced significantly; for example, the Thales Surface Scout radar transmits as little as 10 mW (Thales Nederland 2010). This low power level is very difficult for intercept receivers to detect, which means that FMCW radar can be used in otherwise restrictive emissions control (EMCON) conditions that would preclude the operation of pulsed radar (Pace 2004).

1.2 Frequency sweep linearity

In FMCW radar systems, successful range processing depends critically on the linearity of the FM sweep, or equivalently, on the presence of phase errors in the transmitted signal[4]. Deviations of the frequency sweep from linearity cause spreading the beat frequency spectrum resulting in degraded range performance as illustrated in Figure 6. Sinusoidal phase errors manifest themselves as spurious "ghost" targets or "paired echoes" placed symmetrically at both sides of the desired target peak (Griffiths 1991), whereas frequency nonlinearities following a power law lead to biased range estimates as well as spurious (Sheehan and Griffiths 1992). The ratio (in decibels) of the target peak signal to worst-case spurious sidelobe defines the *spurious-free dynamic range* (SFDR) of the radar.

[4] Amplitude errors are also important in principle, but can be removed by operating an amplifier in saturation at the end of the chirp generator system. Hence in practice, this effect is generally not so serious (Griffiths 1990).

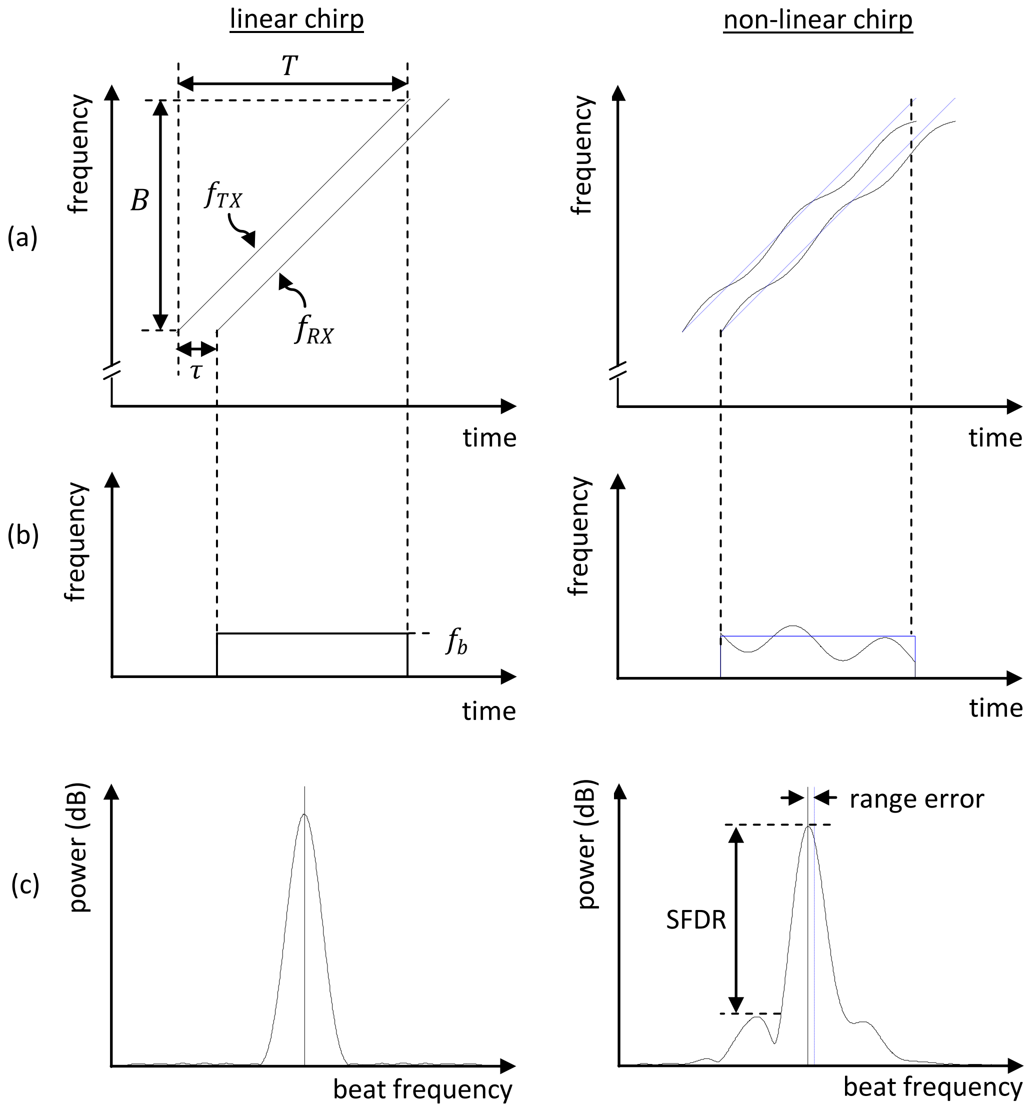

Figure 6 FMCW operation with linear chirps (left), and a non-linear chirps (right). The blue dashed lines on the right figures reproduce the linear case for ease of comparison. From top to bottom, we show (a) time vs. frequency plots of the transmitted and received signals, denoted $f_{TX}(t)$ and $f_{RX}(t)$ respectively; (b) the time vs. frequency plot of the beat signal; and (c) the power spectrum of the beat signal. The range error and spurious-free dynamic range (SFDR) due to the non-linearity of the sweep are indicated.

The sweep linearity of a FMCW radar depends on how the transmitted signal is generated. In the first commercial FMCW navigation radar, the PILOT (**P**hilips **I**ndetectable **L**ow **O**utput **T**ransceiver) developed by Philips Research Laboratories in 1987, the frequency sweep was generated by driving a *YIG-tuned oscillator*[5] with a linear sawtooth current (Beasley, Leonard et al. 2010) as shown in Figure 7.

[5] A YIG (Yttrium, Iron, and Garnet)-tuned oscillator is an oscillators whose frequency varies linearly with the applied current. At its heart is a YIG sphere which, due to its ferrite properties, resonates at microwave frequencies when immersed in a DC magnetic field. The frequency of resonance increases linearly with the applied magnetic field. A coupling structure, often referred to as the "coupling loop", is utilized to couple RF energy to the YIG sphere forming a high quality factor (high-Q) microwave tank circuit. The "YIG resonator" is tied to the negative resistance of an active device – usually a bipolar transistor or a field-effect transistor (FET)

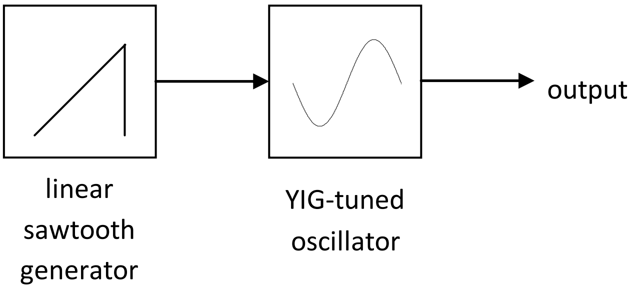

Figure 7 Block diagram of the chirp generator of the PILOT radar.

An advantage is of the YIG-tuned oscillator is that, due to its very high quality factor (the unloaded Q is greater than 8000 at 10 GHz (Teledyne Ferretec 2011)), it produces a very 'clean' output spectrum with little phase noise. However, the system depicted in Figure 7 also has several disadvantages:

- The output frequency of the YIG-tuned oscillator drifts with temperature;
- The linearity of the sweep produced is at best around 0.1% (Beasley and Lawrence 2006), which still limits the range resolution obtainable from the PILOT radar;
- Due to its inductive tuning coil, the YIG-oscillator has a slow switching speed. This limitation manifests itself in particular at the sweep transitions, at when the YIG-tuned oscillator requires of the order of ∼100 µs to 'fly back' to the starting frequency of the next sweep. This "sweep recovery time" effectively limits the duty cycle of the FMCW radar;
- The phase of the output of the YIG-tuned oscillator varies slightly in a random fashion from sweep to sweep. This limits this performance of processing methods which require *coherent* operation of the radar, such as *Doppler processing* and *coherent integration* (see Chapter 2).

In the light of these limitations, much effort has been put into finding improved methods of chirp generation. Here, we consider one such method.

1.3 Digital chirp synthesis

One method for generating FMCW waveforms that promises to have a great impact on next-generation radar is *direct digital synthesis* (DDS) (Stove 1992; Adler, Viveiros et al. 1995). In contrast to traditional concepts, DDS produces an analog waveform by generating a time-varying signal in digital form and then performing digital-to-analog (D/A) conversion.

To generate linear chirp sweep by digital means, the sequence of waveform samples can either be pre-computed, stored, and played back, or calculated directly. The first of these techniques is applicable to any form of modulation, and indeed forms the basis of several arbitrary waveform generators (AWGs). However, for waveforms of very high time-bandwidth product this is likely to require a prohibitive quantity of high-speed memory and, particularly for linear FM waveforms, the first technique is usually preferred (Griffiths 1990).

The calculation of the waveform samples for a linear FM waveform is simple because the linearly varying frequency is equivalent to a quadratically varying phase (modulo $\boldsymbol{2\pi}$). As explained in detail

– to form an oscillator. By varying the DC magnetic field experience by the YIG resonator using a variable current through an electromagnet, one obtains an oscillator which can be tuned over multi-octave microwave frequencies (Castetter 2011).

in Section 2.3, the phase samples may therefore be generated by a cascaded pair of digital *accumulators* which increment their accumulated total by their respective input, once per clock cycle. The resulting phase samples address a sine look-up table (LUT) stored in a read-only memory (ROM), and the ROM outputs are converted to analog form using a digital-to-analog converter (DAC) (see

Figure 8).

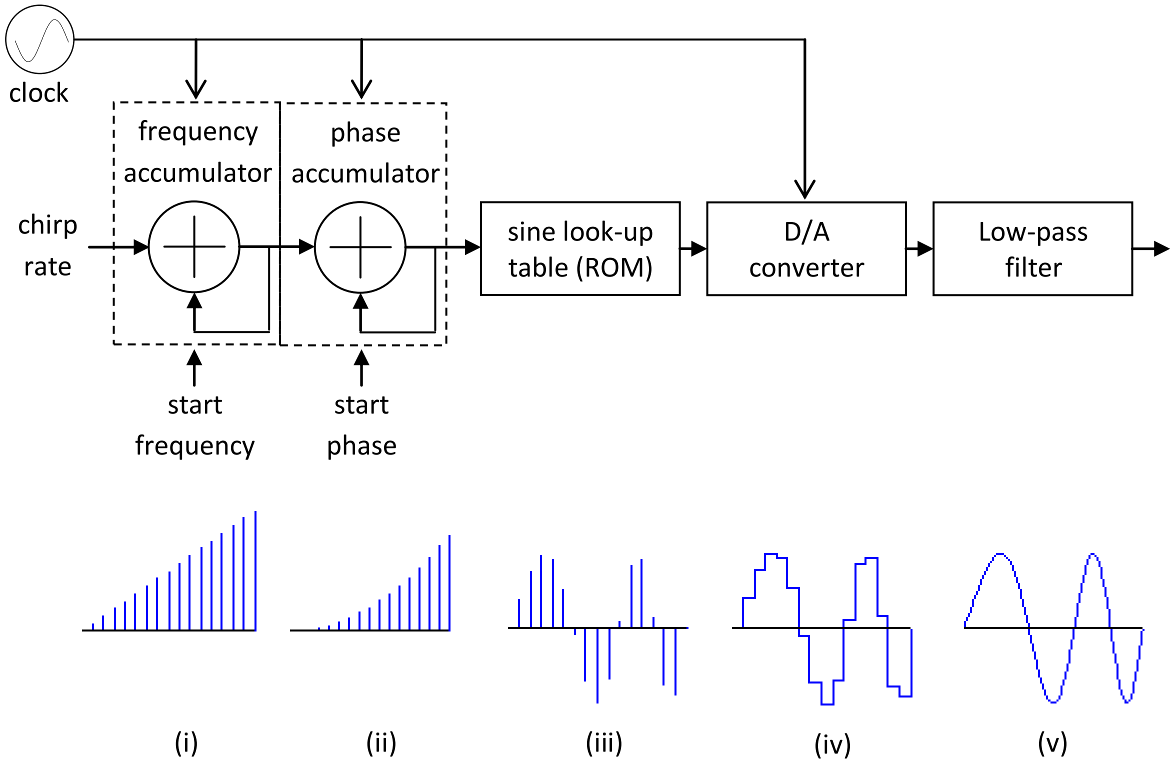

Figure 8 Dual-accumulator chirp DDS architecture and signal flow. From left to right: (i) a digital frequency accumulator is initiating at a start frequency and incremented by a frequency increment, determined by the desired chirp rate, on each clock cycle, to generate a linearly increasing digital frequency; (ii) the output of the frequency accumulator is input to a second phase accumulator, which generates a quadratically increasing phase; (iii) the phase samples are used to address a look-up table, implemented as a ROM, which contains amplitudes of the sine wave for a number of phase values on the interval $[0, 2\pi)$. The result is a chirp in the digital domain; (iv) the digital chirp is converted to analog form using a digital-to-analog converter (DAC). Due to the zero-order-hold property of the DAC, discussed in Section 2.3, the DAC output has a 'step-like' shape and contains higher-order harmonics of the desired output signal; (v) the DAC output is passed through a low-pass interpolating filter to remove the higher-order harmonics and obtain the desired chirped output signal. (After (Adler, Viveiros et al. 1995)).

Because DDS chirps are digitally controlled, they have excellent chirp linearity and stability. A DDS can also rapidly "hop" between frequencies, limited only by transients of its low-pass filter, and is less susceptible to thermal drift and aging. However, the quantization from a continuous representation to a discrete one generates a deviation (or error) in the phase and amplitude which causes spurious signals to appear, degrading the linearity of the frequency sweep.

Further, due to limitations in the speed of its digital circuitry and DAC, DDS has a limited frequency range: current state-of-the-art commodity DDS ICs are clocked at 1 GHz (Analog Devices 2010), giving them usable outputs to the lower UHF spectrum, approximately 400 MHz. In order to take advantage of DDS attributes at microwave frequencies, some form of upconversion is required.

1.3.1 Upconversion by mixing

The upconversion method we investigate in this thesis is the so-called *DDS/mixer hybrid* (Vankka 2000) depicted in Figure 9. The DDS chirp is generated at intermediate frequency, within the capacity of the digital components. The intermediate signal is then mixed to the desired output frequency, and alias components are filtered. If the intermediate output carrier frequency is much lower than the transmit frequency, up-mixing results in components that lie relatively close to the desired components in the frequency spectrum. The filtering of these unwanted frequencies can become a very demanding task, and several stages of mixing and filtering might be required (Cushing 2000; van Rooyen and Lourens 2000).

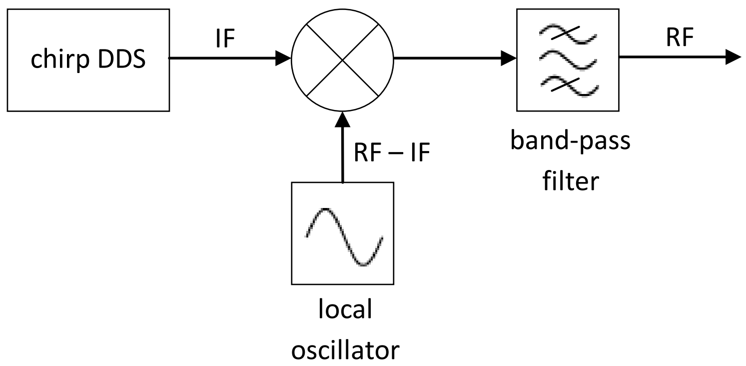

Figure 9 DDS/mixer hybrid. As explained in detail in Section 3.1.2, a chirp DDS at intermediate frequency (IF) is mixed with a local oscillator whose frequency is the difference between the radio frequency (RF) of the desired output and the IF. The output from the mixer is passed through a bandpass filter to select the upper sideband, so that the desired output at RF is obtained.

A distinct advantage of the DDS/mixer hybrid is the ability to generate very low phase noise output, due to the use of components (such as mixers) with negligibly low residual phase noise, compared with the base frequency source. This method also provides excellent sweep-to-sweep coherence, which is essentially limited by drifting of the X-band local oscillator.

A disadvantage of the DDS/mixer hybrid, however, is the remaining presence of the spurious signals due to the digital chirp generation. Within the digital domain, there are actually three sources of errors:

1) **Sampling of the modulating signal.** In so-called dual-clock architectures, the frequency accumulator is updated at a lower rate than the phase accumulator. The effect is a ‘staircase’ approximation of ideal linear time-frequency characteristic of the chirp. The ramifications of this error on the beat signal spectrum have been investigated by Salous and Green (Salous and Green 1994).
2) **Phase truncation**. Prior to addressing the sine ROM, the value of the phase accumulator is truncated, and only the most significant bits are used to look up the sine amplitude. This is done to reduce requirements on the memory of the ROM.
3) **Amplitude quantization**. As the DAC can only produce a finite number of amplitudes, the amplitude of each sample is quantized or ‘rounded’ from its ideal value.

The effect of the ‘staircase’ approximation has been investigated by Salous and Green (Salous and Green 1994). To the best of our knowledge, the effects of phase truncation and amplitude quantization on the performance of FMCW radar has not been described in the extant literature. According to Stove (Stove 2004), however, the practical effects of amplitude quantization are well described by modeling it as noise which is uniformly distributed over ±0.5 bits.

1.4 This thesis

This thesis makes a contribution towards the understanding of these spurious signals by analyzing and simulating the effects of digital phase errors on the beat spectrum of a FCMW-Doppler radar employing a direct digital chirp synthesizer. Specifically, we focus on the two sources of digital phase errors, namely, the sampling of the modulating signal and phase truncation. The effects of amplitude truncation and DAC nonlinearities, the latter of which become increasingly important at higher output frequencies, are not investigated in this work.

A topical outline of the text is as follows. In Chapter 2, we go beyond the tutorial introduction to FMCW radar given in this introduction and discuss FMCW signal processing in more mathematical detail. We also explain the concept of direct digital chirp synthesis (DDCS) in more detail, and enumerate sources of errors. These concepts serve as a basis for Chapter 3, in which we derive an analytical model for the effect of digital phase errors on the output spectrum of the chirp DDS and, in turn, on the beat signal spectrum of the FMCW radar. An upper bound for the spurious-free dynamic range (SFDR) of the beat signal due these digital phase errors is established. In Chapter 4, we investigate the effect of phase errors in general on *Doppler* processing. It is shown that phase errors that are coherent with the transmitted sweep, such as the digital phase errors considered here, have a negligible effect on Doppler processing. In Chapter 5, we devise an algorithm for choosing DDCS chirp parameters such as to effectuate periodic and phase-continuous sweep transitions, which are desirable for generating FMCW-Doppler waveforms. Finally, in Chapter 6, we draw conclusions from our results and discuss their significance.

2 Theory of operation of a model FMCW-Doppler transceiver

In this chapter, we review the fundamentals of homodyne FMCW-Doppler radar, and present a model system which employs a direct digital chirp synthesizer (DDCS) in its transmitter. The model system also serves as an example in subsequent chapters, where we analyze the effect of digital phase errors on its performance.

An outline of this chapter is as follows. In Section 2.1, we briefly describe the architecture and operation of the model FMCW-Doppler transceiver. In Section 2.2, we tutorially review the theory behind FMCW-Doppler signal processing, and explain how target range and velocity information can be extracted from the received echoes. In Section 2.3, we describe in more detail the operation of the DDCS, and enumerate sources of error. Finally, in Section 2.4, we formulate our research question using the fundamentals established in this chapter.

2.1 Description of the model system

In this section, we describe the architecture of our model FMCW-Doppler transceiver and briefly describe its operation. The brief description of the operation of the microwave FMCW surveillance radar given here concerns only those aspects of the FMCW radar that are needed to develop the Doppler data processing concept.

A simplified block diagram of our model FMCW Doppler radar is shown in Figure 10. At its heart is a direct digital chirp synthesizer (DDCS), clocked by a 1 GHz master clock, which generates a chirp in the digital domain and converts it to analog form using an integrated digital-to-analog converter (DAC). The output is passed through a low-pass interpolating filter to produce a chirp at intermediate frequency (IF), which is converted up to radio frequency (RF) by a mixer and a bandpass filter[6]. The upconverted signal is transmitted through a transmit (TX) antenna. After reflection off a target, an echo is received by a receive (RX) antenna and fed to the RF port of a frequency mixer. Simultaneously, the local oscillator (LO) port of the mixer is fed by a 'reference' signal which is a version of the transmitted signal obtained through a directional coupler[7]. The mixing process produces a 'beat' signal which contains the range information obtainable from the radar.

[6] Practical implementations of single-sideband (SSB) upconversion often use a *pair* of cascaded mixers and bandpass filters to reduce requirements on the transition width of the individual bandpass filters.
[7] Typically, an image reject mixer (IRM) is used in order to reduce noise from the image sideband, which can lead to gain in signal-to-noise ratio of up to 3 dB (Willis and Griffiths 2007).

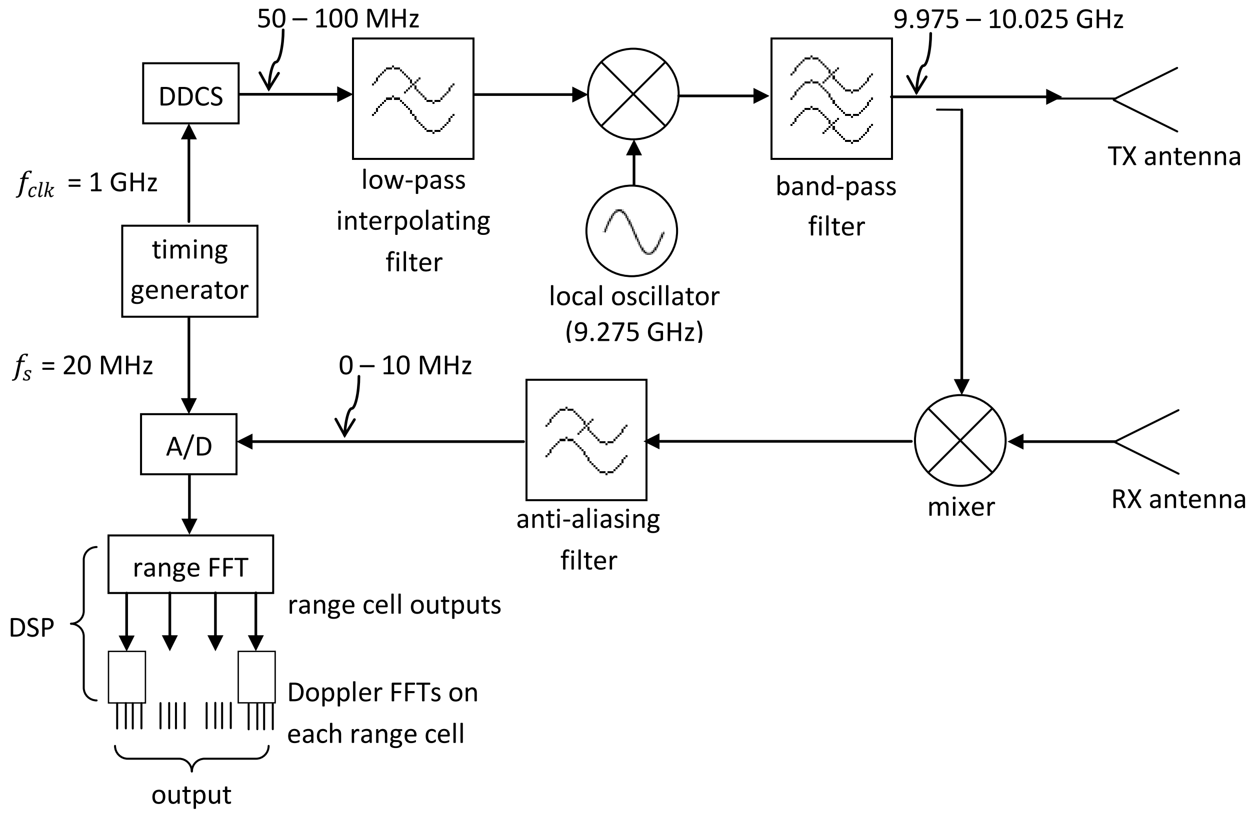

Figure 10 Simplified block diagram of a FMCW-Doppler transceiver. A direct digital chirp synthesizer (DDCS) generates a linear chirp from 50 MHz to 100 MHz, which is passed through a low-pass interpolating filter to eliminate higher harmonics. The resulting signal at intermediate frequency (IF) is mixed with a local oscillator at 9.275 GHz. The resulting double-sideband (DSB) signal is passed through a band-pass filter to select the upper sidelobe, which is a chirp from 9.975 GHz to 10.025 GHz. The main part of this chirp is transmitted through a transmit (TX) antenna while a portion is coupled to the local oscillator (LO) of a second mixer. The radio frequency (RF) port of the second mixer is fed by a separate receive (RX) antenna. The output of the second mixer is passed through an anti-aliasing filter with a cutoff frequency of 10 MHz. The resulting bandlimited signal is sampled by an analog-to-digital (A/D) converter at a rate of f_s = 20 MHz, and resulting time series is fed to a digital signal processing (DSP) unit, which performs the range and Doppler fast Fourier transform (FFT) operations required to output a range-Doppler profile of the target scene.

After passing an analog anti-aliasing filter, which ensures that beat frequencies above half the sample frequency cannot pass[8], the beat signal is sampled by a 16-bit analog-to-digital converter (ADC) at a rate of f_s = 20 MHz using N = 10,000 samples on each upgoing sweep of the modulating sawtooth signal. The ADC collects N samples in each of M consecutive sweeps (the *coherent processing interval*). The samples are arranged in a $M \times N$ matrix, in which the rows consist of samples collected within each sweep, or in *fast time*, and the columns of samples collected across sweeps, or in *slow time*.

After weighting the rows of this matrix by a window function to reduce sidelobes (see Section 2.2.6), a first FFT is performed over the rows of the matrix. The output of the FFT is a complex array, of

[8] Although not shown in the figure, the IF signal is typically also passed thorugh a high-pass filter which compensates for the dependence of signal strength on radar distance by using a gain function that increases by 6 dB/octave. This prevents strong returns from close-in targets from saturating the receiver, and is called 'range gain control' (Stove 1992) or 'sensitivity frequency control' in analogy to 'sensitivity time control' used in pulse radars (Skolnik 2008).

which only the first $N/2$ points are retained. The signals at each of these points then correspond to radar target echo signals that come from progressively greater ranges[9]. These $N/2$ complex array points are collected as rows of a matrix every sweep repetition interval until a total of M rows are obtained, over a period of time that corresponds to the reciprocal of the desired Doppler frequency resolution. Then another window vector multiples each column (or range cell) of this matrix, and a second FFT is performed over each column. The latter provides Doppler processing of each range cell, and since it operates on a complex input array, the output preserves the sense of Doppler (positive or negative), just as though in-phase and quadrature channels had been used (Barrick, Lipa et al. 1994). These digital processing steps can be implemented using field programmable gate arrays (FPGAs) or commercially available digital signal processing (DSP) boards.

In actual radar applications, the output range-Doppler data serves as input to a target tracking algorithms, which can greatly improve the detection of targets against a background of noise. Here, however, we are interested on the effects of certain hardware non-idealities on raw range-Doppler data itself. However, before discussing these effects (Section 2.3), we first explain in more detail how the range-Doppler data is obtained.

2.2 FMCW Doppler signal processing

The objective of this section is to present a simple and concise analysis – backed by an example – of the application of a FMCW signal format in radar systems. Following Barrick (Barrick 1973), it is shown how both time-delay (range) and Doppler (radial velocity) information can be extracted unambiguously.

2.2.1 Application

For the sake of illustration, we pick the following application and example. The RF radar carrier frequency is to be f_c = 10 GHz[10]. Targets are to observed by the radar out to a range of 15 km (corresponding to time delays up to 100 µs). At a center frequency of 10 GHz, echoes from targets moving at a velocity of up to 15 m/s in the radar's line of sight will Doppler shifts of less than 1 kHz. In order to display such echoes unambiguously, a sweep repetition frequency (SRF) of 2 kHz is selected, corresponding to a sweep repetition interval (SRI) of 500 µs. To show sufficient detail, a Doppler processing resolution of 31.25 Hz is desired, and a range resolution of 3.75 m is desired; the latter two requirements translate, as we show in subsequent sections, to a coherent integration time of 32 ms and a chirp bandwidth of 50 MHz.

2.2.2 Transmitted signal

We select a 100% duty factor signal whose frequency sweeps upward, linearly, over one sweep repetition interval T (T = 500 µs for our example). Since a 50 MHz bandwidth is desired, the signal can be written

$$s_{TX}(t) = V_{TX} \cos\left[2\pi\left(f_c t + \frac{1}{2}\alpha t^2\right)\right] \equiv V_{TX} \cos[\phi_{TX}(t)], \tag{1.4}$$

[9] Actually, what is actually measured is the "pseudo-range" since Doppler frequency shifts cannot yet be distinguished from target beat frequencies. Typically, however, the Doppler frequency shift corresponds to less than one range cell.

[10] A radar operating at a center frequency of 10 GHz is said to operate in the *X-band*, which extends from 8.0 to 12.0 GHz according to the specification by the IEEE (Institute of Electrical and Electronics Engineers). In the NATO frequency designation, the radar is said to operate in the I (8.0 - 10.0 GHz) and J (10.0 - 20.0 GHz) bands.

for $-T/2 < t < T/2$, with repetition satisfying

$$s_{TX}(t+T) = s_{TX}(t), \qquad \forall t. \tag{1.5}$$

Here f_c denotes the center frequency (f_c = 10 GHz) and α the chirp rate, which is defined as the ratio of the chirp bandwidth B to the sweep repetition interval T (α = 100 GHz/s for our example). It is assumed that the signal is periodic, and hence phase-coherent from one repetition interval to the next[11].

It has been found useful to define the internal time t_m within the mth pulse as[12]

$$t_m = t - mT, \qquad -\frac{T}{2} < t_m < \frac{T}{2}, \tag{1.6}$$

so that (1.4) and (1.5) can be expressed as

$$s_{TX}(t) = V_{TX}\cos\left[2\pi\left(f_c t_m + \frac{1}{2}\alpha t_m^2\right)\right]. \tag{1.7}$$

Since the instantaneous frequency, $f_{TX}(t)$, is the derivative of the phase (Carson 1922), we have

$$f_{TX}(t) = \frac{1}{2\pi}\frac{d\phi_{TX}}{dt} = f_c + \alpha t_m. \tag{1.8}$$

where f_c = 10 GHz and α = 10 GHz/s. Thus it can be seen that the frequency excursion of $f_{TX}(t)$ over one sweep repetition interval is

$$\Delta f_{TX} = B = 50 \text{ MHz}. \tag{1.9}$$

The amplitude of the transmitted signal is taken to be unity. The plot of instantaneous frequency vs. time of the transmitted signal is shown as a solid line in Figure 11.

[11] FMCW radars in which the transmit phase has a fixed phase relationship from sweep to sweep, i.e., $\phi_{TX}(t+T) - \phi_{TX}(t) = \text{constant}$, are called *coherent*. The provision of a coherent system is prerequisite for Doppler processing. It also allows for coherent integration over a number of sweeps, N, which improves the signal-to-noise ratio (SNR) by a factor of N, which is greater than the factor of $\sqrt{N}$ typically obtainable with non-coherent integration (Beasley and Lawrence 2006).

[12] In the radar signal processing literature, the internal time t_m within the mth sweep is often referred to as *fast time*. The time across sweeps or sweep number m is referred to as *slow time*. Fast time is sampled at the ADC rate of the receiver, and slow time is sampled at the sweep repetition frequency (SRF) of the system.

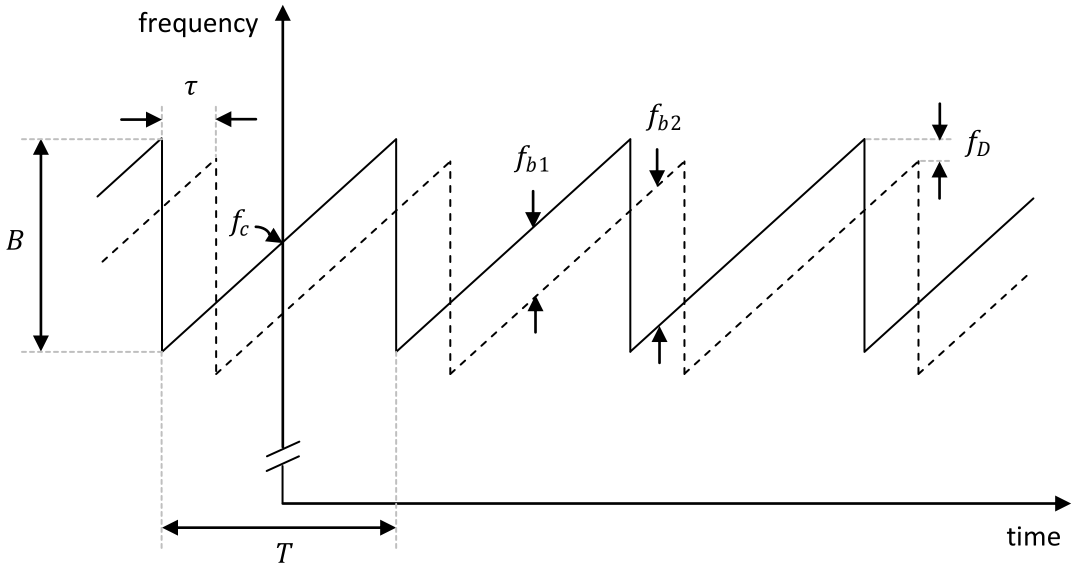

Figure 11 Frequency vs. time of transmitted and delayed/Doppler-shifted received signals. The transmitted chirp (solid line) has a carrier frequency f_c, peak-to-peak frequency deviation B, and sweep period T. The received signal (dashed line) is delayed by the target round-trip delay τ and shifted by the Doppler frequency f_D.

2.2.3 Received signal

The received signal is both delayed in time and shifted in Doppler. To illustrate the situation, we assume that we have a discrete or 'point' target[13] at range 10 km and travelling away from the radar at v = 7.5 m/s. At time t = 0, the target is exactly at R_0 = 10 km from the radar. After that, its range is a function of time as

$$R(t) = R_0 + vt. \tag{1.10}$$

The received signal from this 'point' target is just a replica of the transmitted signal, but with a different amplitude V_{RX} and delayed in position by a factor τ, where $\tau = 2R(t)/c$[14]. It is thus

$$s_{RX} = V_{RX} \cos\left[2\pi\left(f_c(t_m - \tau) + \frac{1}{2}\alpha(t_m - \tau)^2\right)\right] \equiv V_{RX} \cos[\phi_{RX}(t)] \tag{1.11}$$

for $-T/2 + \tau < t_m < T/2$. Its frequency is shown in Figure 11 as the dashed curve.

As seen from Figure 11, the received waveform appears to have the same sawtooth modulation of frequency as the transmit signal, but merely delayed in time and shifted in frequency. Physically, this can be explained as follows. A given transmitted waveform returns, after reflection from a 'point' target approaching the radar at a constant velocity, compressed in time by a certain factor (namely, $1 - 2v/c$). Thus, a sine wave appears to be shifted in frequency by an amount proportional to the

[13] The ideal 'point' target produces a sinusoidal beat signal. In general, however, several targets will be present within the instrumented range, and propagation along the radar path is described by a superposition of a large number of such point targets. However, because the Fourier transform is a linear operator, its response to a weighted sum of sinusoids is just the appropriately weighted sum of 'point' target responses. Consequently, a great deal can be learned about the radar by studying its point-target response. This approach separates algorithm and hardware effects from target and interference phenomenology (Soumekh 1999).

[14] This statement actually represents an approximation which his valid in the case $v \ll c$, which of course is the case for all targets of interest. For a derivation of this approximation, we refer the reader to Hymans and Lait (Hymans 1960) or Kelly and Wishner (Kelly and Wishner 1965).

transmitted frequency. When this sine wave (carrier) is modulated, the echo returns with a higher carrier frequency and with a slightly compressed modulation. For example, an FMCW signal returns with a higher sweep repetition frequency and a higher chirp rate than it had when it left the transmitter. The effects on the modulation are often small, however, and can often be neglected.

A criterion for the validity of this approximation can easily be obtained and expressed in terms of the time-bandwidth product of the transmitted modulation. Since a single sweep has a duration T, its echo has a duration $T(1-2v/c) \equiv T - \Delta T$. This change in length will be noticeable only if ΔT is comparable to the inverse of the bandwidth B of the signal, which measures the "complexity" of the signal and the range accuracy obtainable. Thus, the Doppler stretch effect on the modulation signal can be ignored only if $\Delta T \ll 1/B$, which is equivalent to (Kelly and Wishner 1965)

$$2\frac{v}{c}BT \ll 1. \tag{1.12}$$

In the present example, the maximum value of $2v/c$ is 1×10^{-7}, whereas the time-bandwidth product BT is 25,000 so $2(v/c)BT = 0.0025$ and this approximation is justified. As a result, the received echo can be considered modulated in the same way as the transmitted signal, but shifted in frequency by the *Doppler frequency*

$$f_D \equiv \frac{2v}{c} f_c. \tag{1.13}$$

For a target receding at 7.5 m/s in the radars line of sight and a center frequency of 10 GHz, the Doppler frequency is 500 Hz.

2.2.4 Beat signal

Now after RF amplification, the received signal is 'dechirped' or 'deramped' by 'mixing' or 'beating' it together with a replica of the transmitted signal in a frequency mixer[15]. The resulting signal will contain a product term $GV_{TX}V_{RX}\cos\phi_{TX}\cos\phi_{RX}$, where G is a numerical constant accounting for the voltage conversion loss of the mixer, and other higher-order products. In general, only the lowest-order product will have significant amplitude. The product may be expanded as a sum, namely

$$\frac{1}{2}GV_{TX}V_{RX}[\cos(\phi_{TX}-\phi_{RX}) + \cos(\phi_{TX}+\phi_{RX})].$$

The phase-sum term is an oscillation at twice the carrier frequency, which is generally filtered out either actively, or more usually in radar systems because it is beyond the cut-off frequency of the mixer and subsequent receiver components (Brooker 2005). We are thus interested in the function $\frac{1}{2}GV_{TX}V_{RX}\cos(\phi_{TX}-\phi_{RX})$, which is called the *beat signal*:

$$s_b = \frac{1}{2}GV_{TX}V_{RX}\cos(\phi_{TX}-\phi_{RX}) \equiv V_b\cos\phi_b. \tag{1.14}$$

[15] A mixer is a three-port device that uses a nonlinear or time-varying element to achieve frequency conversion. In its down-conversion configuration, it has two inputs, the *radio frequency* (RF) signal and the *local oscillator* (LO). The output of an idealized mixer is given by the product of the RF and LO signals (Pozar 2005).

Thus, the mixing of the received signal with a replica of the transmitted signal is represented mathematically by subtracting the phase ϕ_{RX} from ϕ_{TX}.

By taking the time derivative of this relation, it follows that the instantaneous frequency of the beat signal, $f_b(t)$, is equal to

$$f_b(t) = f_{TX}(t) - f_{RX}(t), \tag{1.15}$$

where $f_{RX}(t) \equiv f_{TX}(t-\tau)$ is the instantaneous frequency of the received signal. The mixture of the transmitted and received sawtooth frequency waveforms and their subtraction, as shown in Figure 11, thus produces a beat signal whose instantaneous frequency is shown in Figure 12(a).

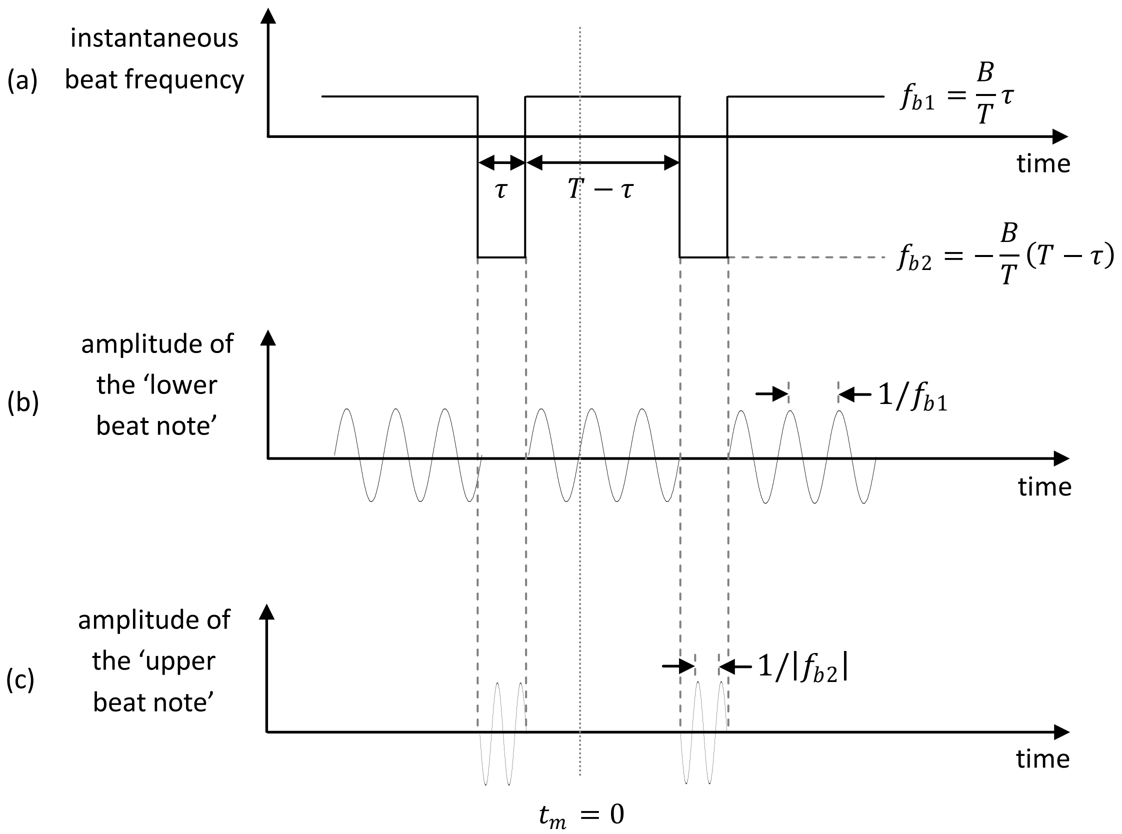

Figure 12 Frequency and amplitude plots versus time of the beat signal. In (a), we see that the instantaneous frequency of the beat signal, $f_b(t)$, alternates between two distinct tones, f_{b1} and f_{b2}. As a result, the beat signal s_b can be regarded as the sum of two pulse trains; (b) illustrates the 'lower beat note' at f_{b1}, and (c) the 'upper beat note' at f_{b2}.

As seen from Figure 12(a), the beat frequency alternates between two distinct tones. In the mth interval, these two frequencies are[16]

(i) During time $-T/2 < t_m < -T/2 + \tau$,
when $f_{RX} = f_c + \frac{B}{T}(t_{m-1} - \tau)$

[16] Here, we implicitly assume that $\tau < T$, or equivalently, $R < cT/2$. The range $cT/2$ is called the radar's *unambiguous range*; typically, the *instrumented range* R_{max} is chosen at less than 20% of the unambiguous range so that the overlap loss is less than 1.9 dB.

and $f_{TX} = f_c + \frac{B}{T} t_m$,

$$f_b(t) = -\frac{B}{T}(T - \tau) \equiv f_{b2}, \tag{1.16}$$

(ii) During time $-T/2 + \tau < t_m < T/2$,
when $f_{RX} = f_c + \frac{B}{T}(t_m - \tau)$
and f_{TX} is as in (i),

$$f_b(t) = \frac{B}{T}\tau \equiv f_{b1}. \tag{1.17}$$

The beat signal can thus be represented as the sum of two pulse trains as shown in Figure 12(b) and Figure 12(c). One, the 'lower beat note', is at frequency f_{b1} and the width of its pulses is $T - \tau$. The other, the 'upper beat note', is at frequency f_{b2} and the width of its pulses is τ.

The 'upper beat note' f_{b2} occurring during $-T/2 < t_m < -T/2 + \tau$ is offset in frequency from the 'lower beat note' f_{b1} by the sweep width, B, as shown by equations (1.16) and (1.17). This is because during $-T/2 < t_m < -T/2 + \tau$, the local oscillator starts the mth sweep while the received RF signal corresponds to the $(m-1)$th sweep. Since B is much greater than the bandwidth of the receiver, the mixer output for $-T/2 < t_m < -T/2 + \tau$ will therefore be filtered and rejected. Hence, for $-T/2 < t_m < -T/2 + \tau$ the beat signal will be a transient pulse. If an ADC is used to observe the beat signal, the sampling can be delayed at the start of each sweep so that the 'fly-back' or 'retrace' effects of the local oscillator returning to its starting frequency are omitted.

Therefore, we are left with a single pulse train to analyze: the 'lower beat note'. Inserting (1.7) and (1.11) into (1.14), we obtain

$$s_b(t) = V_b \cos\left[2\pi\left(f_c t_m + \frac{1}{2}\alpha t_m^2\right) - 2\pi\left(f_c(t_m - \tau) + \frac{1}{2}\alpha(t_m - \tau)\right)\right], \qquad -\frac{T}{2} + \tau < t_m < \frac{T}{2}$$

or, simplifying,

$$s_b(t) = V_b \cos\left[2\pi\left(f_c\tau + \alpha\tau t_m - \frac{1}{2}\alpha\tau^2\right)\right], \qquad -\frac{T}{2} + \tau < t_m < \frac{T}{2}. \tag{1.18}$$

The two-way propagation delay τ is also time-dependent, and is referenced to the range at $t = 0$ so that

$$\tau(t) = \frac{2R(t)}{c} = \frac{2}{c}[R_0 + vt] = \frac{2}{c}[R_0 + v(t_m + mT)] \equiv \tau_0 + \beta t_m + \beta mT, \tag{1.19}$$

where $\tau_0 \equiv 2R_0/c$ is the transit time corresponding to the initial range and $\beta \equiv 2v/c$ is the normalized velocity. The term βmT is the increase in transition time due to the accumulated range vmT from $t = 0$ to the middle of the mth sweep. This term provides the only difference for the equations for consecutive sweeps as opposed to a single sweep.

With equations (1.18) and (1.19) and some algebra, it follows that

$$s_b(t) = V_b \cos[2\pi(C_1 + C_2 t_m + C_3 t_m^2)] \tag{1.20}$$

for $-T/2+\tau<t_m<T/2$, where

$$C_1 = f_c\tau_0 - \frac{1}{2}\alpha\tau_0^2 + f_c\beta mT - \alpha\tau_0\beta mT, \tag{1.21}$$

$$C_2 = f_c\beta + \alpha\tau_0 + \alpha\beta mT - \alpha\tau_0\beta - \alpha\beta^2 mT, \tag{1.22}$$

and

$$C_3 = \alpha\beta\left(1-\frac{\beta}{2}\right). \tag{1.23}$$

Hence, we have three contributions to the phase: a constant, a linear term in t_m, and a quadratic term in time, t_m^2. Equations (1.20) through (1.23) can be simplified by discarding all terms for which the phase contribution is negligible. The maximum phase contribution for the time-dependent terms occurs when $t_m = T/2$. Each term must be examined to determine if it is small compared to π radians.

With the parameters of Table 2 and assuming that the number of sweeps to be processed is of the order of $m \cong 100$, the fourth term in (1.21), $\alpha\tau_0\beta mT$, is of the order of 0.16 radian and can be discarded. Similarly, the linear terms $\alpha\tau_0\beta$ and $\alpha\beta^2 mT$ in (1.22) contribute at most 0.0016 and 8×10^{-9} radians to the phase, respectively. Finally, the quadratic term in (1.20) is always small within the interval $-T/2+\tau<t_m<T/2$; for example, at $t_m = T/2$, it is of the order of 0.0003 radian.

Equation (1.20) then simplifies to

$$s_{b,m}(t_m) = V_b\cos\left(2\pi f_{b,m}t_m + \phi_m\right), \qquad -\frac{T}{2}+\tau<t_m<\frac{T}{2}, \tag{1.24}$$

where the frequency of the beat signal is

$$f_{b,m} = f_c\beta + \alpha\tau_0 + \alpha\beta mT \tag{1.25}$$

and the phase is

$$\phi_m = 2\pi(f_c\tau_0 - \alpha\tau_0^2/2 + f_c\beta mT) \equiv \phi_0 + 2\pi f_D mT. \tag{1.26}$$

The three terms that comprise the frequency term are

(a) The usual range term for a FMCW radar, $\alpha\tau_0$ or $(2B/cT)R_0$;
(b) The Doppler shift f_D, since $f_c\beta = 2v/\lambda_c = f_D$; and
(c) A term resulting from the accumulated range. The accumulated range is vmT, and since the frequency dependence on range is $(2B/cT)R$, the accumulated range causes an increase in beat frequency $(2B/cT)(vmT) = \alpha\beta mT = \beta mB$.

The two terms that comprise the phase of the signal are:

(a) $f_c\tau_0$, the total number of cycles of f_c that occur during the round-trip propagation time corresponding to the initial range;
(b) $-\alpha\tau_0^2/2$, a range-dependent phase term which is incidentally called the “residual video phase” in synthetic aperture radar (SAR) literature;

(c) $f_c \beta mT$, the number of cycles of f_c that occur during time βmT, the round-trip propagation time for the accumulated range.

Both the frequency, $f_{b,m}$, and the phase, ϕ_m, of the beat signal change from sweep to sweep. The frequency change is caused by the range change during the sweep time. With the parameters assumed above, the total observation time (MT) is 50 ms, and with a velocity of 7.5 m/s, the change in range is only 0.375 m. This is much less than the range resolution assumed (3.75 m). Hence the frequency change during the M sweeps is small compared to the range term, except for the very shortest ranges, and the term $\alpha\beta mT$ in (1.25) is also negligible. The radian phase change from sweep to sweep is $2\pi f_D T$, or about 0.067π radians m/s of velocity. Note that a velocity of $\pm\lambda_c/4T$ or 15 m/s will cause a phase shift of π radians between consecutive sweeps. When the phase shift is this large it is not possible to determine if the phase in increasing from sweep to sweep (positive velocity) or decreasing (negative velocity).

Two other effects occur within the pulse; its width, being $T - \tau$, changes very slightly from pulse to pulse. Since T = 500 µs, $\tau = \tau_0 + \beta mT$ we have for $m = 0$, $T - \tau$ = 400 µs; for $m = 100$ we have $T - \tau$ = 400 µs – 2.5 ns. Thus the change in pulse width is negligible. A very important second effect, however, is the change in phase from pulse to pulse, as represented by the third term in (1.26). This phase change shall in fact prove to be the basis for the Doppler processing.

2.2.5 Double-FFT digital processing

Here we demonstrate how a double Fourier-transformation process can be used – often in real time using the fast-Fourier-transform (FFT) algorithm – to produce a time-delay (range) and Doppler (velocity) display of the radar target data. The first Fourier transform process is performed over a pulse repetition period, T (i.e., within a pulse) to obtain target range. The second Fourier transform is performed over several pulses of these data to obtain target Doppler velocity.

2.2.5.1 Range FFT

First, let us perform a Fourier transform on a single pulse. This is shown in Figure 13. In order to perform the Fourier transform digitally, the beat signal is sampled in by an analog-to-digital converter (ADC), after which a fast Fourier transform (FFT) is performed on the resulting samples. We discuss two practical aspects relating to the A/D conversion.

- **Sampling interval**. In order to avoid sampling 'fly-back' transients from the previous sweep, the beat signal is sampled on an interval

$$T_{AD} \equiv T - \tau_{max} \tag{1.27}$$

  so that the 'lower' beat signal is observed for all targets within the instrumented range, and the 'upper' beat signal is omitted (cf. (Wojtkiewicz, Misiurewicz et al. 1997)). For the parameters of our example, the sampling interval is T_{AD} = 500 µs – 100 µs = 400 µs.

- **Sampling rate criterion.** In order to satisfy the Nyquist sampling criterion, we have to sample at a rate f_s that is at least twice the maximum value the beat frequency f_b can assume:

$$f_s \geq 2 f_{b,max}\,. \tag{1.28}$$

  Since for our example the maximum beat frequency is $f_{b,max}$ = 10 MHz, a sampling rate of f_s = 25 MHz would suffice; hence the number of samples collected per sweep is

$$N \equiv f_s T_{AD}, \tag{1.29}$$

or N = 10,000 for the example considered here[17].

In Figure 13(a), we depict a fly-back transient, and illustrate the concept of sampling on a 'fly-back free interval'.

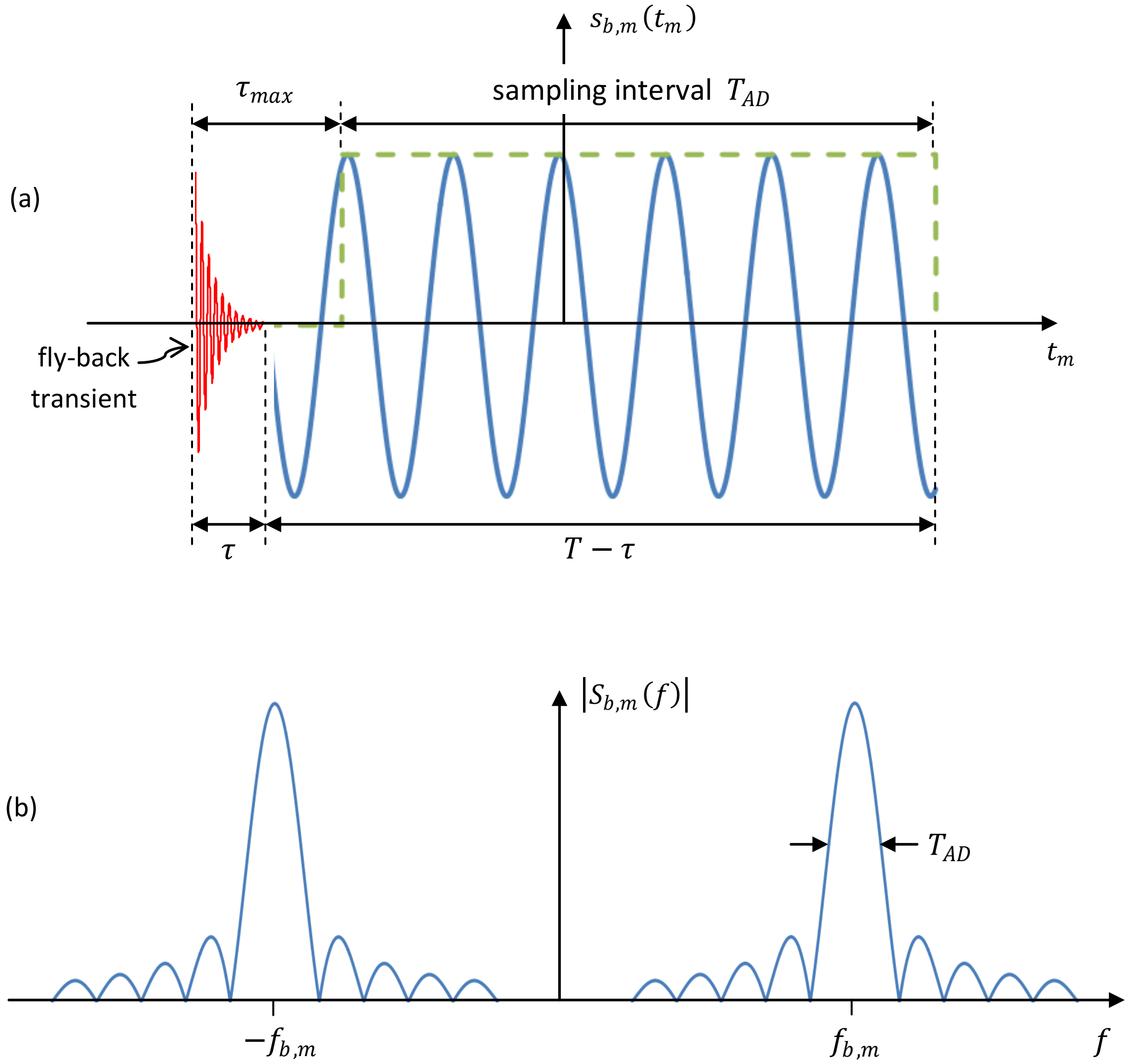

Figure 13 Single pulse and its Fourier transform. (a) Illustrates a single pulse of the 'lower' beat signal $s_{b,m}(t_m)$ during one sweep repetition interval. During the initial transit time τ following the beginning of each sweep, the beat signal is a transient pulse due to the 'fly-back' of the local oscillator to its starting frequency and the filtering of the 'upper' beat note. In order to avoid sampling this 'retrace' effect, the sampling is delayed from the beginning of the sweep by the maximum transit time τ_{max} (cf. (Piper 1995). (b) The amplitude spectrum $|S_{b,m}(f)|$ of $s_{b,m}(t_m)$ consists of two "sicn" pulses centered at $-f_{b,m}$ and $f_{b,m}$. (After (Barrick 1973)).

The Fourier transform of beat signal in the mth pulse, $s_{b,m}(t_m)$ as given by (1.24), is

[17] In order to avoid out-of-band noise from folding back into the target beat signal spectrum, a practical application includes an anti-alias filter with a cutoff frequency between $f_{b,max}$ and $f_s/2$.

$$S_{b,m}(f) = \int_{-T/2+\tau_{max}}^{T/2} V_b \cos[2\pi f_{b,m} t + \phi_m] \, e^{-j2\pi f t} \, dt \tag{1.30}$$

or

$$\begin{aligned} S_{b,m}(f) = \frac{V_b T_{AD}}{2} \{ \mathrm{sinc}[(f - f_{b,m}) T_{AD}] e^{j\phi_0 + j2\pi f_D mT} \\ + \mathrm{sinc}[(f + f_{b,m}) T_{AD}] e^{-j\phi_0 - j2\pi f_D mT} \}, \end{aligned} \tag{1.31}$$

where $\mathrm{sinc}(\cdot)$ is the normalized sinc function defined as

$$\mathrm{sinc}(x) \equiv \frac{\sin(\pi x)}{\pi x}. \tag{1.32}$$

This Fourier transform is shown in Figure 13(b). Since we started with $N \geq 2f_{b,max} T_{AD}$ samples, we obtain samples in the frequency domain from $-f_{b,max}$ to $f_{b,max}$, i.e., at $N/2 = f_{b,max} T_{AD}$ positive values of frequency. These samples are complex in general, as evidenced by the exponential phase factor containing ϕ_0 and $2\pi f_D mT$. Thus we conceptually have $N/2$ range bins ($N/2 = 5{,}000$ here), permitting us to realize the 3.75 m range resolution over the 15 km window, as initially stipulated. Note that each $N/2$ resolution element can be considered a range bin as long as the Doppler term, $(2v/c)f_c$, is small compared to the range term, $\alpha\tau_0$; this is true for the example considered here. Since each pulse is approximately $1/T_{AD}$ wide at the half-power point (T_{AD} = 400 μs here), we should be able to resolve 4,000 targets within range because the width of each FFT pulse in this 10 MHz window is 2.5 kHz. Hence after one FFT process within a pulse we have range information, but no Doppler information; we now turn to extraction of Doppler.

Note that is we start with the first pulse at $m = 0$ and do this FFT process on each pulse, we obtain a Fourier transform m times, where $m \leq M - 1$ (some maximum value). Since the frequency, F_m, and phase, $2\pi f_D mT$, shifts slightly from pulse to pulse due to the target velocity (as given by equations (1.25) and (1.26)), this "sinc" pulse in the frequency domain will change very slightly after each Fourier transformation. Since the N-point FFT produces numbers at $N/2$ discrete positive frequencies, (1.31) should really be written with f replaced by $f = \frac{k}{N} f_s$, where $k = 0, \ldots, \frac{N}{2} - 1$.

Thus the first FFT process on N samples within a pulse gives $N/2$ range bins for each pulse. For each successive pulse, this FFT gives $N/2$ additional positive frequency samples. Digitally, we store each $N/2$ samples in rows of a matrix, until we have M rows. Thus, we have an M-by-$N/2$ matrix whose columns so far represent range bins.

2.2.5.2 Doppler FFT

Now, we perform another FFT over each column, or range bin. This requires M points altogether. Each matrix element is a complex number whose value changes in a column because the frequency, $f_{b,m}$, and the phase, $2\pi f_D mT$, are changing from sweep to sweep. Since each of the M vertical elements comes from a different pulse T seconds apart, MT seconds are required to fill this matrix. Hence each column is really a function of time, and the M column elements can be considered (digital) samples of this time function.

To Fourier transform over a typical column (say the nth), let us again refer to our example for the target at R_0 = 7.5 km; this target will appear in the n = 2,000 bin for $N/2$ = 4,000. As we saw before, this produces $f_{b,m}$ = 5 MHz + 500 Hz + 2.5m Hz. Thus for m running from 1 to 100 – corresponding to time running from 0 to 50 milliseconds – two things happen happen to the positive pulse in the nth range bin: its amplitude changes slightly due to the shift of the "sinc" pulse because of $f_{b,m}$, and its phase changes. The amplitude variation from $m = 1$ to $m = 100$ is slow. For the example given, the shift in the pulse due to $f_{b,m}$ is 250 Hz over $M = 100$ pulses; the -3.9 dB width of the "sinc" pulse is $1/T_{AD}$ = 2.5 kHz. Hence amplitude variation within a column is slight, and can be represented in most cases by a constant, i.e., $\mathrm{sinc}\left[\left(f - f_{b,M/2}\right)T_{AD}\right]$, its value midway down the column where $m = M/2$.

Thus the only variation now within the column (at the positive frequency corresponding to n) is the phase factor, i.e.,

$$S_{mn} = K(f)e^{j2\pi f_D mT} = K(f)e^{j2\pi f_D t_m}, \tag{1.33}$$

where

$$K(f) = \frac{V_b T_{AD}}{2}\mathrm{sinc}\left[\left(f - f_{b,M/2}\right)T_{AD}\right]e^{j\phi_0}. \tag{1.34}$$

In the rightmost expression of (1.33), mT has been replaced by t_m to represent the discrete flow of time from pulse to pulse. The Fourier transform of this quantity over t_m from 0 to MT is

$$\mathcal{S}_n = K(f)MT\mathrm{sinc}[(f - f_D)MT]. \tag{1.35}$$

Here again we should note that our digital FFT does not really give a continuous variation over f (frequency), but will compute values at M discrete frequency points. The question arises how we should choose these M frequency points, i.e., how wide a frequency window we want to display. Since our sweep repetition frequency, $1/T$ ($1/T$ = 2.5 kHz here) results in an unambiguous Doppler of 1.25 kHz, we would logically select $f_{D,max}$ = $1/2T$ so as to display all of the unambiguous Doppler window. Then the frequency window in Doppler will be from $-f_{D,max}$ to $f_{D,max}$ at a spacing $f_{D,max}/M$, which turns out to every $2f_{D,max}/M$ Hz, or 20 Hz here. Note also in (1.33) that if the Doppler shift f_D exceeds $1/2T$, then from pulse to pulse we will be sampling at less than the required Nyquist sampling rate. Hence our sweep repetition frequency, $1/T$, must always be *at least* twice the maximum expected Doppler frequency[18].

Observe now an important fact in (1.35): the displacement of the "sinc" pulse resulting from the second Fourier transformation over the columns occurs at the Doppler shift $f_D = (2v/c)f_c$ that results from a target at (radial) velocity v with a backscatter radar having a carrier frequency f_c. Furthermore, the -3.9 dB width of the pulse represented by (1.35) is $1/MT$ Hz, as shown in Figure 14. Thus, we produce M (or 100) Doppler frequency points every $1/MT$ Hz (or 20 Hz here). Since MT is the coherent integration time (in this scheme, it is the time required to fill the matrix), $1/MT$ is exactly the Doppler resolution one would expect from any coherent pulse-Doppler radar.

[18] The unambiguous velocity measurement range can be extended by using multiple (appropriately chosen) sweep repetition frequencies (Musa and Salous 2000) ; however, the algorithm used to achieve this is beyond the scope of this thesis.

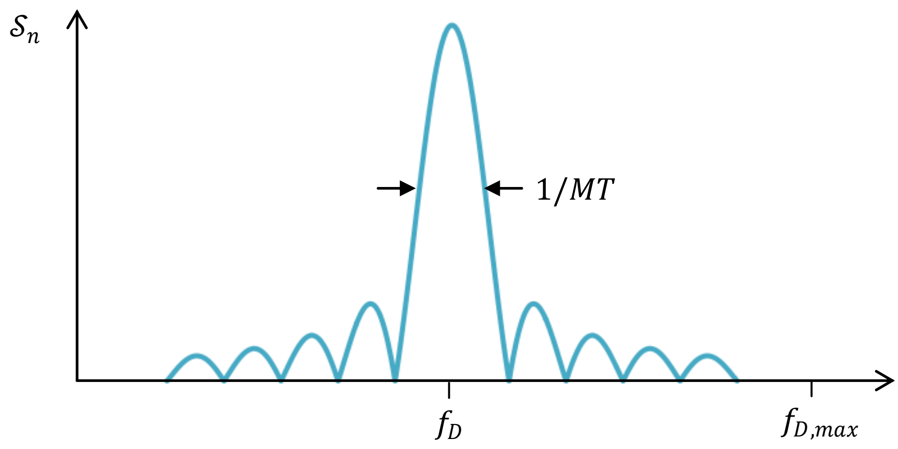

Figure 14 Doppler spectrum after second Fourier transformation within a given range. (After (Barrick 1973)).

Therefore, in summary, we have done two sets of FFTs. One set within each pulse at N points to give $N/2$ range bins; these bins are elements of a row of a matrix. The second set is over M pulses, or over M column elements of the matrix, to give M Doppler bins for each range bin. Note that the original target range also contained a small offset due to Doppler. If this offset is objectionable, it can now be removed – in the case of a discrete target – by using the Doppler information to correct the target range.

2.2.6 Sidelobe apodization

The spectrum of a truncated sine wave output by a FMCW radar for a single target has the characteristic 'sin *x*/*x*' shape as predicted by Fourier theory. The range side lobes in this case are only 13.3 dB lower than the main lobe, which is not satisfactory as it can result in the occlusion of small nearby targets as well as introducing clutter from the adjacent lobes into the main lobes. To counter these undesirable effects, a window function is usually applied to the sampled IF signal prior to FFT frequency estimation.

Many window functions with a wide range of properties have been published by various authors and their effects on fixed-frequency signals well documented (e.g. see an extensive review given by Harris (Harris 1978)). Consideration in this report is restricted to three commonly employed window functions: Hamming, Hanning, and Blackman (Pace 2004). Each of these windows has the generic form

$$w[n] = a_0 - a_1 \cos\left(2\pi \frac{n}{N-1}\right) + a_2 \cos\left(4\pi \frac{n}{N-1}\right), \qquad 0 \le n \le N-1, \qquad (1.36)$$

where n is the sample index, N is the total number of samples, and a_0, a_1, and a_2 are coefficients specific to each window. As summarized in Table 1, the resulting spectra offer poorer resolution but improved sidelobe levels that can accommodate almost any requirement.

Window	Rectangle	Hamming	Hanning	Blackman
Worst side lobe (dB)	–13.3	–42.2	–31.5	–58
3 dB bandwidth (bins)	0.88	1.32	1.48	1.68
Scalloping loss (dB)[19]	3.92	1.78	1.36	1.1
SNR loss (dB)	0	1.34	1.76	2.37
Main lobe width (bins)	2	4	4	6
a_0	1	0.54	0.50	0.42
a_1		0.46	0.50	0.50
a_2				0.08

Table 1 Properties of some weighting functions. (After (Pace 2004)).

Figure 15 and Figure 16 below compare these windows in the time and frequency domains. Of particular interest are the Hamming and Hanning weighting functions that offer similar SNR and resolutions, but with completely different sidelobe characteristics. As can be seen in Figure 15, the former has the form of a cosine-squared-plus-pedestal, while the latter is just a standard cosine-squared function. In the Hamming case, the close-in side lobe is suppressed to produce a maximum level of -42.2 dB, but the energy is spread into the remaining sidelobes resulting in a falloff of only 6 dB/octave, while in the Hanning case the first lobe is higher at -31.5 dB, but with a falloff of 18 dB/octave (Willis and Griffiths 2007).

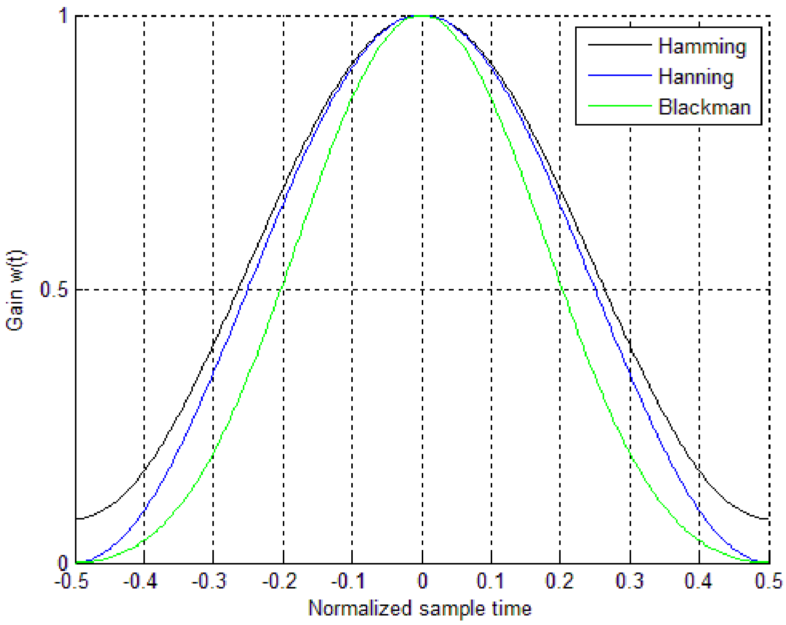

Figure 15 Window function gains. (After (Willis and Griffiths 2007)).

[19] *Scalloping loss* is the apparent attenuation of the measured value for a frequency component that falls exactly half way between FFT bins. It is defined as the ratio of the power gain for a signal frequency component located half way between bins to that of a component located exactly on the FFT bin (source: http://www.bores.com/courses/advanced/windows/10_pl.htm).

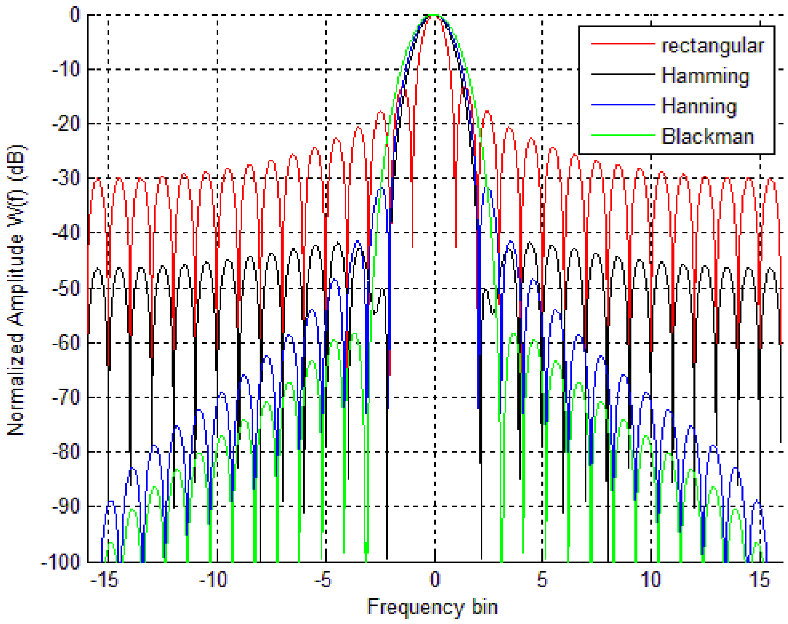

Figure 16 Normalized window amplitude spectra as a function of bin number. (After (Willis and Griffiths 2007)).

For most FMCW applications, the Hamming window is used as it provides a good balance between sidelobe levels (-42.2 dB), beam width (1.32 bins), and loss in SNR compared to a matched filter (1.34 dB) (Willis and Griffiths 2007).

2.2.7 Simulation

We have implemented a simulation of a FMCW Doppler radar in MATLAB. The simulation code is given in the Appendix[20]. The parameters of our model FMCW Doppler radar are tabulated in Table 2.

[20] Actually, the code given in the Appendix also provides the ability to investigate the effect of sinusoidal phase errors, which we investigate in Chapter 4. For this simulation, however, we have set the amplitude of the sinusoidal phase error equal to zero, corresponding to an ideal frequency sweep.

Parameter	Symbol / Formula	Value	Unit
RF center frequency	f_c	10	GHz
RF wavelength	λ_c	30	mm
Frequency excursion, peak-to-peak	B	50	MHz
Ideal time resolution		20	ns
Ideal range resolution	$c/2B$	3	m
Sweep repetition frequency (SRF)		2	kHz
Sweep repetition interval (SRI)	T	500	µs
Maximum unambiguous Doppler shift	$f_{D,max} = 1/2T$	1	kHz
Maximum unambiguous target velocity	$v_{max} = \lambda_c/4T$	15	m/s
Sweep rate	$\alpha = B/T$	100	GHz/s
Beat frequency / range ratio	$2B/cT$	6.67	kHz/m
Range / beat frequency ratio	$cT/2B$	0.15	m/kHz
Maximum ('instrumented') range	R_{max}	15	km
Maximum transit time	τ_{max}	100	µs
Maximum beat frequency	$f_{b,max}$	10	MHz
Minimum beat frequency interval	$T - \tau_{max}$	400	µs
Minimum beat frequency spectral width	$1/(T - \tau_{max})$	2.5	kHz
Minimum range resolution	$cT/[2B(T - \tau_{max})]$	3.75	m
ADC sample rate	f_s	31.25	MHz
ADC sampling period	T_s	32	ns
ADC sampling interval	T_{AD}	400	µs
Number of samples collected per sweep	N	12,500	samples
Range FFT length	N_{FFT}	16,384	samples
Number of padded zeroes	$N_{FFT} - N$	3,884	
FFT frequency sample spacing	f_s/N_{FFT}	1.907	kHz
FFT range sample spacing	$(cT/2B)(f_s/N_{FFT})$	0.286	m
Doppler FFT length	M	64	samples
Doppler FFT frequency sample spacing	$1/MT$	31.25	Hz
Radial velocity sample spacing	$\lambda_c/2MT$	0.47	m/s

Table 2 FMCW Doppler radar parameters.

In Figure 17, we show a contour plot (linear scale) of the simulated response of a 'point' target at an initial range R_0 = 10 km receding in the radar's line of sight direction at a velocity of v = 7.5 m/s. We haved used Hamming weighting for both the range and Doppler FFTs.

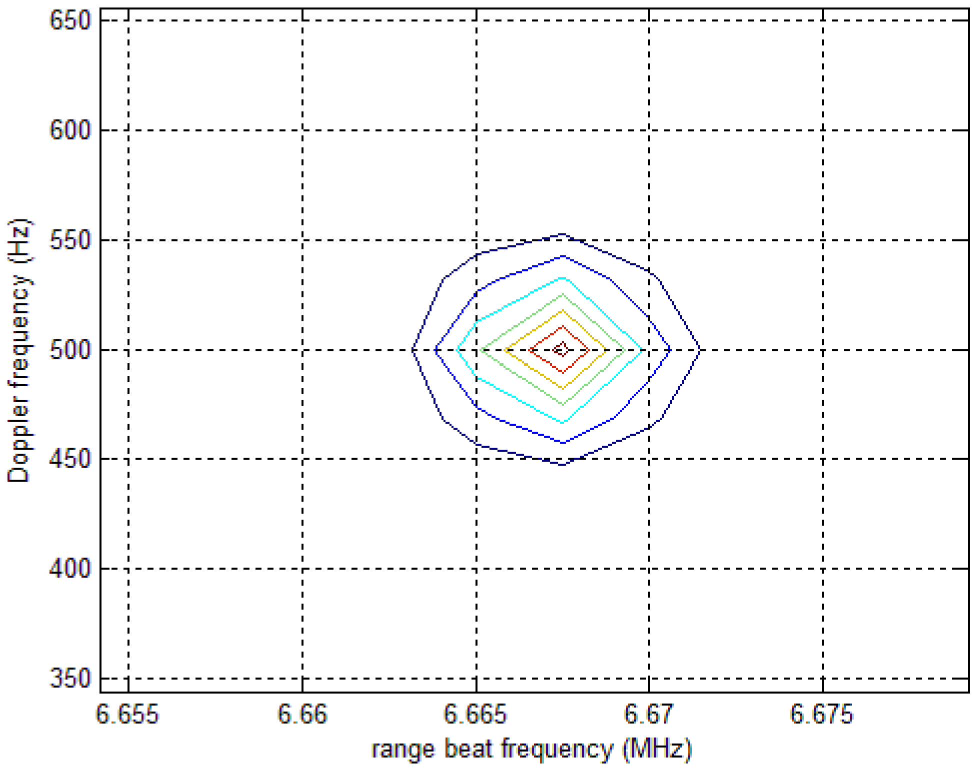

Figure 17 Contour plot (linear scale) of the response of a 'point' target at an initial range of 10 km, receding at a radial velocity of 7.5 m/s, for the simulation parameters given in Table 2.

Figure 17 shows that the 'point' target response is a peak at a range beat frequency of 6.667 MHz and a Doppler frequency of 500 Hz, as expected.

2.2.8 Discussion of the 'point' target model

The true physics of scattering of a radar signal by a target would indicate that the 'point' model is too simplistic. In fact many assumptions must be made in order to end up with the above system model. For instance:

- Scattering by a target can also impart a phase shift to the reflected wave, which we have omitted here. In a more general development, we would adopt a complex representation of the transmitted and received signals (Jakowatz, Wahl et al. 1996) and allow g to take complex values to incorporate this phase shift. The phase shift can also vary with frequency, which gives rise to target 'signature' responses (Soumekh 1999).
- The medium through which the radar signal travels is assumed to be non-dispersive. This also precludes waveguide dispersion or group delay in the filters. In practice, group delay in the filters is a significant problem (Perez-Martinez, Burgos-Garcia et al. 2001).
- The radar system and its environment are assumed to be linear and time-invariant (LTI). A violation of this assumption with important practical consequences is non-linear behavior in the receiver electronics – most notably the mixer and high-gain preamplifier (also called a low-noise amplifier, or LNA) which amplifies the received signal prior to mixing – which can result in the generation of signal harmonics and intermodulation between multiple signals (Morgan, Beasley et al. 2006).

- One should associate an amplitude factor with the target return, which varies with range as $\sim 1/R^4$ for point targets and $\sim 1/R^2$ for extended targets or 'clutter'. For targets within a range of typically 1 km, however, this amplitude factor is compensated for by a sensitivity frequency control (SFC) filter; beyond this range, the effect of this factor is often negligible compared to radar system errors such as the quantization noise, thermal additive noise, and multiplicative noise (instability of the radar) (Soumekh 1999).

Despite its limitations, however, the 'point' target model is a convenient way to separate algorithm and hardware effects from target and interference phenomenology.

2.2.9 Concluding remarks and outlook

We have discussed how a FMCW-Doppler transceiver transmitting coherent frequency sweeps can extract target range and velocity information. Up till now we have assumed that the transmitted chirps were ideally linear. However, a chirp generated by a direct digital chirp synthesizer (DDCS) is affected certain inherent non-idealities due to the digital nature of the DDCS, and these non-idealities will in turn affect the observed range-Doppler output. Before determining these effects, which is the subject of Chapters 3 and 4, we first discuss the operation of the DDCS in more detail in Section 2.3.

2.3 Direct digital synthesis

Before digital technology became widely available, analog techniques were employed to generate radar transmit waveforms. FMCW signals were generated using a voltage-controlled oscillator (VCO) or YIG (Yttrium Iron Garnet)-tuned oscillator. However, it is difficult to achieve adequate linearity over a wide bandwidth and preserve coherence from sweep to sweep, and such oscillators can be susceptible to mismatches and to drift with temperature. Digital technology, however, presents the radar system designer flexibility and accuracy of digital waveform control.

In this section, we describe the direct digital synthesis (DDS) technique commonly used to generate radar transmit signals digitally. An outline of this section is as follows. First, we review the basic principles of direct digital *frequency* synthesis (DDFS) in Section 2.3.1. This will serve as a prelude to our subsequent discussion of the direct digital *chirp* synthesizer (DDCS) in Section 2.3.2. Finally, in Section 2.3.3, we enumerate sources of noise and spurious signals in DDCSs.

2.3.1 Direct digital frequency synthesis

The most popular technique for direct digital frequency synthesis (DDFS) is the sine look-up table method first introduced by Tierney, Rader, and Gold (Tierney, Rader et al. 1971). This method, which is well described in the literature, is illustrated in

Figure 18. A *phase accumulator* stores a phase pointer which is advanced by a given step, the *frequency tuning word* (FTW) or *phase increment*, at each clock cycle of a stable frequency reference. The phase position is converted into amplitude by addressing a look-up table stored in a

(programmable) read-only memory ((P)ROM). Finally, a digital-to-analog converter (DAC) followed by a low-pass interpolating filter converts the digital signal to analog form[21].

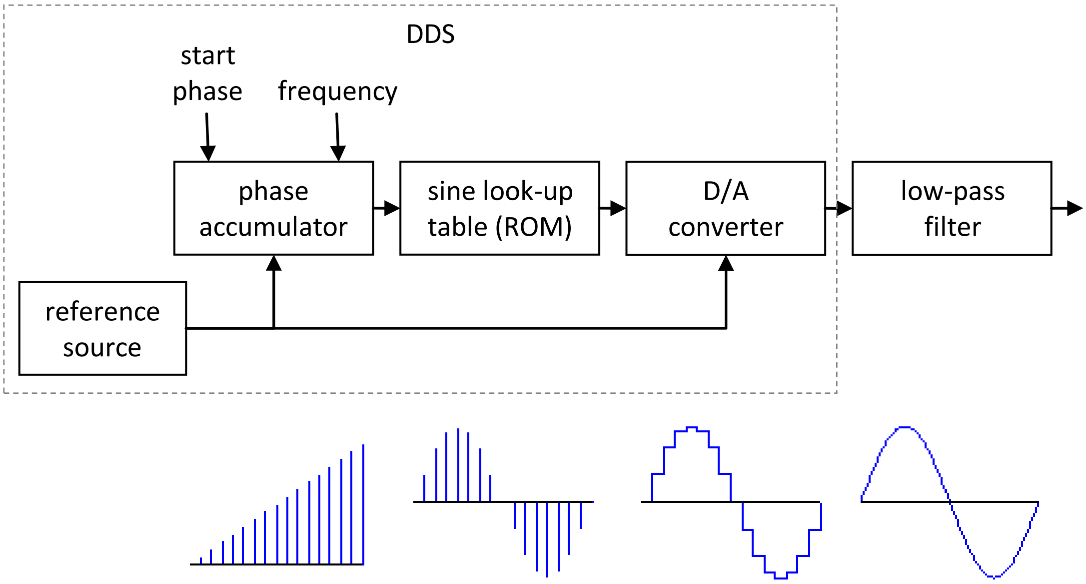

Figure 18 Block diagram of a DDFS (above) and signal flow through it (below). (After (Adler, Viveiros et al. 1995)).

The detailed operation of the digital part of the DDS, called a numerically controlled oscillator (NCO), is illustrated in Figure 19. The phase increment is expressed in a format called Binary Angle Measurement (BAM), in which the most significant bit (MSB) of the word represents 180°, the next bit 90°, and so on. In the phase accumulator, the tuning word is added to the output of a running sum, implemented as an adder followed by a register. This produces a uniformly increasing phase, incremented at the system clock rate. The W MSBs of the running sum are sent to the phase-to-amplitude converter, which is a look-up table that produces an S-bit value that represents the amplitude of the sine wave at the input phase.

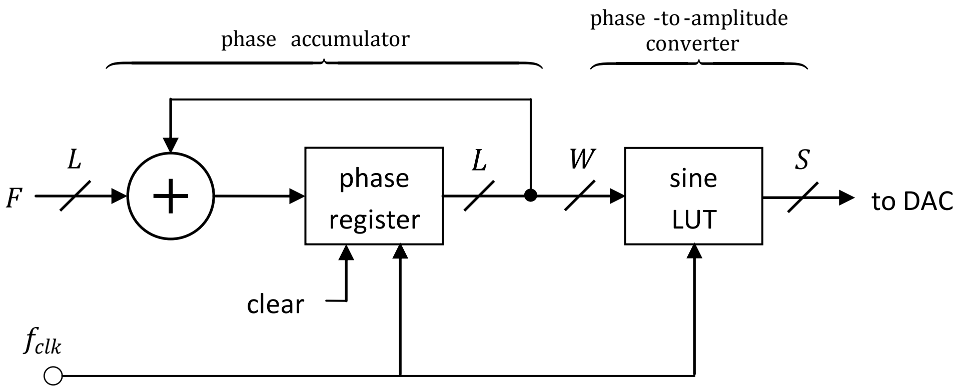

Figure 19 NCO block diagram. (After (Skolnik 2008)

[21]The term "DDS" is also used to refer only to the system up to and including the DAC. The integration of a DAC and a DDS onto a single chip is commonly known as a *complete* DDS solution, a property common to the Analog Devices DDSs investigated in this report.

The counter's carry function allows the phase accumulator to act as a 'digital phase wheel' in the DDS implementation. To understand this basic function, visualize the sine-wave oscillation as a vector rotating around a phase circle (see Figure 20). Each designated point on the phase 'wheel' corresponds to the equivalent point on a cycle of a sine wave. As the vector rotates around the wheel, the sine of the angle generates a corresponding output sine wave. Thus, one revolution of the vector around the phase wheel results in one complete cycle of the output sine wave.

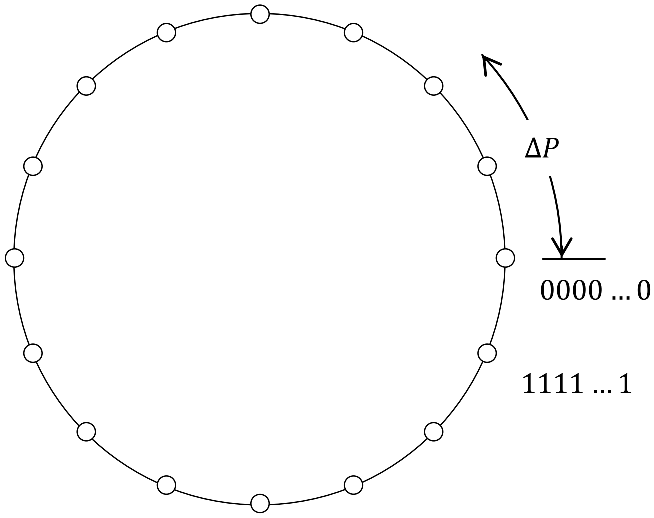

Figure 20 Digital phase wheel. (After (Murphy and Slattery 2004)).

At each clock pulse, the phase accumulator increments its stored number by the phase increment word ΔP. The phase increment word ΔP forms the phase step between reference clock updates; it effectively sets how many points to 'skip' around the phase wheel. The larger the jump size, the faster the phase accumulator overflows and completes its equivalent of a sine wave cycle. The rate of accumulator overflows determines the output frequency:

$$f_o = \frac{\Delta P}{2^L} f_{clk}, \tag{1.37}$$

where f_o is the DDS output frequency, ΔP is the phase increment word, L is the number of accumulator bits, and f_{clk} is the system clock frequency. Due to the discrete-time nature of the system, the phase increments ΔP and $2^L - \Delta P$ will result in the same (aliased) output frequency, although the two output signals will be offset in phase by 180°. Thus there are $2^L/2$ discrete output frequencies that can be generated, each corresponding to a unique value of ΔP less than 2^{L-1}.

Using the above architecture, both the frequency and phase resolution of the DDFS are determined by the word-length (also known as bit-depth) L of the phase accumulator. Specifically, the frequency resolution is obtained by setting $\Delta P = 1$ in Eq. (1.37):

$$\Delta f = \frac{f_{clk}}{2^L}. \tag{1.38}$$

In most applications, L is chosen to be of the order of 24 to 48 in order to achieve acceptable resolution. However, to address the waveform memory with such a large number of bits would require a prohibitively large ROM, because the memory size grows exponentially with the number of address bits. For this reason, usually only the W most significant bits of the phase accumulator are driven to the memory, and the least significant ones are discarded. This process is known as *phase truncation*. The memory length is thus reduced to 2^W words, with W taking values around 14-19 in practical systems .

The truncated output of the phase accumulator serves as the address to the sine (or cosine) look-up table. Each address in the look-up table corresponds to a phase point on the sine wave from 0° to 360°. The look-up table contains the corresponding digital amplitude information for one complete cycle of a sine wave. (Actually, only data for 90° is required because the quadrature data is contained in the two MSBs). The look-up table therefore maps the phase information from the phase accumulator into an m-bit digital amplitude word, which in turn drives the DAC (Kester 2002).

The DAC output spectrum contains frequencies $nf_{clk} \pm f_{out}$, where $n = 0,1$, ... Assuming it operates by the widely used sample-and-hold principle, the amplitudes of these components are weighted by the function

$$\mathrm{sinc}\left(\frac{f}{f_{clk}}\right). \tag{1.39}$$

The roll-off occurs because the DAC output is not a series of zero-width impulses (as in a perfect impulse resampler), but a series of rectangular pulses whose width is equal to the reciprocal of the update rate (Kester 2005). This effect can be mitigated by using an inverse $\mathrm{sinc}(f/f_{clk})$ filter, which can be implemented digitally in the DDS (Analog Devices 2009). The resolution of the DAC is typically 2 to 4 bits less than the width of the lookup table, although even a perfect W-bit DAC will add quantization noise to the output.

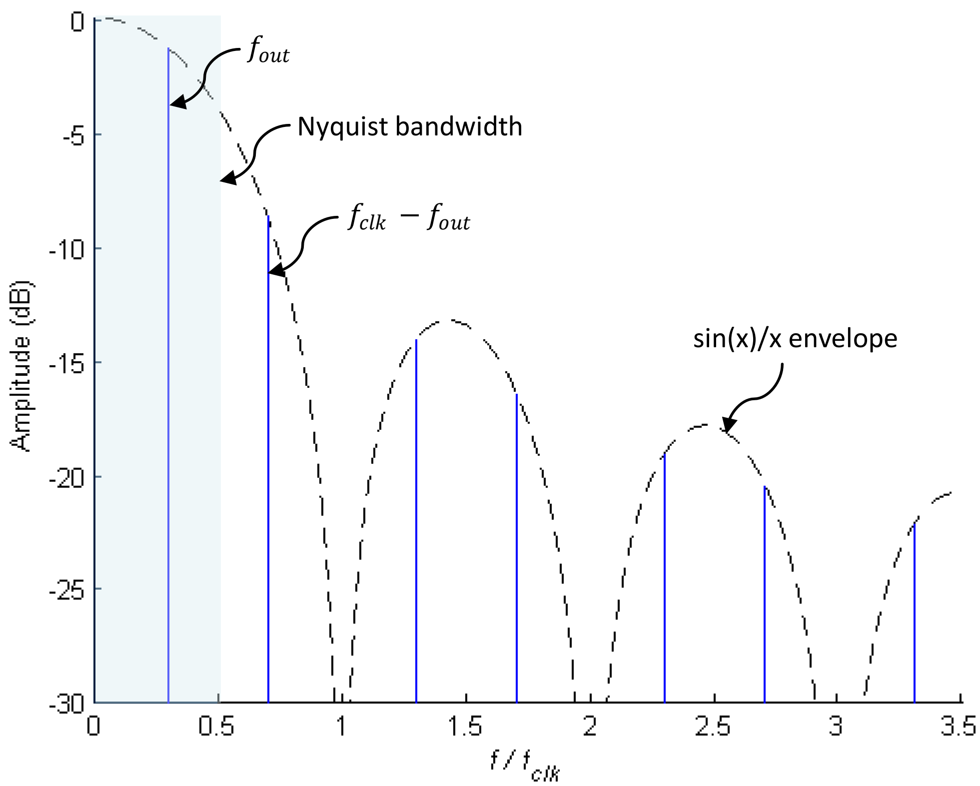

Figure 21 Amplitude spectrum of the output of a DDS generating a single tone at $f_{out} = 0.3f_{clk}$.

The reconstruction filter that follows the D/A converter removes the high frequency sampling components and provides a pure sine wave output. As the DDS generates frequencies close to f_{clk} / 2, the first image $(f_{clk} - f_{out})$ becomes more difficult to filter. This results in a narrower transition band for the filter, and increasing filter complexity. Therefore, in order to keep the filter simple, the DDS operation is limited to less than 40% of the clock frequency in practical applications.

In short, we have discussed theThe direct digital frequency synthesizer (DDFS) pro

2.3.2 Direct digital chirp synthesis

A direct digital chirp synthesizer (DDCS) is similar to a DDFS, except that the input ΔP of the phase accumulator, instead being a fixed value, is now provided by the output of an additional *frequency accumulator* (Durbridge and Warne 1991; Adler, Viveiros et al. 1995) or *digital ramp generator* (DRG) (Analog Devices 2010). As we shall explain below, the two *cascaded* (or *pipelined*) accumulators act as a double integrator and generate a parabolic output, which translates to the parabolic phase of a linear FM signal (Figure 22).

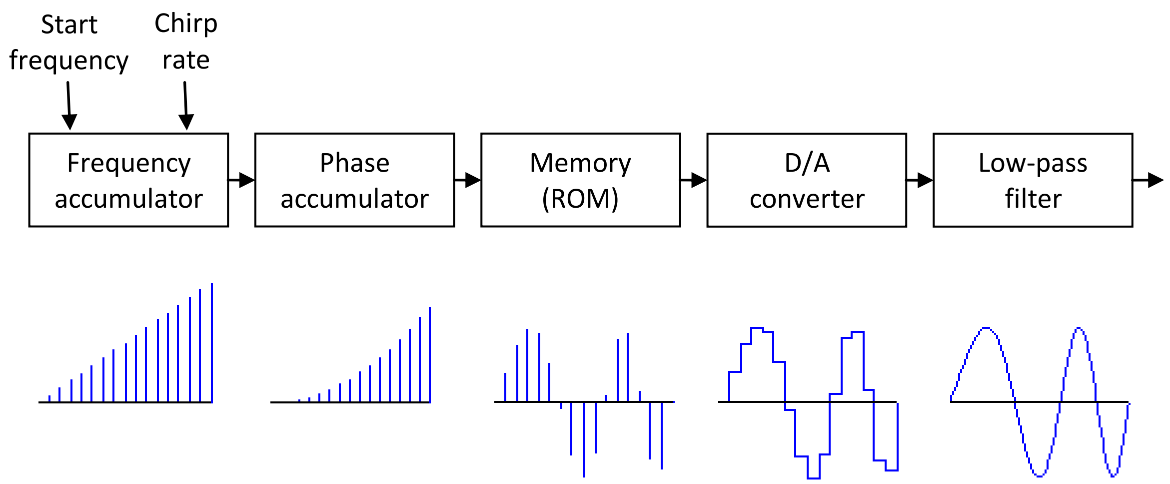

Figure 22 DDCS architecture (above) and the signal flow through it (below). Vertical bars represent digital time series, while continuous graphs presents analog signals. From left to right the signal flow

2.3.2.1 Single-clock DDCS

The DDCS is based on the realization that the quadratic phase sequence

$$P[n] = Cn^2 + Bn + A \tag{1.40}$$

can be generated numerically at high speed using addition only. Figure 23 shows a block diagram of a DDCS with two cascaded accumulators. The outputs of the accumulators are stored in registers. Assuming for the moment that the phase and frequency accumulators are clocked synchronously with a single master clock, **Error! Reference source not found.** presents the contents of the chirp ate register (ΔF) and the two accumulator registers, frequency (F) and phase (P), for the first few clock cycles in a chirp generation sequence. The parameter ΔF is called the *frequency increment*, and is also known as the *phase increment increment* (Durbridge and Warne 1991) or the *delta frequency tuning word* (DFTW) (Analog Devices 2009).

n (clock cycle)	ΔF (chirp rate)	$F[n]$ (frequency)	$P[n]$ (phase)
initial values	$2C$	$C + B$	A
1	$2C$	$3C + B$	$1^2C + 1B + A$
2	$2C$	$5C + B$	$2^2C + 2B + A$
3	$2C$	$7C + B$	$3^2C + 3B + A$
4	$\vdots$	$\vdots$	$\vdots$
5	$2C$	$(2n + 1)C + B$	$n^2C + nB + A$

Table 3 Generation of quadratic time base using a pipelined double accumulator. (After (Andrews, Chang et al. 1992)).

After register initialization, at each clock cycle n, the register value P (or F) is obtained as sum of the data stored within the register the value of F (or R) at the previous clock cycle. By loading the registers in Figure 23 with the initial conditions described in Table 3, all pipeline delays are accounted for and the quadratically increasing phase has its origin at the time of loading of the initial conditions.

2.3.2.2 Dual-clock DDCS

As mentioned before, the quadratic phase word generation illustrated in Table 3 is based on the assumption that the frequency and phase accumulators are clocked at the same rate. While many chirp DDSs are implemented in this way (Durbridge and Warne 1991; Durrant and Parkes 1991; Andrews, Chang et al. 1992), in some cases it may be necessary to use a dual clock architecture in which the frequency accumulator is clocked at sub-multiple K of the master clock frequency. This reduces the speed requirements for the frequency accumulator and provides a finer chirp rate resolution (Salous and Green 1994).

Such is the case for the Analog Devices AD9858 and AD9910 DDSs we wish to model in this report. According to Kester (Kester 2002; Kester 2005), these DDSs require a serial, or byte-loading sequence to get the new frequency word into an internal buffer register which precedes the parallel-output frequency register. After the new word is loaded into the buffer register, the parallel-output frequency register is clocked, thereby changing all the bits simultaneously. The number of clock cycles required to load the frequency buffer register determines the maximum rate at which the output frequency can be changed. For the AD9858 this requires K = 8 clock cycles (Analog Devices 2009), and for the AD9910 K = 4 (Analog Devices 2010).

Figure 23 shows a block diagram of the model dual-clock DDCS that we shall investigate in this report. Note that there is no 'frequency truncation', i.e., the frequency accumulator has the same word length L as the phase accumulator[22]. Although not shown in Figure 23 for simplicity, both accumulators can be cleared (or reset). By resetting the accumulators at intervals of the modulation period, the output waveform becomes a repetitive frequency sawtooth, or FMCW waveform.

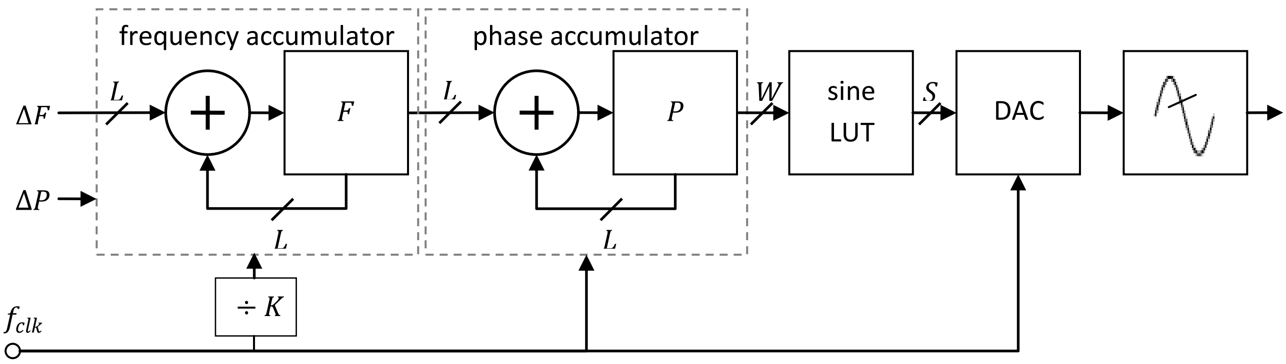

Figure 23 Chirp DDS block diagram.

A detailed derivation of the chirp DDS output is deferred to Chapter 3.

[22] In the AD9910, ΔF is an L-bit unsigned integer, and the ramp direction is controlled using a separate pin (Analog Devices 2010). In the AD9858, ΔF is a signed (two's complement) value, but the MSB is not necessary anyways since it would produce aliased frequencies (Analog Devices 2009).

2.3.3 Sources of noise and spurs in DDS

The output of a DDCS contains spurious signals, whose origin can be attributed to one (or several) of the following distortion sources. Some of them are common to all digital systems, while others are specific to the chirp DDS structure.

- Errors due to sampling of the modulating signal. To digitize the phase in steps equal to those of an ideal linear chirp, the two accumulators have to be clocked at the same rate. However, as explained is Section 2.3.2.2, in our model chirp DDS the frequency increment word can only be changed at a sub-multiple K of the master clock frequency. This results in a 'staircase' or 'stepped CW' approximation of the linear frequency ramp, the effect of which has been analyzed by Barry and Fenwick (Barry and Fenwick 1967) and subsequently refined by Salous and Green (Salous and Green 1994).

- Phase truncation. The synthesizer resolution is determined by the flock frequency and the number of bits (L) of the phase accumulator. Usually L is of the order of 24 to 32, giving a resolution of $f_{clk}/2^L$. It is not feasible to address the waveform memory with such a large number of bits, because the memory size grows exponentially with the number of address bits. For this reason, usually only the W most significant bits (MSBs) of phase accumulator are driven to the memory, and the least significant ones are discarded. The memory length is thus reduced to 2^W words, with W taking values around 14 to 19 in practical systems.

- Amplitude truncation. The amplitude samples stored in the waveform memory have finite precision, usually limited by the maximum number of bits that can drive the DAC.

- Zero-order-sample-and-hold distortion. Typical DACs are sample-and-hold devices. That is, they continue to output the last sampled value throughout the sample period. This effect acts as a filter having a frequency response:

$$H(f) = \mathrm{sinc}\left(\frac{f}{f_s}\right) \tag{1.41}$$

  This results in a high-frequency roll-off that is quite undesirable in many circumstances. For example, if the output frequency is one quarter of the sample frequency, an attenuation of 1 dB will occur (Smith 1998).

- DAC non-linearities. Both DAC errors (in its several definitions) and transients energy (usually represented by "glitch energy") cause distortions that are difficult to evaluate, although simulation and empirical tests can be done.

- Sampling components. Due to the sampling process, there are aliased components present in the DAC output. If the output signal is bandlimited below the Nyquist frequency ($f < f_{clk}/2$), these components can be eliminated by low-pass filtering.

- Post-filter errors. Most notably, if the group delay in the low-pass filter deviates from linear phase, it will affect the frequency slope accuracy, especially at the high end of the band. Therefore, it is desirable to choose low-pass filters with linear phase characteristics, such as

Bessel and Butterworth filters. A drawback of these filters, however, is that they provide less attenuation in the stop band than filters with a more nonlinear phase characteristic (e.g., Chebyshev and Cauer filters) and a trade-off must be made (Tierney, Rader et al. 1971; Smith 2003).

There are thus a myriad of sources of error in a DDS-based chirp synthesizer. The scope of this thesis, however, is limited to just a few of them.

2.4 Statement of the problem

In this report, we shall focus on the digital sources of error. Our model system will be based on the Analog Devices AD9858 and AD9910 direct digital synthesizers, of which the relevant technical specifications are listed in Table 4.

DDS	Internal clock speed (GSPS)	Frequency accumulator bits	Phase accumulator bits	DRG clock division factor	DAC bits	Phase accumulator address bits
AD9858	1	32	32	8	10	15
AD9910	1	32	32	4	14	19

Table 4 Parameters of Analog Devices direct digital synthesizers.

As stated earlier, in this report we focus on the digital phase errors due to sampling of the modulating signal and phase truncation. The question we set out to answer in Chapter 3 is: how do these digital phase errors affect the 'point' target response of a FMCW radar after performing the range FFT, and what is the worst-case amplitude of a resulting spurious sidelobe relative to the target signal? In Chapter 4, we also investigate what their effect is on Doppler processing.

3 An analysis of the effect of digital phase errors in the transmit signal on the beat signal spectrum

As discussed in Section 2.3, a chirp DDS has several sources of error due to the non-ideality of both its digital and analog components. In this chapter we focus on two digital sources of error, namely, (1) the staircase approximation of the linear FM time-frequency characteristic by the frequency accumulator and (2) the subsequent truncation of phase samples generated by the phase accumulator prior to addressing the sine ROM. We derive an upper bound for the degradation of the spurious-free dynamic range (SFDR) in a FMCW radar's range profile due to these error sources.

This chapter is organized into six sections. In Section 3.1, we construct a mathematical model of a FMCW transceiver in which the transmit signal is generated by single-sideband (SSB) upconversion of a signal at intermediate frequency (IF) which is generated by bandlimited interpolation of *amplitude* samples. In Section 3.2, we posit a model of a direct digital chirp synthesizer (DDCS), by which these amplitude samples are generated from ideal *phase* samples perturbed by a periodic digital phase error. In Section 3.3, we compute the effects of such digital phase errors on the performance of our model FMCW transceiver. In Section 3.4, we apply these general results to an actual DDCS by considering in detail the operation of a DDCS, and derive the form of the periodic digital phase error. Finally, in Section 3.5, we combine the results of Sections 3.3 and 3.4 to derive an upper bound for the spurious-to-peak level (SPL) of spurious signals in the spectrum of the beat signal of our model FMCW transceiver.

3.1 Mathematical model of a FMCW transceiver

In this section, we construct a mathematical model of a FMCW radar transceiver which generates a chirp at intermediate frequency (IF) from digital samples and up-converts the IF signal to radio frequency (RF) by single-sideband (SSB) upconversion. The IF signal is considered to be generated by a direct digital synthesizer (DDS), but our general discussion at this stage also applies to systems which, for example, read out waveform samples from memory.

In Section 3.1.1, we describe an ideal DDS as a bandlimited interpolator of digital samples. In Section 3.1.2, we discuss the single-sideband upconversion, and show that the transmitted signal can be expressed in terms of the 'analytic signal' of the DDS output. In Section 3.1.3, we consider the special case that the digital samples are of an ideal linear chirp, and show that in this case, within the 'stationary phase approximation', the transmit signal is also an ideal linear chirp. Finally, in Section 3.1.4, we obtain an expression for the beat signal observed by the FMCW transceiver in terms of the analytic signal of the DDS output, a result we use in subsequent sections to characterize the effect of digital phase errors on the FMCW transceiver's performance.

3.1.1 Bandlimited interpolation of discrete amplitude samples

In a complete direct digital synthesizer (DDS), a bandlimited analog output signal $s(t)$ is generated from a digital sample sequence $s[n]$. Ideally, $s(t)$ is the *bandlimited interpolant* of $s[n]$ given by the *Whittaker-Shannon interpolation formula*:

$$s(t) = \sum_{n=-\infty}^{\infty} s[n]\operatorname{sinc}\left(\frac{t - nT_{clk}}{T_{clk}}\right), \tag{2.1}$$

where T_{clk} is the DDS clock frequency[23]. The ideal DDS output (2.1) would be produced if the DDS's digital-to-analog converter (DAC) was an ideal impulse modulator and the low-pass filter was an ideal "brick-wall" low-pass filter with a cutoff frequency at the Nyquist frequency of the DDS, $f_{clk}/2$, where $f_{clk} = 1/T_{clk}$ is the DDS clock frequency.

In practice, neither an ideal impulse modulator nor an ideal low-pass filter is realizable. Instead, the digital output of the DDS is typically fed to a zero-order hold (ZOH) circuit which has a frequency response which 'droops' with frequency as $\mathrm{sinc}(f/f_{clk})$ as discussed in Section 2.3. However, this effect can partially be compensation by pre-distorting the DDS output with a so-called 'inverse sinc' filter (Analog Devices 2010), so that (2.1) still reasonably approximates the output from the complete DDS system.

Equation (2.1) can also be written as a convolution product:

$$s(t) = \bar{s}(t) * \frac{1}{T_{clk}} \mathrm{sinc}\left(\frac{t}{T_{clk}}\right), \tag{2.2}$$

where $\bar{s}(t)$ is modulated train of impulses

$$\bar{s}(t) = T_{clk} \sum_{n=-\infty}^{\infty} s[n]\delta(t - nT_{clk}). \tag{2.3}$$

The Fourier transform of $\bar{s}(t)$,

$$\bar{S}(f) = T_{clk} \sum_{n=-\infty}^{\infty} s[n] \exp(-j2\pi f T_{clk} n), \tag{2.4}$$

is, following Jenq (Jenq 1988), called the *digital spectrum* of the sequence $s[n]$. It can be shown (Cooley, Lewis et al. 1967) that if $s[n]$ represents the sampled values of a continuous-time function $s_c(t)$, i.e.,

$$s[n] = s_c(nT_{clk}), \tag{2.5}$$

then the digital spectrum $\bar{S}(f)$ of the sequence $s[n]$ is the *periodic repetition* of the analog spectrum $S_c(f)$ of $s_c(t)$:

$$\bar{S}(f) = \sum_{k=-\infty}^{\infty} S_c(f - kf_{clk}), \tag{2.6}$$

where $f_{clk} = 1/T_{clk}$ is the DDS clock frequency. The terms which are offset by $\pm f_{clk}$, $\pm 2f_{clk}$, ... are referred to as *aliases* of $S_c(f)$ (Oppenheim, Schafer et al. 1999).

The spectrum of the DDS output signal, $S(f)$, can be expressed in terms of the digital spectrum $\bar{S}(f)$ of its output sequence $s[n]$ by taking the Fourier transform of (2.2), which, by the convolution theorem, is given by

[23] End effects due to the starting and stopping of the DDS output sequence are neglected in this analysis.

$$S(f) = \bar{S}(f)\text{rect}\left(\frac{f}{f_{clk}}\right). \quad (2.7)$$

Thus, under the assumption that of an ideal low-pass interpolating filter, the spectrum of the DDS output signal is simply the digital spectrum of its digital sequence $s[n]$ confined to the *Nyquist interval* $(-f_{clk}/2, f_{clk}/2)$. Note that if the sequence $s[n]$ represents the sampled values of an $s_c(t)$ which is bandlimited within the Nyquist interval, then by (2.7), the DDS output perfectly reproduces the underlying signal: $s(t) = s_c(t)$.

3.1.2 Single sideband upconversion

As mentioned in chapter 2, due to limitations in the speed of their digital circuitry, direct digital synthesizers are not yet able to generate signals directly at radio frequency (RF), and some form of upconversion is required. In this thesis, we focus on one such way, namely *single-sideband* (SSB) upconversion by the *filter method*. A block diagram of this principle is shown in Figure 24.

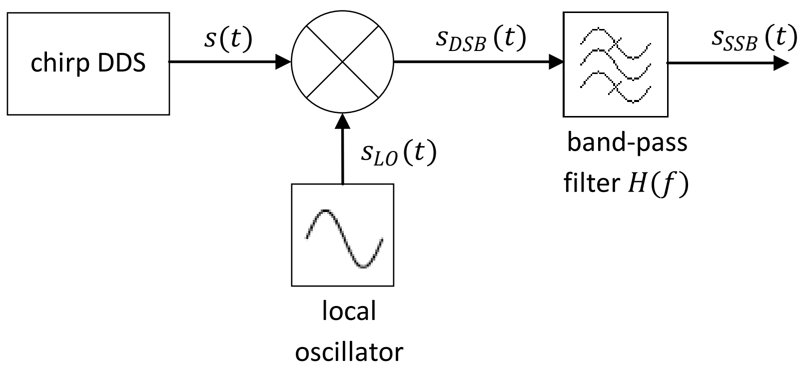

Figure 24 Single-sideband (SSB) modulation by the filter method. A direct digital chirp synthesizer (DDCS, or chirp DDS) generates a signal $s(t)$ at an intermediate frequency (IF) which is mixed with a local oscillator (LO) signal $s_{LO}(t)$ to yield a double-sideband (DSB) mixer output $s_{DSB}(t)$. One of the sidebands of $s_{DSB}(t)$ is filtered out by a band-pass filter with transfer function $H(f)$ to obtain a single-sideband (SSB) output $s_{SSB}(t)$.

The operation of SSB modulation in the frequency domain is illustrated in Figure 25. The baseband signal $s(t)$ generated by the chirp DDS is assumed to be band-limited with a cut-off frequency f_M. (In our case, $f_M \leq f_{clk}/2$, since the DDS is only used to generate frequencies up to its Nyquist frequency). Since $s(t)$ is a real signal, it has a symmetric amplitude spectrum $|S(f)|$ as shown in Figure 25(a).

The baseband signal $s(t)$ is mixed (multiplied) with a local oscillator signal $s_{LO}(t)$, which we represent, without loss of generality, as a cosine at the local oscillator frequency f_{LO}:

$$s_{LO}(t) = 2\cos(2\pi f_{LO} t). \quad (2.8)$$

The spectrum $S_{LO}(f)$ of $s_{LO}(t)$ consists of a pair of Dirac delta functions centered at $\pm f_{LO}$:

$$S_{LO}(f) = \delta(f + f_{LO}) + \delta(f - f_{LO}). \quad (2.9)$$

Multiplication of the baseband signal $s(t)$ and the local oscillator signal $s_{LO}(t)$ yields the double-sideband (DSB) signal[24]

$$s_{DSB}(t) = s(t)s_{LO}(t). \tag{2.10}$$

The spectrum $S_{DSB}(f)$ of $s_{DSB}(t)$ is obtained by convolving the baseband spectrum $S(f)$ with $S_{LO}(f)$ as given by (2.9) to yield

$$S_{DSB}(f) = S(f + f_{LO}) + S(f - f_{LO}). \tag{2.11}$$

Thus, if we assume that $f_M < f_{LO}$, then the spectrum of the double-sideband modulated signal consists of two replicas of the baseband signal spectrum centered at $\pm f_{LO}$ as depicted in Figure 25(c).

Next, the double-sideband amplitude-modulated signal $s_{DSB}(t)$ is filtered to select the desired sideband and eliminate the unwanted 'image' sideband as well as the carrier. Here we choose *upper* sideband modulation, which uses a band-pass filter which can ideally be represented as

$$H_u(f) = \begin{cases} 1, & \text{for } f_{LO} < |f| < f_{LO} + f_M, \\ 0, & \text{elsewhere.} \end{cases} \tag{2.12}$$

The transfer function of the upper-sideband bandpass filter $H_u(f)$ is illustrated in Figure 25(d).

After multiplying $S_{DSB}(f)$ by this transfer function, we obtain the SSB-modulated transmit signal

$$S_{SSB}(f) = \frac{1}{2}[S_a(f - f_{LO}) + S_a^*(-f - f_{LO})] \tag{2.13}$$

where $S_a(f)$ is the spectrum of the *pre-envelope* or *analytic signal* (Boashash 1992)given by:

$$S_a(f) = 2U(f)S(f), \tag{2.14}$$

with $U(f)$ the Heaviside step function. The spectrum of the single-sideband transmit signal, $S_{SSB}(f)$, is depicted in Figure 25(e).

[24] If the mixer employed is a *balanced* mixer, meaning that it suppresses the local oscillator (LO) frequency at its output, then the resulting signal is called *double sideband suppressed carrier* (DSB-SC). In practice, mixers employed are almost always (double-)balanced, so we have chosen to omit the "SC" suffix for brevity.

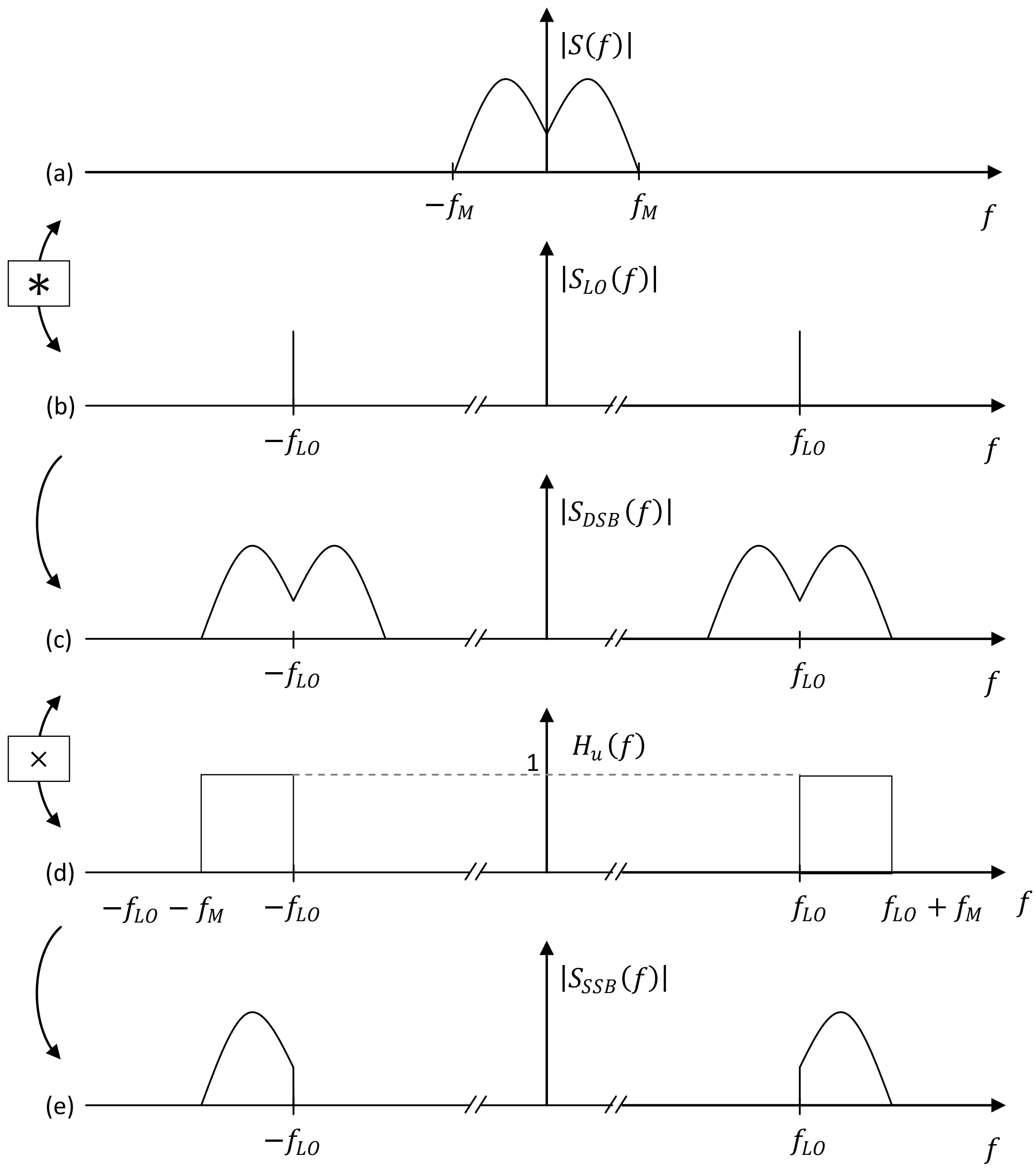

Figure 25 Single-sideband (SSB) modulation with transmission of the upper sideband by the filter method. From top to bottom are depicted the amplitude spectra of (a) the modulating signal $S(f)$ generated by the DDS; (b) the local oscillator signal $S_{LO}(f)$, which constitutes a pair of delta functions at $\pm f_{LO}$; (c) the double-sideband (DSB) signal spectrum $S_{DSB}(f)$ generated by convolving $S(f)$ and $S_{LO}(f)$; (d) the transfer function of the band-pass filter $H_u(f)$ used to transmit the upper sideband (USB) and reject the 'image' lower sideband and any out-of-band noise; (e) the final single-sideband modulated signal $S_{SSB}(f)$.

Taking the inverse Fourier transform of (2.13), the single sideband transmit signal $s_{SSB}(t)$ can be expressed in the time domain as

$$s_{SSB}(t) = \mathcal{R}e\{s_a(t)\exp(j2\pi f_{LO}t)\} \tag{2.15}$$

where $s_a(t)$ is the analytical signal of $s(t)$ defined through its Fourier transform (2.14), or equivalently, as

$$s_a(t) \equiv s(t) + j\hat{s}(t), \tag{2.16}$$

where $\hat{s}(t)$ is the *Hilbert transform* of $s(t)$, defined as the principal value of the convolution integral

$$\hat{s}(t) \equiv s(t) * \frac{1}{\pi t}. \tag{2.17}$$

In short, when single-sideband modulation is employed to up-convert an intermediate frequency (IF) signal $s(t)$, the up-converted signal $s_{SSB}(t)$ can be expressed as the real part of the analytic signal $s_a(t)$ of the IF signal $s(t)$ modulated by a complex exponential at the local oscillator frequency f_{LO}.

3.1.3 The analytic signal of an ideal linear chirp at intermediate frequency

In the previous sections, we showed that the single sideband transmit signal can be expressed in terms of the analytic signal $s_a(t)$ of the DDS output $s(t)$. Since $s(t)$ is bandlimited to the Nyquist interval $(-f_{clk}/2, f_{clk}/2)$ and its analytic signal contains only its positive frequencies, it follows that $s_a(t)$ is bandlimited to the interval $(0, f_{clk}/2)$.

Now, consider the ideal case in which the DDS sequence $s[n]$ represents sampled values of a continuous-time function $s_c(t)$ which is an ideal FMCW signal, that is, a periodic repetition of chirps. This periodic signal can be expressed in terms of its Fourier *series*, the coefficients of which are (apart from a factor $1/T$, where T is the sweep period) equal to the sampled values of the Fourier *transform* of a single sweep of the FMCW signal (Oppenheim, Schafer et al. 1999). However, since a single sweep of the FMCW signal is time-limited, it *cannot* simultaneously be bandlimited (Slepian 1983). Therefore, transmit signal $s_{SSB}(t)$ from our model system given by (2.15) *cannot* represent the ideal FMCW transmit signal.

Physically, $s_{SSB}(t)$ is affected by truncation of the of 'skirts' in the spectrum of the ideal chirp, as well as spectral interference with the skirts of the aliases of the desired upper sideband and those of (the aliases of) its image, the lower sideband. In this section, however, we show that if the underlying continuous-time signal $s_c(t)$ is a chirp with a large *time-bandwidth product*,

$$BT \gg 1, \tag{2.18}$$

then it can be considered as approximately bandlimited to its 'nominal' bandwidth – that is, its instantaneous frequency excursion B during its sweep period T. Consequently, if $s_c(t)$ is chosen such that its 'nominal' frequency support lies within the support $(0, f_{clk}/2)$ of $s_a(t)$, then the effect of the 'skirts' of aliases and images is negligible provided that (2.18) holds. It is also shown that in this case, the analytic signal $s_a(t)$ is approximately obtained simply by replacing the sine or cosine in the expression for $s_c(t)$ by a complex exponential.

We proceed to show the results stated above. Suppose that the underlying continuous-time signal $s_c(t)$ is an ideal chirp:

$$s_c(t) = \mathrm{rect}\left(\frac{t}{T}\right) \cos\left[2\pi\left(f_{c,IF}t + \frac{1}{2}\alpha t^2\right)\right], \tag{2.19}$$

where T is the sweep period, $f_{c,IF}$ the center frequency of the IF signal, and α the sweep rate. (2.19) can, in turn, be expressed in terms of complex exponentials using Euler's formula:

$$s_c(t) = \mathcal{R}e\{\tilde{x}(t)\}, \tag{2.20}$$

where

$$\tilde{x}(t) \equiv \mathrm{rect}\left(\frac{t}{T}\right) \exp\left[j2\pi\left(f_{c,IF}t + \frac{1}{2}\alpha t^2\right)\right]. \tag{2.21}$$

is the “real plus imaginary quadrature” (RQ) (Boashash 1992) version of $s_c(t)$, which is obtained by replacing the cosine in (2.19) by a complex exponential. As shown by Nuttall (Nuttall and Bedrosian 1966), the RQ signal (2.21) is equal to the analytic signal $s_{c,a}(t)$ of $s_c(t)$ if both are *spectrally one-sided*, that is, contain only positive frequencies. Below, we show that if $f_{c,IF} > B/2$, then this is asymptotically the case in the limit that BT tends to infinity.

Taking the Fourier transform of (2.21) yields

$$\tilde{X}(f) = \int_{-T/2}^{T/2} \exp\left[j\pi\left(\alpha t^2 - 2\left(f - f_{c,IF}\right)t\right)\right] dt$$

which, upon “completing the square” in the argument of the complex exponential, can be written as

$$\tilde{X}(f) = \exp\left[-j\frac{\pi}{\alpha}\left(f - f_{c,IF}\right)^2\right] \int_{-T/2}^{T/2} \exp\left[j\pi\alpha\left(t - \frac{f - f_{c,IF}}{\alpha}\right)^2\right] dt. \tag{2.22}$$

Performing the substitution $u = \sqrt{2\alpha}\left(t - \left(f - f_{c,IF}\right)/\alpha\right)$, we find

$$\tilde{X}(f) = \frac{1}{\sqrt{2\alpha}} \exp\left[-j\frac{\pi}{\alpha}\left(f - f_{c,IF}\right)^2\right] \int_{\sqrt{2\alpha}\left(-\frac{T}{2} - \frac{f - f_{c,IF}}{\alpha}\right)}^{\sqrt{2\alpha}\left(\frac{T}{2} - \frac{f - f_{c,IF}}{\alpha}\right)} \exp\left(j\frac{\pi}{2}u^2\right) du.$$

Defining the *complex Fresnel integral*

$$Z(x) \equiv \int_0^x \exp\left(j\frac{\pi}{2}u^2\right) du \tag{2.23}$$

and using the property $Z(-x) = -Z(x)$, we finally obtain

$$\tilde{X}(f) = \frac{1}{\sqrt{2\alpha}} \exp\left[-j\frac{\pi}{\alpha}\left(f - f_{c,IF}\right)^2\right] \left\{ Z\left[\sqrt{\frac{2}{\alpha}}\left(f - f_{c,IF} + \frac{B}{2}\right)\right] - Z\left[\sqrt{\frac{2}{\alpha}}\left(f - f_{c,IF} - \frac{B}{2}\right)\right] \right\}, \tag{2.24}$$

where $B = \alpha T$ is the chirp bandwidth. Defining the dimensionless variables[25]

$$D \equiv \alpha T^2 = BT, \qquad v \equiv \frac{f - f_{c,IF}}{B}, \qquad \tilde{\mathcal{X}} = \tilde{X}\sqrt{\alpha},$$

(2.24) can be expressed in dimensionless form as follows:

$$\tilde{\mathcal{X}}(v) = \frac{1}{\sqrt{2}} \exp(-j\pi D v^2) \left\{ Z\left[\sqrt{2D}\left(v + \frac{1}{2}\right)\right] - Z\left[\sqrt{2D}\left(v - \frac{1}{2}\right)\right] \right\}. \tag{2.25}$$

[25] Incidentally, the time-bandwidth product D has historically been called the “dispersion factor” in relation to conventional pulse compression radars in which chirps were generated passively (Klauder 1960).

The spectral amplitude of this function is plotted below in Figure 26 for values of the time-bandwidth product BT increasing from 10 to 100. The complex Fresnel integrals $Z(\cdot)$ were evaluated numerically to a tolerance of 10^{-10} using a Matlab function contributed by Volegov (Volegov 2004) based on the algorithm of Mielenz (Mielenz 2000).

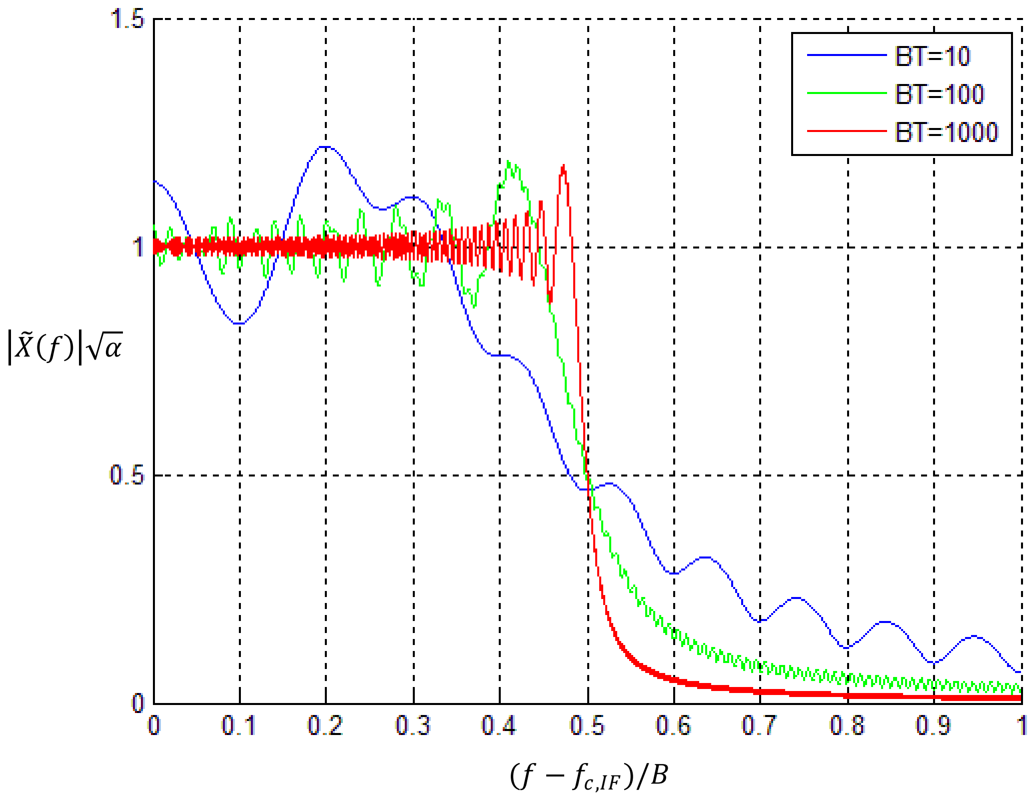

Figure 26 Spectral amplitude of rectangular chirps with time-bandwidth products BT = 10, 100, and 1000. The plot is symmetric about $(f - f_{c,IF})/B = 0$, therefore only its right half is shown. (After (Klauder 1960)).

As seen from Figure 26, for increasing values BT, the amplitude spectrum becomes more 'step-like' at the edge of its nominal bandwidth B. In fact, it can be shown that this is actually the case in the limit that α tends to infinity. To this end, we write (2.22) as

$$\tilde{X}(f) = \exp\left[-j\frac{\pi}{\alpha}\left(f - f_{c,IF}\right)^2\right]\int_{-\infty}^{\infty} \mathrm{rect}\left(\frac{t}{T}\right)\exp\left[\pi\alpha\left(t - \frac{f - f_{c,IF}}{\alpha}\right)^2\right]dt. \tag{2.26}$$

The integral in (2.26) is seen to have the form of the convolution product, evaluated at $\left(f - f_{c,IF}\right)/\alpha$, of the function $\mathrm{rect}(t/T)$ with the function $\exp(j\pi\alpha t^2)$. The normalized version of the latter function,

$$q_\alpha(t) \equiv \sqrt{-j\alpha}\,\exp(j\pi\alpha t^2), \tag{2.27}$$

is the impulse response function of a so-called a *quadratic phase filter*, which has applications in areas such as pulse compression and real-time spectrum analysis, fiber-cable communications and dispersion, and Fresnel diffraction and optical filtering (Papoulis 1994). Convolution with the quadratic phase filter (2.27) has even been given a special name: the *Fresnel transform* (Gori 1994). The real and imaginary parts of $q_\alpha(t)$ are plotted in Figure 27.

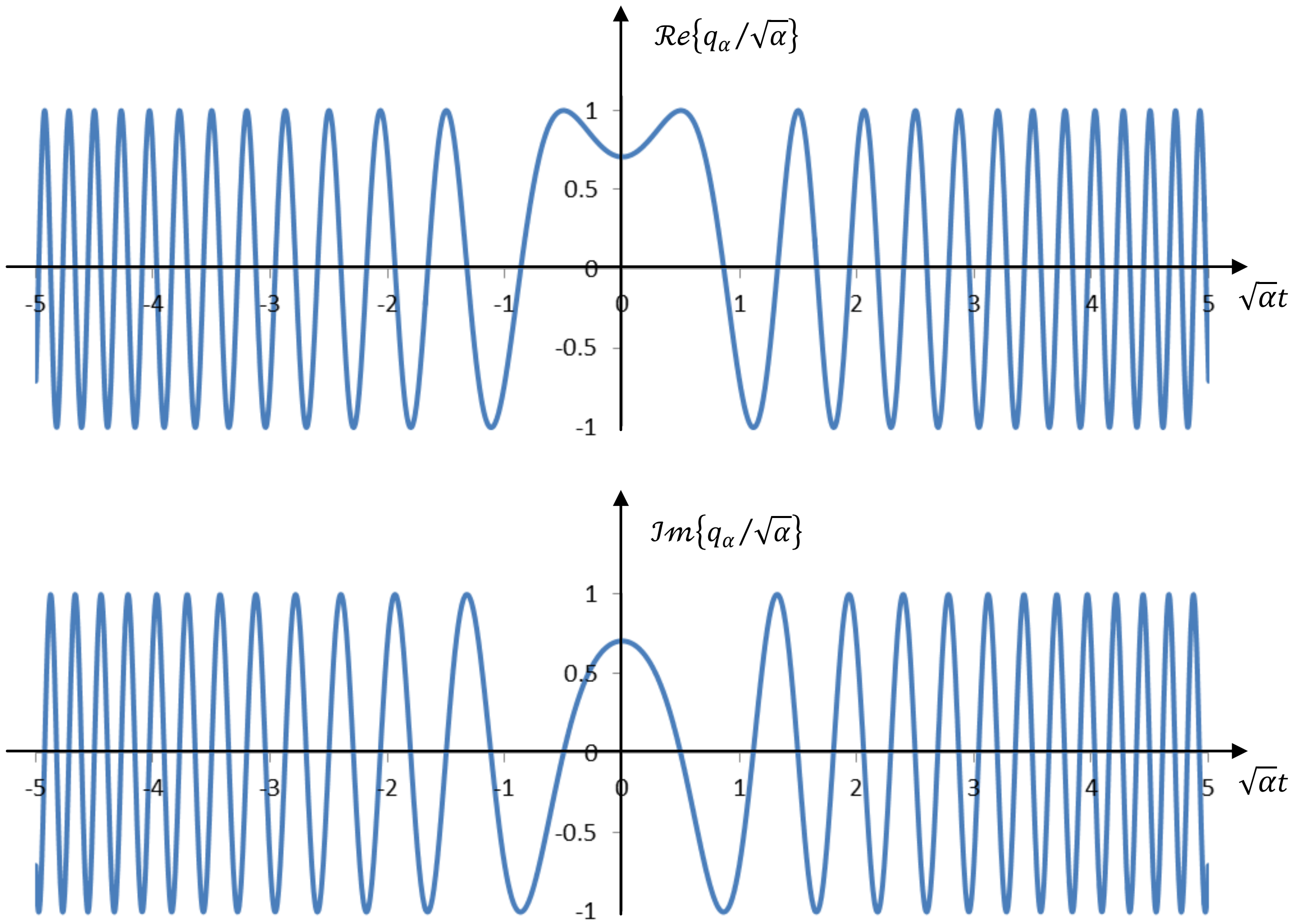

Figure 27 Real (top) and imaginary (bottom) parts of the normalized quadratic phase filter impulse response function, $q_\alpha/\sqrt{\alpha}$, against normalized time, $\sqrt{\alpha}t$.

Here, we will apply results pertaining to the asymptotics of the Fresnel transform. In particular, it can be shown that

$$\lim_{\alpha\to\infty} q_\alpha(t) = \delta(t). \tag{2.28}$$

In other words, in the limit that the chirp rate α tends to infinity, the quadratic phase filter approaches the Dirac delta function. This can also be seen from Figure 27: for values of the dimensionless time $\sqrt{\alpha}t$ much greater than 1, q_α oscillates increasingly rapidly, which leads to cancellation and a diminishing contribution to the integral of q_α times another, more slowly varying function.

Applying the identity (2.28) to the convolution integral (2.26), we find:

$$\lim_{\alpha\to\infty} \tilde{X}(f) = \sqrt{\frac{j}{\alpha}}\operatorname{rect}\left(\frac{f - f_{c,IF}}{\alpha T}\right)\exp\left[-j\frac{\pi}{\alpha}\left(f - f_{c,IF}\right)^2\right]. \tag{2.29}$$

The right-hand side of (2.29) is called the *stationary phase approximation* (Boashash 1992) of the spectrum of a rectangular chirp, and is valid for large time-bandwidth products, $BT \gg 1$. Note that (2.29) *must* be an approximation of the exact spectrum $\tilde{X}(f)$ because it is bandlimited with bandwidth B, whereas $\tilde{x}(t)$ is time-limited with duration T, and as mentioned before, a function cannot be simultaneously bandlimited and time-limited unless it is the trivial always-zero function (Slepian 1983).

In order to give a measure of the 'convergence' of $\tilde{X}(f)$ to its stationary phase approximation, we have determined the fraction of the chirp's power outside frequency intervals $f \in f_{c,IF} + B[-1/2 - b, 1/2 + b]$, where b is a parameter describing the extent by which the integration interval exceeds the nominal bandwidth of the chirp. By Parseval's theorem, this fraction δ can be shown to be equal to

$$\delta = 1 - \int_{-\frac{1}{2}-b}^{\frac{1}{2}+b} \left|\tilde{\mathcal{X}}(v)\right|^2 dv. \tag{2.30}$$

The integrals were evaluated numerically by Gaussian quadrature with a tolerance of 10^{-10} (–200 dB), using a Matlab function contributed by Fig (Fig 2005).

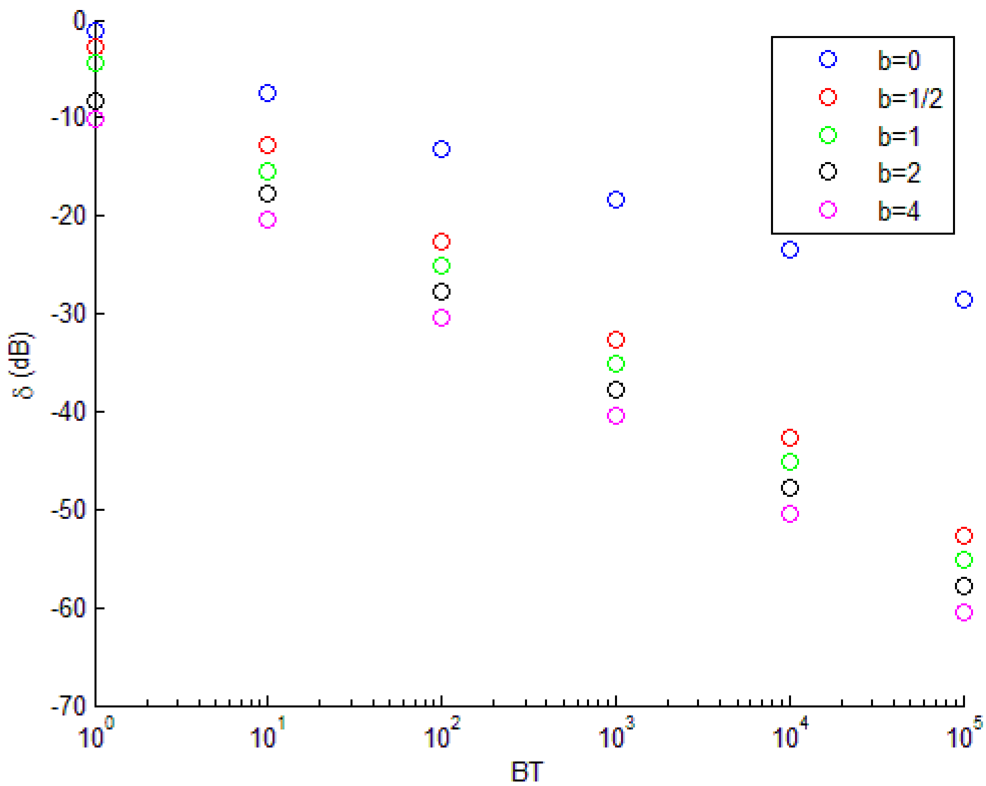

Figure 28 Power outside the nominal bandwidth of a chirp as a function of time-bandwidth product (BT). The parameter b represents, as a ratio of the chirp bandwidth B, the extent by which the integration interval exceeds the nominal bandwidth of the chirp.

As seen from Figure 28, the fraction of power outside the 'nominal' bandwidth $[f_{c,IF} - B/2, f_{c,IF} + B/2]$ of the chirp (this corresponds to the the case $b = 0$) decreases with the time-bandwidth product as $\sim 1/\sqrt{BT}$. If the integration interval does not contain the edge of the 'nominal' bandwidth, however, the power outside the interval decreases faster, as $\sim 1/BT$, as seen in Figure 28 for b = ½, 1, 2, and 4. For a sweep of bandwidth 50 MHz and duration 400 µs, the time-bandwidth product is 20,000, in which case only about 0.3% of the power is outside the nominal signal bandwidth.

The preceding results show that within the stationary phase approximation, a chirp is bandlimited to its ‘nominal’ frequency support. We maintain that as a result, if the ‘nominal’ support of the continuous-time signal $s_c(t)$ given by (2.19) lies within the interval $(0, f_{clk}/2)$, i.e.,

$$0 < f_{c,IF} - \frac{B}{2} \quad \text{and} \quad f_{c,IF} + \frac{B}{2} < \frac{f_{clk}}{2}, \tag{2.31}$$

then, provided the time-bandwidth product of the chirp is large, the analytical signal $s_a(t)$ of the DDS output $s(t)$ approaches the “real plus imaginary quadrature” signal $\tilde{x}(t)$ defined by (2.21), that is,

$$s_a(t) \approx \tilde{x}(t), \qquad BT \gg 1. \tag{2.32}$$

The approximation (2.32) is the result of combining two approximations. Firstly, because $s_c(t)$ is approximately bandlimited to the Nyquist interval $(-f_{clk}/2, f_{clk}/2)$, its digital spectrum $\bar{S}(f)$ is approximately equal to the analog spectrum $S_c(f)$ on that interval, so that, after low-pass filtering in accordance with (2.7),

$$s(t) \approx s_c(t), \qquad BT \gg 1, \tag{2.33}$$

where $s(t)$ is the DDS output given by (2.1). Secondly, because “real plus imaginary quadrature” signal $\tilde{x}(t)$ of $s_c(t)$ is, within the stationary phase approximation, spectrally one-sided (since $f_{c,IF} > B/2$), it approximates the analytic signal $s_{c,a}(t)$ of $s_c(t)$, i.e.,

$$s_{c,a}(t) \approx \tilde{x}(t), \qquad BT \gg 1. \tag{2.34}$$

Combining the analytic part of (2.33) with (2.34) leads to our stated result (2.32).

The combined results of the Sections 3.1.1, 3.1.2, and 3.1.3 show that if a DDS generates a chirp at intermediate frequency from samples of an *ideal* linear chirp, then the final single-sideband transmit signal is, within the stationary phase approximation, also an ideal chirp:

$$s_{SSB}(t) \approx \mathrm{rect}\left(\frac{t}{T}\right) \cos\left[2\pi\left(f_c t + \frac{1}{2}\alpha t^2\right)\right], \qquad BT \gg 1, \tag{2.35}$$

where $f_c = f_{c,IF} + f_{LO}$ is the final center frequency of the transmitted chirp.

3.1.4 The beat signal in terms of the analytic signal

The signal $s_{SSB}(t)$ is transmitted through the FMCW radar’s antenna and in accordance with the point-target model, a delayed version $s_{SSB}(t-\tau)$ is received. In this chapter, we assume that the target is *stationary* with respect to the radar, so that $\tau = 2R/c$, where R is the constant range of the target. Our focus here is thus on the effects of the DDS spurious signals on the *range processing* in the FMCW receiver; their effect on *Doppler processing* is discussed in Chapter 4.

In the FMCW receiver, the transmitted and received signals, $s_{SSB}(t)$ and $s_{SSB}(t-\tau)$ respectively, are mixed (multiplied) as explained in Section 2.2. We consider the case that $s_{SSB}(t)$ is given by its general representation (2.15) in terms of the analytic signal of the DDS output, $s_a(t)$. In this case, the output of an ideal mixer is

$$\tilde{s}_b(t) = \mathcal{R}e\{s_a(t)\exp(j2\pi f_{LO}t)\} \cdot \mathcal{R}e\{s_a(t-\tau)\exp\big(j2\pi f_{LO}(t-\tau)\big)\}. \tag{2.36}$$

However, as explained in Section 2.2, the sum-frequency terms in the expansion of (2.36) are oscillations at over twice the local oscillator frequency f_{LO}, and thus usually beyond the bandwidth of the mixer or otherwise easily filtered out. (Note that this situation is in contrast to the up-conversion configuration of a mixer discussed in Section 3.1.2, in which the desired sideband and its image are spaced much closer together at a high carrier frequency, making them difficult to separate by filtering). What remains are the difference-frequency terms, so that the actual beat signal at the mixer output can be expressed as (neglecting a factor $1/2$, as we are not concerned with amplitude variations in this derivation):

$$s_b(t) = \mathcal{R}e\{s_a(t)s_a^*(t-\tau)\exp(j2\pi f_{LO}\tau)\}. \tag{2.37}$$

Thus, the beat signal can – apart from a constant phase term $2\pi f_{LO}\tau$ – be expressed entirely in terms of the analytical signal $s_a(t)$ corresponding to the DDS output signal $s(t)$.

It follows that if the DDS chirp is generated from samples of the ideal chirp (2.19), then within approximation (2.32),

$$\begin{aligned} s_b(t) &\approx \mathcal{R}e\{\tilde{x}(t)\tilde{x}^*(t-\tau)\exp(j2\pi f_{LO}\tau)\} \\ &= \cos\left[2\pi\left(f_c\tau - \frac{1}{2}\alpha\tau^2 + \alpha\tau t\right)\right], \qquad -\frac{T}{2}+\tau < t < \frac{T}{2} \end{aligned} \tag{2.38}$$

for $BT \gg 1$. In other words, ideal samples lead to an ideal beat signal within the stationary phase approximation.

To summarize Section 3.1, we have constructed a mathematical model of a FMCW transceiver which employs a direct digital chirp synthesizer with single-sideband upconversion by the filtering method. We have shown that if the sampled values of an ideal chirp are used for the generation of the DDS output signal, then within the stationary phase approximation, the output signal from the transmitter and the resulting beat signal are also ideal. In the remainder of this chapter, we investigate what changes if the DDS samples are *not* ideal.

3.2 Model of the phase errors in the digital samples generated by a DDS

From an engineering perspective, the staircase approximation and phase truncation are simply adaptations made to accommodate for limitations in the speed of the digital circuitry of a DDCS. If we wish to describe the effect of these adaptations mathematically, however, it is desirable to capture these effects succinctly in a mathematical model. In this section, we posit such a model. (Our model is justified in Section 3.4, where we investigate the detailed operation of a DDCS).

In Figure 29 we compare a block diagram of a 'real' DDCS with its posited mathematical model. In the 'real' DDCS (Figure 29(a)), there are three sources of error in the digital domain:

1) In the DDCS the frequency accumulator is clocked at a frequency that is lower than the system clock frequency f_{clk} by a sub-multiple K. (For example, the Analog Devices AD9858 DDS has $K = 8$, and the AD9910 has $K = 4$). This results in a 'staircase' or 'stepped CW' approximation of ideal time-frequency characteristic of a linear chirp.
2) The frequency and phase accumulators are quantized to a large number of bits L in order to give them fine chirp rate and frequency resolutions, respectively. However, to use all of

these L bits to address the look-up table for phase-to-amplitude conversion would require a prohibitive amount of high-speed memory. For this reason, the output of the phase accumulator is truncated from L to W bits prior to addressing the sine ROM. (The AD9858 and AD9910 both have $L = 32$, but $W = 15$ for the AD9858 whereas $W = 19$ for the AD9910).

3) The digital-to-analog converter (DAC) used in the DDCS has a finite precision of S bits. Therefore, the amplitude of the digital output samples is also quantized to S bits.

As shown in Section 3.4, the first two of these distortions have the combined effect of perturbing the 'ideal' phase register value by an 'effective' periodic phase error $\epsilon_P[n]$. This is shown schematically in Figure 29(b).

The third source of error, amplitude quantization, is neglected in this analysis, as was done by Mehrgardt (Mehrgardt 1983) and Nicholas and Samueli (Nicholas and Samueli 1987) in their analyses of the effect of phase truncation errors on direct digital *frequency* synthesizers. An empirical noise model for the effects of amplitude quantization, which assumes that the quantization error is uniformly distributed over ±0.5 bits, was proposed by Stove (Stove 2004) and reported to accurately describe its practical effects. Here, however, we are interested in the worst-case spurious given by amplitude quantization, a value for which is given in Section 3.5. For the moment, we assume the phase-to-amplitude mapping is ideal, as represented in Figure 29(b) by an 'infinite' number of bits.

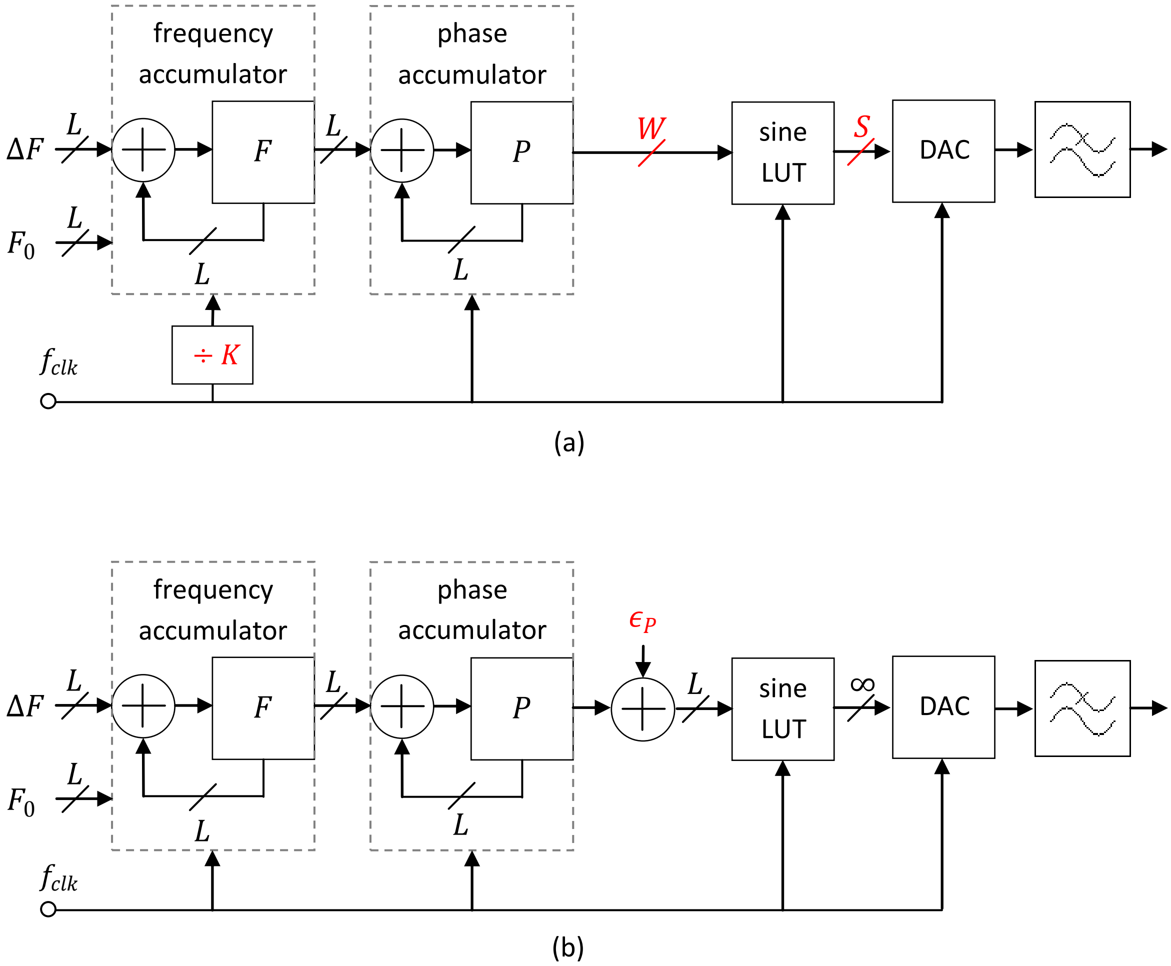

f_{clk}	=	system clock frequency (Hz)
ΔF	=	frequency increment word
F_0	=	initial frequency tuning word
L	=	number of bits of the frequency and phase accumulators
F	=	frequency register value
P	=	phase register value
ϵ_P	=	effective digital phase error
K	=	frequency accumulator clock division ratio
W	=	number of bits used to address the sine look-up table (LUT)
S	=	number of bits of the digital-to-analog converter (DAC)

Figure 29 Block diagram of (a) a 'real' DDCS and (b) its mathematical model. Sources of error are highlighted red. In the model the sources of digital phase errors, the 'staircase' approximation and phase truncation, are replaced by an effective phase error ϵ_P.

Mathematically, we model the DDS output sequence as

$$s[n] = \cos\left(\frac{2\pi}{2^L}P[n]\right), \tag{2.39}$$

where $P[n] \in \mathbb{Z}_{2^L}$ is the phase register value which can be written as

$$P[n] = \tilde{P}[n] - \epsilon_P[n] \tag{2.40}$$

where $\tilde{P}[n]$ represents the sampled values of the digital phase of an ideal linear chirp and $\epsilon_P[n]$ is a phase error term. (Both $\tilde{P}$ and ϵ_P are not necessarily integer-valued). It is for the moment assumed (and shown in Section 3.4) that $\epsilon_P[n]$ is periodic with some period M, i.e.,

$$\epsilon_P[n+M] = \epsilon_P[n], \qquad \forall n. \tag{2.41}$$

Equations (2.39)-(2.41) are expressed in units of phase accumulator bits.

In short, we have posited a model of the digital phase errors in a direct digital chirp synthesizer, by which the output phase sequence can be expressed as the ideal output perturbed by a *periodic* phase error sequence. In the following section, we investigate the ramifications of this phase error model on the FMCW transceiver described in Section 3.1.

3.3 The effect of periodic digital phase errors on the FMCW transceiver

In this section, we analyze how the periodic digital phase error model posited in Section 3.2 affects the performance of our model FMCW transceiver described in Section 3.1. Firstly, in Section 3.3.1, we establish a "real plus imaginary quadrature" complex representation $x[n]$ of the DDS samples $s[n]$. In Section 3.3.2, we show that the digital spectrum $X(f)$ of $x[n]$ can be expressed as a "main" signal proportional to the desired spectrum $\tilde{X}(f)$, plus a series of "replicas" shifted in frequency by $1/MT_{clk}$, where M is the periodicity of the phase errors, and weighted in amplitude by the discrete Fourier transform (DFT) of the complex exponential of the phase error sequence.

3.3.1 Complex representation of the DDS output samples

Similarly to Sections 3.1.1 and 3.1.2, we express the DDS output sequence as the real part of a complex exponential sequence:

$$s[n] = \mathcal{R}e\{x[n]\}, \tag{2.42}$$

where, by comparison with our DDS model (2.39) and (2.40),

$$x[n] \equiv \exp\left(j\frac{2\pi}{2^L}\left(\tilde{P}[n] - \epsilon_P[n]\right)\right). \tag{2.43}$$

Now, since $(2\pi/2^L)\tilde{P}[n]$ are by assumption samples of the phase of an ideal linear chirp, (2.43) can be expressed as

$$x[n] = \tilde{x}(nT_{clk})\exp(-j\theta_n), \tag{2.44}$$

where $\tilde{x}(t)$ is the "real plus imaginary quadrature" representation of an ideal chirp given by (2.21), and θ_n is the phase error sequence in radians:

$$\theta_n \equiv \frac{2\pi}{2^L}\epsilon_P[n]. \tag{2.45}$$

Of course, the periodicity assumption (2.41) of $\epsilon_P[n]$ also carries over to θ_n, i.e.,

$$\theta_{n+M} = \theta_n, \qquad \forall n. \tag{2.46}$$

Taking the “digital Fourier transform”[26] of (2.42), the digital spectrum $\bar{S}(f)$ of the DDS sample sequence $s[n]$ is given by

$$\bar{S}(f) = \frac{1}{2}[X(f) + X^*(-f)], \tag{2.47}$$

where $X(f)$ denotes the digital spectrum of the complex exponential sequence $x[n]$:

$$X(f) = T_{clk} \sum_{n=-\infty}^{\infty} x[n] e^{-j2\pi f n T_{clk}}. \tag{2.48}$$

In the following section, we show that using the assumption of periodicity of the phase errors, Eq. (2.46), the digital spectrum can be expressed as a “main” signal which is proportional to the ideal chirp spectrum $\tilde{X}(f)$ given by (2.24) (or, within the stationary phase approximation, (2.29)), plus a series of frequency-shifted “replicas”. These “replicas” are then shown to produce spurious or “ghost” targets in the spectrum of the beat signal.

3.3.2 The digital spectrum of a signal perturbed by periodic phase errors

The subject of this section is to express the digital spectrum of a sequence which can be expressed as an ‘ideal’ sequence perturbed by some periodic phase error, in terms of the digital spectrum of the ‘ideal’ sequence. Our discussion follows, whose derivation in turn is based on Jenq. Successively, we – following Salis (Riera Salis 1994) and Jenq (Jenq 1988) – derive our main result (Section 3.3.2.1), discuss its significance and properties (Section 3.3.2.2), and confirm it by a simulation (Section 3.3.2.3).

3.3.2.1 Derivation

Let $\tilde{x}(t)$ be an analog signal with its Fourier transform $\tilde{X}(f)$. The signal $\tilde{x}(t)$ is sampled in such a way that each sample has a phase error θ_n:

$$x[n] = \tilde{x}(nT_{clk}) e^{-j\theta_n}. \tag{2.49}$$

The phase error is assumed to be periodic with period M, so that it is characterized by the finite sequence

$$\theta_0, \theta_1, \ldots, \theta_{M-1}.$$

The sampled data sequence is then treated as if it were obtained by sampling another function $x(t)$ at a rate $1/T_{clk}$. We are interested in finding the representation of the digital spectrum of $x(t)$, $X(f)$, in terms of the Fourier transform, $\tilde{X}(f)$, of $\tilde{x}(t)$.

The basic principle used to derive the representation of a digital spectrum is to decompose the original sampled data sequence $x[n]$ into M subsequences, each affected by a value of θ_m. The general expression for the mth subsequence is

$$x_m = \left[\ \tilde{x}(mT_{clk}) e^{-j\theta_m},\ \ \tilde{x}\big((m+M)T_{clk}\big) e^{-j\theta_m},\ \ \tilde{x}\big((m+2M)T_{clk}\big) e^{-j\theta_m},\ \ \ldots\ \right] \tag{2.50}$$

[26] Apart from a normalizing factor T_{clk}, our “digital Fourier transform” is simply the discrete-time Fourier transform (DTFT) with the dimensionless angular frequency ω replaced by its dimensional counterpart $2\pi f T_{clk}$ (cf. (Oppenheim, Schafer et al. 1999)).

The individual spectrum of each sequence is easily calculated, as it is the result of sampling the analog signal $\tilde{x}(t + mT_{clk})$ every MT_{clk} seconds and multiplying the result by a constant $e^{-j\theta_m}$. The result is:

$$X_m(f) = \frac{1}{M} e^{-j\theta_m} \sum_{k=-\infty}^{\infty} X^a\left(f - \frac{k}{MT_{clk}}\right) e^{j2\pi\left(f - \frac{k}{MT_{clk}}\right)mT_{clk}}. \quad (2.51)$$

The sequence $X(f)$ is obtained by summing the subsequences $X_m(f)$ delayed by mT_{clk} seconds, so that they add coherently:

$$X(f) = \sum_{m=0}^{M-1} X_m(f) e^{-j2\pi fmT_{clk}}. \quad (2.52)$$

Inserting (2.51) into (2.52) and interchanging the order of summation, we obtain

$$X(f) = \sum_{k=-\infty}^{\infty} A(k)\tilde{X}\left(f - \frac{k}{MT_{clk}}\right), \quad (2.53)$$

where $A(k)$ is given by

$$A(k) = \frac{1}{M} \sum_{m=0}^{M-1} e^{-j\theta_m} e^{-j\frac{2\pi km}{M}}. \quad (2.54)$$

3.3.2.2 Properties

Let us now explore some important properties of the digital spectrum of the periodically phase-perturbed signal. From (2.54), it is seen that the weight coefficients $A(k)$ are the result of applying the discrete Fourier transform (DFT) to the sequence $\exp(-j\theta_m)$. Consequently, $A(k)$ is periodic in k with period M, hence the digital spectrum (2.53) is periodic in f with period $1/T_{clk} = f_{clk}$ as expected. The term in (2.53) with coefficient $A(0)$ corresponds to the desired signal $\tilde{X}(f)$, which we refer to as the 'main' signal or 'signal' for short, while the coefficients $A(k)$, $k = 1, \dots, M-1$ correspond to 'replicas' of the desired signal offset in frequency by k/MT_{clk}, respectively.

Further, in the original baseband, $(-1/2T_{clk}, 1/2T_{clk})$, there are M components centered within the interval, plus contributions of neighboring components. As the separation between components can be very small (M can be large), contiguous ones are likely to overlap. The main component is located at the center frequency $f_{c,IF}$ of the desired signal with magnitude $|A(0)|$, while the kth component is located at $f_{c,IF} + (k/M)f_s$ with magnitude $|A(k)|$.

Since $\exp(-j\theta_m)$ is not a real-valued sequence, we do not have $A(k) = A^*(-k)$. However, for small phase errors, $\theta_m \ll 1$, we have

$$e^{-j\theta_m} \approx 1 - j\theta_m. \quad (2.55)$$

The real component of the sequence $\exp(-j\theta_m)$ is thus seen to be much greater than its imaginary component, whence we still have

$$|A(k)| \approx |A(-k)| \quad (2.56)$$

as noted by Jenq (Jenq 1988).

Next, we derive an upper bound for the amplitude of the amplitudes $|A(k)|$, $k = 1, \dots, M-1$ of the "replicas" of the transmitted signal. Firstly, inserting (2.55) into (2.54) yields

$$A(k) \approx \frac{1}{M} \sum_{m=0}^{M-1} (1 - j\theta_m) e^{-j\frac{2\pi km}{M}}. \tag{2.57}$$

For $k = 1, \dots, M-1$, the contributions from first term in the summand of (2.57) sum to zero, so that

$$A(k) \approx -\frac{j}{M} \sum_{m=0}^{M-1} \theta_m e^{-j\frac{2\pi km}{M}}, \qquad k = 1, \dots, M-1. \tag{2.58}$$

From (2.58), it follows that $|A(k)|$ satisfies the upper bound

$$\begin{aligned} |A(k)| &\approx \frac{1}{M} \left| \sum_{m=0}^{M-1} \theta_m \right| \\ &\leq \frac{1}{M} \sum_{m=0}^{M-1} |\theta_m| \\ &\leq \theta_{max}, \end{aligned} \tag{2.59}$$

where $\theta_{max} \equiv \max_m |\theta_m|$. Therefore, within the small-angle approximation, the amplitude of the "replicas" is bounded by the maximum phase error.

Finally, since $|\exp(-j\theta_m)| = 1$, Parseval's theorem applied to (2.54) yields

$$\sum_{k=0}^{M-1} |A(k)|^2 = 1. \tag{2.60}$$

These properties will prove useful in deriving an upper bound for the effects of digital phase errors on the beat signal.

3.3.2.3 Simulation

We have visualized these properties of the digital spectrum $X(f)$ of "real plus imaginary quadrature" DDS output through a simulation. The clock frequency f_{clk} was chosen at 1 GHz, equal to the clock frequency of commercial DDSs such as the AD9858 and AD9910. Samples $\tilde{x}(nT_{clk})$ of an ideal chirp with period T = 500 µs, bandwidth B = 50 MHz, and intermediate center frequency $f_{c,IF}$ = 75 MHz were perturbed by an error sequence constituting repetitions of the base sequence

$$\theta_m = [0, \ 0.01, \ 0.02, \ 0.03, \ 0.04, \ 0.05, \ 0.06, \ 0.07].$$

The resulting normalized digital power spectrum, $|X(f)|^2/\alpha$, was evaluated at 16,384 points on the Nyquist interval $(-500 \text{ MHz}, 500 \text{ MHz})$ of the DDS using a 16,384-point FFT, and is shown in Figure 30.

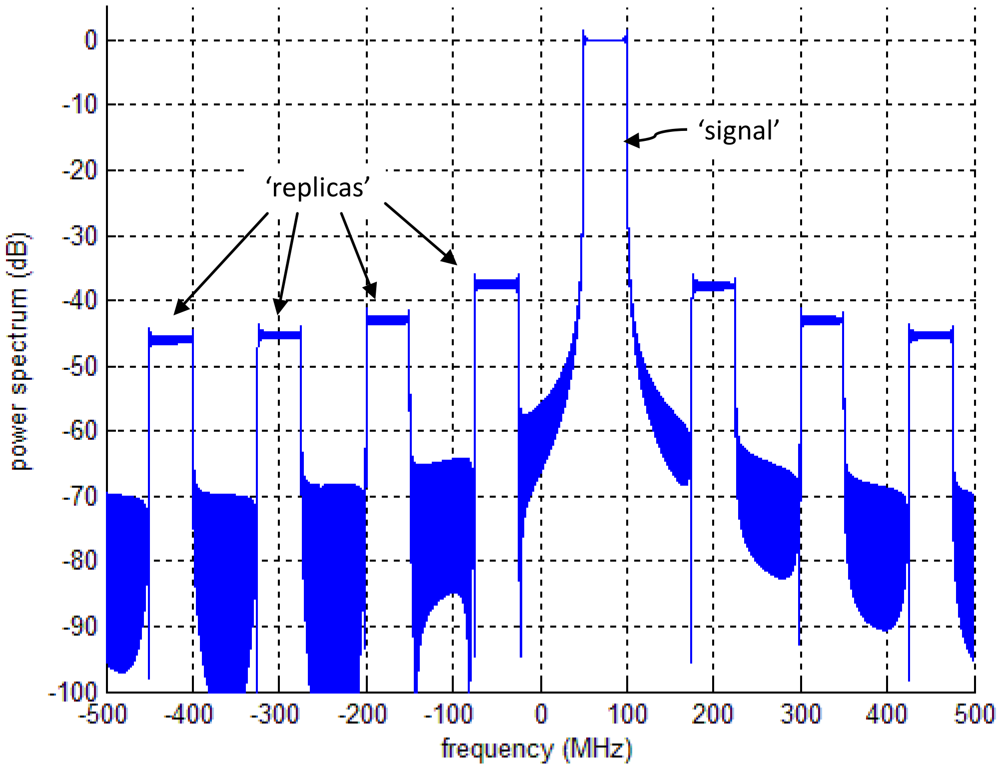

Figure 30 Power spectrum of the normalized digital spectrum $X(f)/\sqrt{\alpha}$ of the sequence $x[n] = \tilde{x}(nT_{clk})e^{-j\theta_n}$, where $\tilde{x}(t)$ is an ideal linear chirp with starting frequency 50 MHz, stop frequency 100 MHz, and duration 500 µs, and the phase error sequence θ_m is periodic with one period constituting the sequence $[0,1,2,3,4,5,6,7]/100$ radian. The desired 'signal' and unwanted 'replicas' are indicated.

As seen from Figure 30, on the interval $(-f_{clk}/2, f_{clk}/2)$, $X(f)$ contains one main 'signal' plus seven 'replicas' as expected. As an internal check, the amplitudes of the 'signal' and 'replicas' were compared directly to those of the normalized DFT of $e^{-j\theta_m}$, in accordance with (2.54), and found to be in excellent agreement. It is also seen from Figure 30 that $|A(k)| \approx |A(-k)|$ for the small phase errors involved, in agreement with (2.56).

Thus, we have characterized the digital spectrum of the "real plus imaginary quadrature" signal of the DDS output in the case that the ideal phase samples are perturbed by a periodic sequence of phase errors. It remains to apply these results to characterize the beat signal spectrum which, being a scaled version of the target range profile, is the ultimate measure of the performance of the model FMCW transceiver.

3.3.3 Effect of replicas on the beat signal spectrum

As shown in Section 3.1.4, the beat signal of our model FMCW transceiver is generally characterized by the analytic signal $s_a(t)$ of the DDS output $s(t)$. We showed in Section 3.1.3 that if a chirp is generated from ideal samples, then within the stationary phase approximation, the analytic signal $s_a(t)$ of $s(t)$ is equal to "real plus imaginary quadrature" signal $\tilde{x}(t)$ of $s(t)$ – that is, the two ways of obtaining a complex signal from a real one produce the same result. This is no longer the case, however, if $s(t)$ is perturbed by replicas, since these replicas can cross over to the negative side of the spectrum.

To illustrate the situation, we retrace the steps to obtain the analytic signal spectrum $S_a(f)$ from the "real plus imaginary quadrature" digital spectrum $X(f)$ following Section 3.1. There are three steps involved:

1. Add $X(f)$ to its mirrored conjugate version $X^*(f)$ and multiply by 1/2 to obtain the digital spectrum $\bar{S}(f)$ in accordance with (2.47);
2. Multiply $\bar{S}(f)$ with the ideal low-pass filter transfer function $\mathrm{rect}(f/f_{clk})$ to obtain the DDS output spectrum $S(f)$ in accordance with (2.7);
3. Discard negative frequencies and multiply positive ones by 2 to obtain the analytic signal spectrum $S_a(f)$ in accordance with (2.14).

Performing these steps in sequence, we arrive at the expression

$$S_a(f) = H(f)[X(f) + X^*(-f)], \tag{2.61}$$

where the filter $H(f)$ is given by

$$H(f) = \begin{cases} \frac{1}{2}, & f = 0, \\ 1, & 0 < f < \frac{f_{clk}}{2}, \\ \frac{1}{2}, & f = \frac{f_{clk}}{2}, \\ 0, & \text{otherwise.} \end{cases} \tag{2.62}$$

(Apart from a factor 2, $H(f)$ can be regarded as an ideal low-pass filter cascaded with a Hilbert transform filter (Oppenheim, Schafer et al. 1999)). Substituting our result (2.53) from the previous section into (2.61), we find

$$S_a(f) = H(f) \sum_{k=-\infty}^{\infty} \left[A(k)\tilde{X}\left(f - \frac{k}{MT_{clk}}\right) + A^*(k)\tilde{X}^*\left(-f - \frac{k}{MT_{clk}}\right)\right]. \tag{2.63}$$

Due to the action of the of the filter $H(f)$, the replicas for large absolute values of k will be filtered out. This was modeled by Jenq (Jenq 1997) by limiting the summation range in to contain M 'versions' ('signal' and 'replicas') of $\tilde{X}(f)$ (in his case, the frequency range of interest was the full Nyquist interval $(-f_{clk}/2, f_{clk}/2)$). Since here we are only investigating worst-case scenarios, however, we simply proceed on the assumption that *any* of the $M-1$ 'replicas' can have its 'nominal' support within the support of $H(f)$.

We also make a small-angle assumption: for $\theta_m \ll 1$, the 'replica' amplitudes $A(k)$, $k = 1, \dots, M-1$ are much smaller than $A(0)$, so that 'second-order' spurious signals resulting from the mixing of replicas with each other can be neglected compared to 'first-order' spurious resulting from the mixing of the replicas with the 'main' signal.

Now, to the extent which they are not filtered, it is seen from (2.63) that there are two kinds of replicas in the spectrum $S_a(f)$ of the analytic signal:

- 'signal replicas' $\tilde{X}(f - k/(MT_{clk}))$ of the desired signal $\tilde{X}(f)$, and
- 'image replicas' $\tilde{X}^*(-f - k/(MT_{clk}))$ of its unwanted image $\tilde{X}^*(-f)$.

As stated earlier, the 'image replicas' must be taken in to account because they can 'cross over' to the positive half of the spectrum for sufficiently negative values of k. We consider the effect of the 'image' and 'signal' replicas on the beat signal spectrum in Sections 3.3.3.1 and 3.3.3.2, respectively.

3.3.3.1 Effect of the 'image replicas'

The 'image replicas' can be characterized by the inverse Fourier transform

$$A^*(k)\tilde{X}^*\left(-f-\frac{k}{MT_{clk}}\right) \leftrightarrow A^*(k)\tilde{x}^*(t)\exp\left(-j2\pi\frac{k}{MT_{clk}}\right) \equiv i_k(t), \tag{2.64}$$

where $i_k(t)$ stands for the kth image replica. Inserting the ideal chirp expression (2.21) into (2.64), we find

$$i_k(t) = A^*(k)\exp\left[j2\pi\left(\left(-\frac{k}{MT_{clk}}-f_{c,IF}\right)t-\frac{1}{2}\alpha t^2\right)\right], \qquad -\frac{T}{2}<t<\frac{T}{2} \tag{2.65}$$

Therefore, the 'image replica' has a *negative* chirp rate. As a result, it will not correlate with the 'main' signal in the mixing process.

Specifically, the mixture of kth image replica $i_k(t)$ with the 'main' signal $A(0)\tilde{x}(t)$ will, according to (2.37), contribute a term to the beat signal which is the real part of

$$A(0)\tilde{x}(t)i_k^*(t-\tau)\exp(j2\pi f_{LO}\tau) \propto A(0)A^*(k)\exp(j2\pi\alpha t^2), \qquad -\frac{T}{2}+\tau<t<\frac{T}{2}, \tag{2.66}$$

where the symbol "∝" denotes "proportional to". (We have omitted phase and frequency offset terms from (2.66), which are not important for our discussion here). The beat signal term (2.66) is chirped at twice the original chirp rate α of the transmit signal. According to (2.29), its amplitude spectrum will therefore be approximately rectangular with a height $A(0)A^*(k)/\sqrt{2\alpha}$.

By contrast, as shown in the next section, 'signal replicas' produce pure sinusoidal signals upon mixture with the 'main signal', which therefore have 'sinc' spectra with amplitudes $A(0)A^*(k)(T-\tau)$. As a result, the spurious signals resulting from the 'image replicas' are of the order of $-10\log_{10}\big(B(T-\tau)\big)$ dB down in power with respect to those resulting from the 'signal replicas', which for $B(T-\tau)=20{,}000$ amounts to -43 dB. Therefore, the effect of the 'image replicas' on the spectrum of the beat signal is negligible compared to that of the 'signal replicas', which we discuss presently.

3.3.3.2 Effect of the 'signal replicas'

In order to investigate the effect of the transmitted 'signal replicas' on the beat signal, we first investigate the contribution of a single pair of replicas which are symmetrically placed about the transmit chirp at a frequency offset $f_k = k/MT_{clk}$ for some integer k. Figure 31 shows time-frequency characteristics of the transmit/receive signals and beat signals in the presence of these replicas.

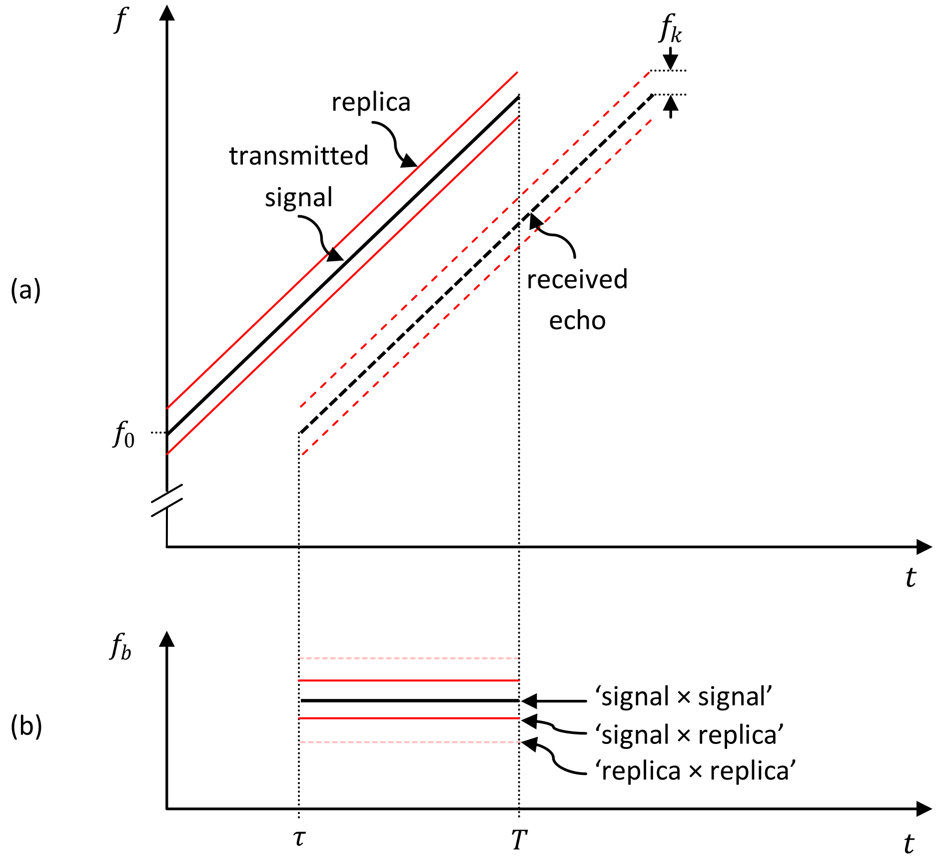

Figure 31 The generation of 'paired echoes' due to frequency-shifted replicas of the transmit chirp.

As seen in Figure 31, each pair of replicas offset by $\pm f_k$ from the transmit chirp produces 'paired echoes' in the beat signal spectrum at $\pm f_k$ from the desired target beat signal, as a result of mixing with the main transmit signal (the solid lines in Figure 31(b)), as well as a weaker pair of echoes at $\pm 2f_k$ as a result of mixing of the error signals with each other (the dashed lines in Figure 31(b)).

In general, the amplitude in the beat spectrum of the echo resulting from the mixing of the kth transmit and lth receive replica is equal to $A(k)A^*(l)$, and in the presence of many replicas, there will be several contributions at each multiple of $1/MT_{clk}$ in the beat signal. For small phase errors, however, $A(0) \gg A(k)$ for $k = 1, 2, \ldots, M-1$, and the contributions resulting from the mixing of replicas with each other can be neglected. In this approximation, the amplitude of the spurious peak in the beat spectrum offset by k/MT_{clk} (with $k \neq 0$) from the true target peak is

$$B(k) \approx A(k)A^*(0) + A(0)A^*(-k). \tag{2.67}$$

Applying the triangle inequality and using the small-angle approximation $|A(k)| \approx |A(-k)|$ (Eq. (2.56)), we obtain the bound

$$|B(k)| \leq 2|A(0)||A(k)| \tag{2.68}$$

or, since $|A(0)| \leq 1$ by Parseval's theorem (Eq. (2.60); there almost no loss of tightness here because $|A(0)| \approx 1$ for $\theta_m \ll 1$) and due to the upper bound (2.59), we have

$$|B(k)| \leq 2\theta_{max}\,. \tag{2.69}$$

Since in the small-angle approximation $\theta_{max} \ll 1$, the amplitude of the signal is $|A(0)|^2 \approx 1$, we thus obtain the following bound for the level of the highest spurious sidelobe due to the digital phase errors relative to the main target peak, or *spurious-to-peak level* (SPL):

$$SPL \leq 6.02 + 20 \log_{10}(\theta_{max}). \quad (2.70)$$

For example, for a maximum phase error of 0.01 radian, the spurious sidelobes are at -34 dB or less from the desired beat signal.

3.3.3.3 Simulation

We have confirmed the results derived above by a simulation using the same parameters as in Section 3.3.2.3. We first discuss the simulation of the return signal (Section 3.3.3.3.1), then simulate the beat signal resulting, conceptually, from the transmission of the "real plus imaginary quadrature" signal $x(t)$. We then simulate the analytic signal $s_a(t)$ (Section 3.3.3.3.2) and its corresponding beat signal (Section 3.3.3.3.3), which is represents the output from our model FMCW transceiver. It is confirmed that although the analytic signal contains 'image replicas' in addition to the 'signal replicas' of the "real plus imaginary quadrature" signal, it is the 'signal replicas' that determine the worst-case spurious sidelobes in the beat signal spectrum.

3.3.3.3.1 Simulation of the return signal

To simulate the beat signal, we require an additional parameter: the target transit time τ. In general, τ can take continuous values; however, in our simulation the time variable is discretized according to the sampling rate used for the simulation, which we have chosen equal to the DDS clock frequency T_{clk}. (In a practical coherent FMCW receiver, the beat frequency will be sampled in at a sub-multiple f_s of the system clock frequency f_{clk}, but for the purpose of illustration we choose a higher rate here). In order to allow τ to nonetheless take continuous values, we have implemented a *fractional delay filter* (FDF), which produces samples of the delayed bandlimited interpolant (2.1) (Laakso, Valimaki et al. 1996).

In order to capture the effects of the bandlimited interpolation (2.1) in our simulation, we have purposely chosen the target delay to not be a multiple of T_{clk} = 1 ns. Specifically, we chose

$$\tau = \frac{12497 + \exp(1)}{12500} \times 100 \text{ µs} \approx 99.9977 \text{ µs},$$

which corresponds to a non-integer delay of

$$d \equiv f_{clk}\tau \approx 9999.77.$$

We have thus also avoided choosing the target delay a multiple of the period of the phase error, 8 ns in the example of Section 3.3.2.3, since in that case the transmitted and received phase errors would cancel in the phase of the beat signal and their effects on the beat signal spectrum would not be visible (Salous and Green 1994).

3.3.3.3.2 Beat signal of the "real plus imaginary quadrature" signal

The resulting beat signal spectrum is shown below in. We started with the "real plus imaginary quadrature" sequence $x[n]$ given by (2.49), with the same phase error θ_m as in Section 3.3.2.3. A version of $x[n]$ was delayed, using an FDF, by a fractional delay $d \equiv f_{clk}\tau \approx 9999.77$ to obtain a ‘return’ sequence $x[n-d]$. The beat signal sequence $x_b[n]$, sampled at the same rate f_{clk}, was then calculated via the relation

$$x_b[n] = x[n]x^*[n-d]. \tag{2.71}$$

The first $\lfloor d \rfloor$ samples of the sequence $x_b[n]$ were set to zero to avoid the ‘fly-back’ portion of the sweep, and the digital spectrum $X_b(f)$ of the resulting sequence was evaluated using a 16,384-point FFT. Figure 32 shows the resulting plot of the normalized power spectrum $|X_b(f)|^2/(T-\tau)^2$ of the beat signal.

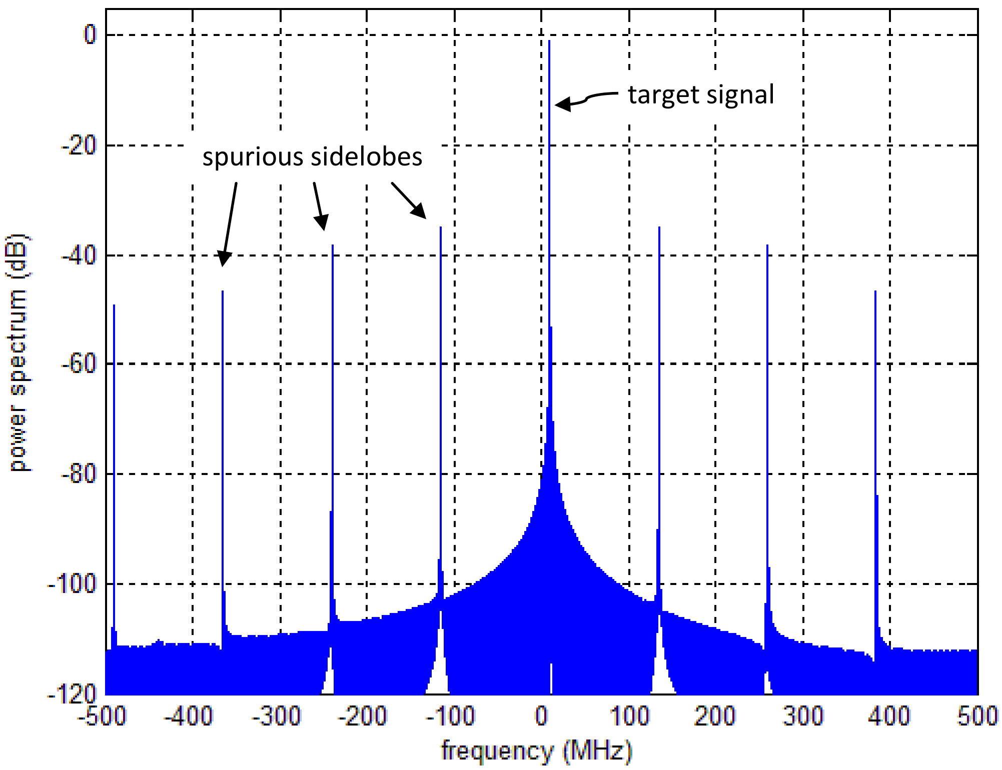

Figure 32 Power spectrum of the normalized beat signal $X_b(f)/(T-\tau)$ corresponding to the “real plus imaginary quadrature” sequence $x[n]$. The target signal at ~ 10 MHz and spurious sidelobes spaced at multiples of $1/(MT_{clk})$ = 125 MHz from it are indicated.

As seen from Figure 32, the beat signal spectrum $X_b(f)$ contains a series of replicas spaced at $1/(MT_{clk}) = 125$ MHz from the ‘main’ signal and each other. The peak sidelobe is -33.9 dB down from the ‘main’ signal, which is less than the -37.8 dB predicted by the coefficient $|A(0)A^*(1)|$ due to the ‘second-order’ effects of the mixing of the replicas with each other. The observed peak-to-sidelobe ratio is well below the upper bound of -23.1 dB given by (2.70) with $\theta_{max} = 0.07$ radian.

3.3.3.3.3 Approximation of the analytic signal

In order to approximate the analytic signal, we have evaluated the discrete-time “analytic” signal $s_a[n]$ described by Marple (Marple 1999). This sequence is obtained by the following steps:

1. Taking the N-point DFT of the real-valued DDS signal $s[n]$ given by (2.42), where $N = T/T_{clk}$ is the number of samples per sweep (that is, the length of $s[n]$);

2. Multiplying the negative frequencies by zero, the positive frequencies by two, and the DC and Nyquist components by unity;
3. Taking the inverse DFT to obtain the discrete-time analytic signal $s_a[n]$.

These steps are implemented by Matlab's built-in "`hilbert`" function. Figure 33 shows the digital spectrum of the discrete-time analytic signal $s_a[n]$ thus obtained, evaluated using a 16,384-point FFT. Since the negative frequencies are zero, only the interval $(0, f_{clk}/2)$ is shown.

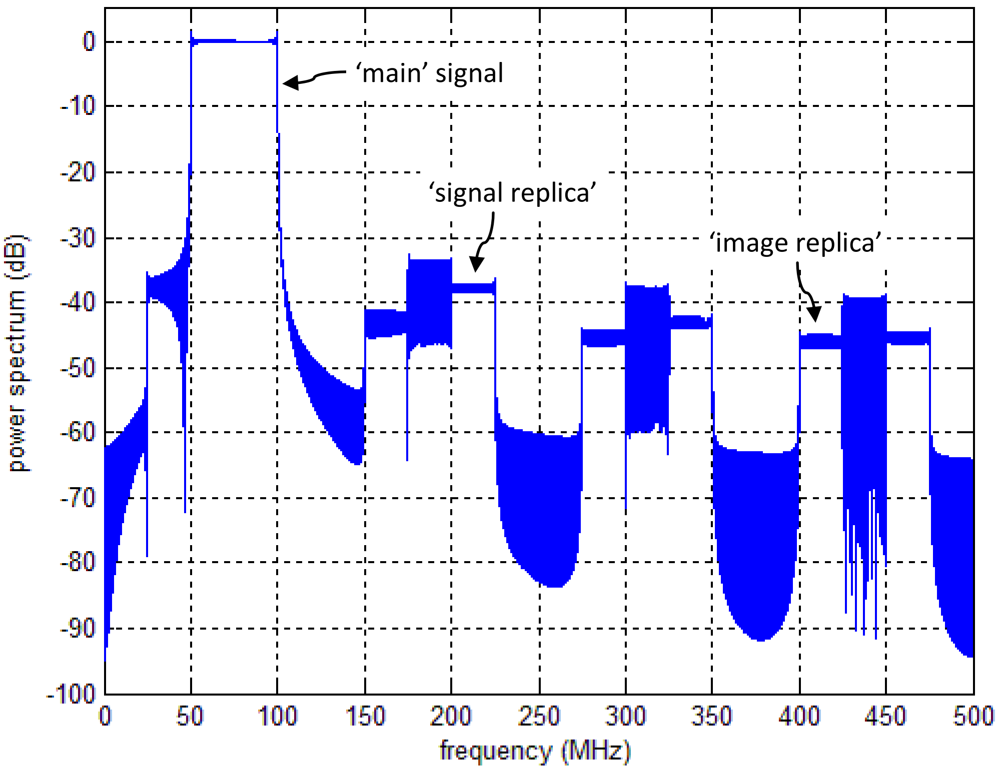

Figure 33 Power spectrum of discrete-time analytic signal $s_a[n]$.

As seen from Figure 33, the spectrum $S_a(f)$ of the analytic signal also contains 'signal replicas' just as $X(f)$ illustrated in Figure 30, as well as 'image replicas', which are frequency-shifted versions of the image $X^*(-f)$.

3.3.3.3.4 Beat signal of the model FMCW transceiver

Finally, in order evaluate the performance of the actual model FMCW transceiver, we approximate the samples $s_b[n] \equiv s_b(nT_{clk})$ of the beat signal given by (2.37) as follows:

$$s_b[n] = \mathcal{Re}\{s_a[n]s_a^*[n-d]\}, \qquad (2.72)$$

where $s_a[n]$ is the discrete-time analytic signal of the DDS output sequence $s[n]$, and $s_a[n-d]$ its counterpart fractionally delayed by $d = f_{clk}\tau$ as in Section 3.3.3.3.2. We have omitted a constant phase factor $\exp(j2\pi f_{LO}\tau)$ in (2.72) since it does not have any effect on the power spectrum of the beat signal. The discrete spectrum $S_b(f)$ of $s_b[n]$ was evaluated using a 16,384-point FFT, and is shown in Figure 34.

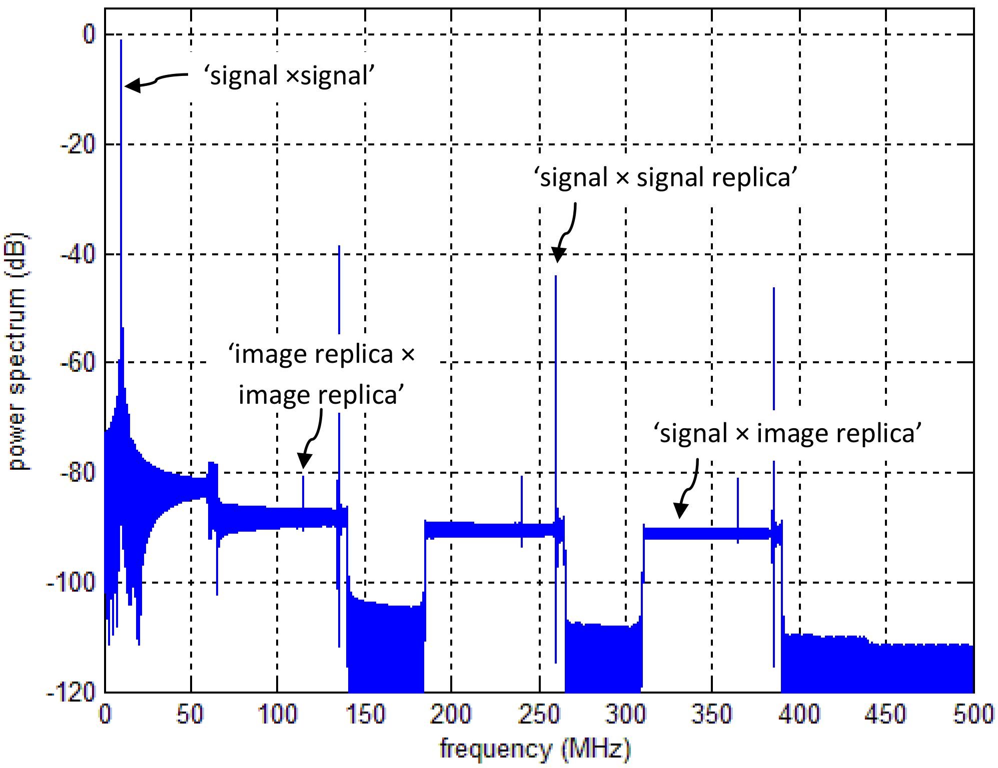

Figure 34 Power spectrum of the normalized beat signal $S_b(f)/(T-\tau)$ corresponding to the discrete-time analytic signal sequence $s_a[n]$. Besides the target signal at ~ 10 MHz ("signal × signal"), there are also spurious sidelobes at multiples of $1/(MT_{clk})$ = 125 MHz from the target signal, which are caused by mixing of the 'signal replicas' with the 'main' signal and each other ("signal × signal replica"). Around 90 dB down from the target signal, there are chirps with bandwidths of $2\alpha(T-\tau) = 80$ MHz, which result from the mixture of replicas of the image signal $\tilde{x}^*(t)$ with the desired transmit signal $\tilde{x}(t)$ ("signal × image replica"). Finally, around 80 dB down from the target signal, there are spurious sidelobes which result from 'second-order' effect of mixing of the 'image replicas' with each other ("image replica × image replica").

As seen from comparison of beat signal of the "real plus imaginary quadrature" Figure 32 with Figure 34, the beat signal of the analytic signal contains some additional 'structure' compared to that of the "real plus imaginary quadrature" signal due to the presence of replicas of the image signal. However, since the 'image replicas' have the opposite chirp rate from the 'main' signal, they are 'expanded' in the beat signal spectrum instead of 'compressed' as the 'signal replicas'. Although the mixture of the 'image replicas' with each other does result in an additional set of spurious sidelobes, the level of these sidelobes is negligible compared to that of the "signal × signal replica" sidelobes in the small-angle approximation.

3.3.3.3.5 Concluding remarks

In short, we have shown that the upper bound (2.70) for the peak-to-sidelobe ratio (PLSR) derived in Section 3.3.2.2 by considering only the effect of the 'signal replicas' is remains valid, within the small phase error approximation, to the beat signal spectrum of the full analytic signal including 'image replicas'. Since the latter, by (2.37), corresponds to what is observed by the model FMCW transceiver, we have thus derived a means to evaluate the worst-case degradation of its performance.

In order to apply these results to a *real* FMCW transceiver, we must evaluate the form of the digital phase error sequence θ_n (or equivalently, the error sequence in bits, $\epsilon_P[n]$) in order to justify the model posited in Section 3.2 and to determine the value of the maximum phase error θ_{max} . This is done in the following section.

3.4 Form of the digital phase error

In this section, we investigate the exact form of the digital phase error sequence θ_n, and determine its maximum amplitude and period. As stated in Section 3.2, θ_n is attributable to two sources: the 'staircase' approximation of the linear chirp and phase truncation. The first is discussed in Section 3.4.1 and the second in 3.4.2, after which we determine the amplitude and period of θ_n in Section 3.4.3.

3.4.1 Phase error sequence to due submultiple-K clocking of frequency accumulator

A quadratic phase can also be generated with the dual-clock principle. This is illustrated schematically in Figure 35, which shows a staircase approximation to a linear FM signal with K = 4. As we shall elucidate shortly, by drawing a straight "fit" through the sampled frequency register values, the staircase can be "decomposed" into an ideal, linear chirp and a periodic error term.

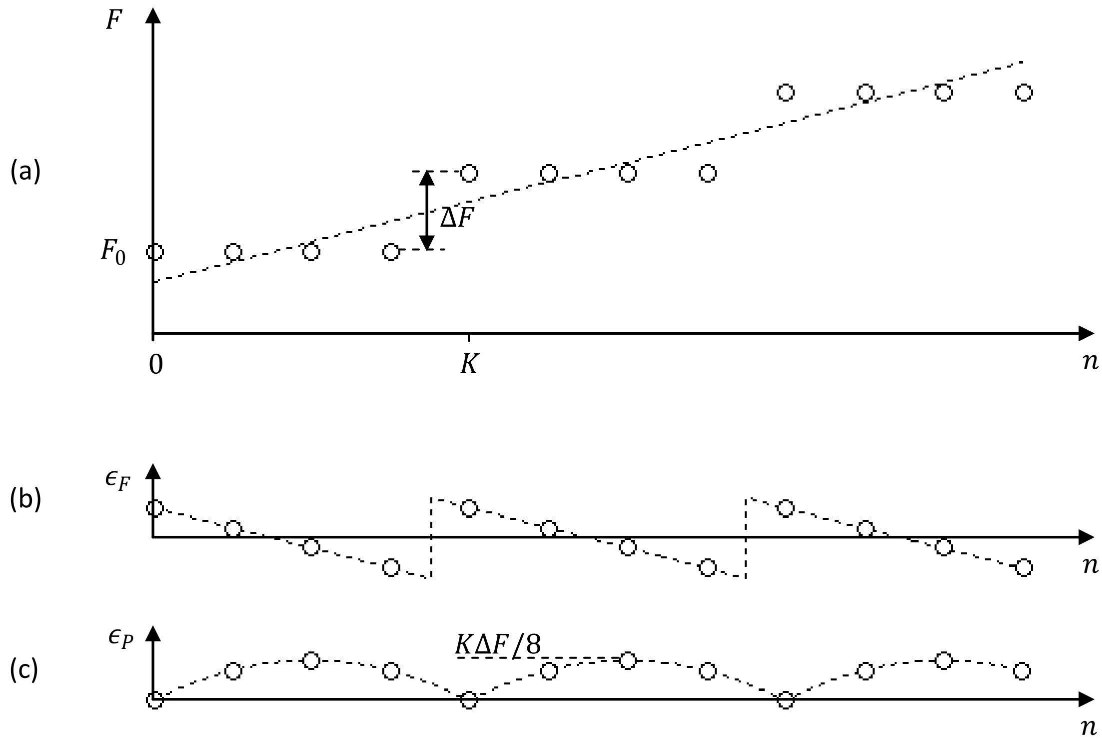

Figure 35 Dual-clock generation of approximately quadratic phase with $K = 4$. The dashed lines are guides for the eye.

This process of phase accumulation is depicted numerically in Table 5. The first four columns are analogous to Table 3, and depict the values of the chirp rate, frequency, and phase registers for each clock cycle n. As in Table 3, each register value is generated as the sum of itself and the value of the previously cascade accumulator at the previous clock cycle.

clock cycle (n)	rate (R)	frequency (F)	phase (P)	$\frac{\Delta F}{2K}n^2 + F_0 n$	$\epsilon_P[n]$
initial values	0	$F_0 + \frac{1}{2}\Delta F$	0	0	0
1	0	$F_0 + \frac{1}{2}\Delta F$	$1F_0 + \frac{1}{2}\Delta F$	$1F_0 + \frac{1}{8}\Delta F$	$\frac{3}{8}\Delta F$
2	0	$F_0 + \frac{1}{2}\Delta F$	$2F_0 + \frac{2}{2}\Delta F$	$2F_0 + \frac{4}{8}\Delta F$	$\frac{4}{8}\Delta F$
3	ΔF	$F_0 + \frac{1}{2}\Delta F$	$3F_0 + \frac{3}{2}\Delta F$	$3F_0 + \frac{9}{8}\Delta F$	$\frac{3}{8}\Delta F$
4	0	$F_0 + \frac{3}{2}\Delta F$	$4F_0 + \frac{4}{2}\Delta F$	$4F_0 + \frac{16}{8}\Delta F$	0
5	0	$F_0 + \frac{3}{2}\Delta F$	$5F_0 + \frac{7}{2}\Delta F$	$5F_0 + \frac{25}{8}\Delta F$	$\frac{3}{8}\Delta F$
6	0	$F_0 + \frac{3}{2}\Delta F$	$6F_0 + \frac{10}{2}\Delta F$	$6F_0 + \frac{36}{8}\Delta F$	$\frac{4}{8}\Delta F$
7	ΔF	$F_0 + \frac{3}{2}\Delta F$	$7F_0 + \frac{13}{2}\Delta F$	$7F_0 + \frac{49}{8}\Delta F$	$\frac{3}{8}\Delta F$
8	0	$F_0 + \frac{5}{2}\Delta F$	$8F_0 + \frac{16}{2}\Delta F$	$8F_0 + \frac{64}{8}\Delta F$	0

Table 5 Dual-clock generation of a quadratic phase perturbed by a periodic error for $K = 4$. The digital chirp rate R is equal to the frequency increment word ΔF each K clock cycles. As a result, the frequency tuning word F increases in a staircase fashion

Mathematically, this can be cast in the following form. The frequency tuning word can be expressed as

$$F[n] = F_0 + \frac{\Delta F}{2} + \Delta F \left\lfloor \frac{n}{K} \right\rfloor \tag{2.73}$$

where $\lfloor \cdot \rfloor$ denotes truncation to integer values. The phase can be expressed as a cumulative sum of the frequency samples:

$$P[n] = \sum_{k=0}^{n-1} F[k]. \tag{2.74}$$

We wish to express the phase register value P as the sum of an 'ideal' phase $\tilde{P}$ and a periodic phase error ϵ_P. To this end, we first express the frequency register value F as the sum of an 'ideal' frequency F and a zero-mean, periodic frequency error $\epsilon_{F,s}$:

$$F[n] = \tilde{F}[n] + \epsilon_{F,s}[n], \tag{2.75}$$

where

$$\tilde{F}[n] = F_0 + \frac{\Delta F}{2K} + \frac{\Delta F}{K} n \tag{2.76}$$

and

$$\epsilon_{F,s}[n] = \frac{\Delta F}{K}\left(\frac{K-1}{2} - \langle n \rangle_K\right), \tag{2.77}$$

where $\langle n \rangle_K = n - K\lfloor n/K \rfloor$ denotes the residue of n modulo K.

Inserting (2.75)-(2.77) into (2.74), we obtain

$$P[n] = \tilde{P}[n] + \epsilon_{P,s}[n], \tag{2.78}$$

where

$$\tilde{P}[n] = \frac{\Delta F}{2K} n^2 + F_0 n \tag{2.79}$$

represents an 'ideal' phase term[27], and

$$\epsilon_{P,s}[n] = \frac{\Delta F}{2K} \langle n \rangle_K (K - \langle n \rangle_K) \tag{2.80}$$

a periodic phase error term, as evidenced by the fact that it is a function of of n through $\langle n \rangle_K$ only. (Note that if we had not chosen ϵ_F to have zero mean, this would not have been the case).

The maximum phase error is attained when $\langle n \rangle_K = K/2$, and is equal to

$$\max\{\epsilon_{P,s}[n]\} = \frac{K\Delta F}{8}. \tag{2.81}$$

Thus, the of the frequency accumulator every K clock cycles causes the output phase to lead the ideal output phase by at most $\frac{2\pi}{2^L}\left(\frac{K\Delta F}{8}\right)$. For a 32-bit accumulator with $K = 4$ and a frequency increment of $\Delta F = 2148$ corresponding to our model system, this amounts to a maximum phase error of 1.6×10^{-6} radian.

3.4.2 Additional effect of phase truncation

The phase from the phase accumulator is subsequently truncated to generate the output phase:

$$P_t = 2^B \left\lfloor \frac{P}{2^B} \right\rfloor \tag{2.82}$$

This can be expressed as

$$P_t[n] = P[n] - \epsilon_{Pt}[n], \tag{2.83}$$

where

$$\epsilon_{Pt}[n] = \langle P[n] \rangle_{2^B}. \tag{2.84}$$

In Eq. (2.83), the phase register value $P[n]$ is itself perturbed from its ideal values $\tilde{P}[n]$ by the phase error $\epsilon_P[n]$ due to clocking the frequency accumulator at a sub-multiple of the phase accumulator clocking frequency. Inserting (2.78) into (2.83) yields

---

[27] Conceptually, $\tilde{P}[n]$ can be regarded as the phase register value that would be obtained if the frequency register were update every clock cycle instead of every K clock cycles, with a frequency increment $\Delta F/K$ and an initial phase value of $F_0 + \Delta F/2K$ (cf. Section 2.3.2.2).

$$P[n] = \tilde{P}[n] + \epsilon_P[n], \tag{2.85}$$

where

$$\epsilon_P[n] = \epsilon_{P,s}[n] - \epsilon_{P,t}[n] \tag{2.86}$$

is the total phase error, including the effects of the staircase approximation and phase truncation.

3.4.3 Properties of the digital phase error ϵ_P

From its expression (2.86), we can derive several interesting properties of the phase error $\epsilon_P[n]$.

3.4.3.1 *Maximum amplitude*

The total phase error ϵ_P is seen by (2.86) to be the difference between $\epsilon_{P,s}$ and $\epsilon_{P,t}$. From (2.81), we have $\max \epsilon_{P,s} = K\Delta F/8$. Further, it is clear from Figure 35(c) and from Eq. (2.80) that $\epsilon_{P,s}$ is a non-negative sequence.

The error contribution from phase truncation $\epsilon_{P,t}$ has the form, as seen from Eq. (2.84), of an expression modulo 2^B, from which we can immediately infer its maximum value:

$$\max \epsilon_{P,t} = 2^B - 1. \tag{2.87}$$

Further, $\epsilon_{P,t}$ is also a non-negative sequence. It follows that the maximum absolute value of the difference is

$$\max|\epsilon_p| = \max\left\{\frac{K\Delta F}{8}, 2^B - 1\right\}. \tag{2.88}$$

The staircase approximation phase error $K\Delta F/8$ was shown in Section 3.4.1 to have a maximum value of 1.6×10^6 radian; for a 32-bit accumulator of which 19 bits are used to address the sine ROM, the maximum phase error due to phase truncation is $\frac{(2^{32-19})}{2^{32}} \times 2\pi \approx 1.2 \times 10^{-5}$ radian. Hence, for our practical application, maximum phase error is determined by phase truncation.

3.4.3.2 *Periodicity*

In Section 3.2, we assumed a phase error that was periodic with period M. Here, we show that ϵ_P is indeed periodic with a period of at most $M = K \cdot 2^B$. To this end, it clearly suffices to show that $\epsilon_{P,s}$ and $\epsilon_{P,t}$ are both individually periodic with a period of at most $K \cdot 2^B$.

Recall that the staircase approximation phase error $\epsilon_{P,s}$ is periodic with period K, where K is the clock division factor between the phase and frequency accumulators. It follows immediately that $\epsilon_{P,s}$ is also periodic with period $K \cdot 2^B$, since this is just a multiple of fundamental periods K.

It remains to show that $\epsilon_{P,t}$ is also periodic with a period of at most $K \cdot 2^B$, i.e,

$$\epsilon_{P,t}[n + K \cdot 2^B] = \epsilon_{P,t}[n], \qquad \forall n. \tag{2.89}$$

Recall that $\epsilon_{P,t}$ was of the form $\epsilon_{P,t} = \langle P[n] \rangle_{2^B}$, where $P[n]$ is the output from the phase accumulator (Eq. (2.84)). Hence, it will suffice to show that $P[n + K \cdot 2^B] = P[n] + Q \cdot 2^B$, where Q is an integer, since then the remaining term is equivalent to zero modulo 2^B.

To this end, it is useful to express $P[n]$ in the following form, due to Salous and Green (Salous and Green 1994):

$$P[n_1, n_2] = F_0(Kn_1 + n_2) + \frac{n_1(n_1+1)}{2} K\Delta F + n_1 n_2 \Delta F, \tag{2.90}$$

where $n_1 \equiv \mathrm{floor}(n/K)$ and $n_2 \equiv \mathrm{mod}(n, K)$.

Clearly, increasing n by the amount $K \cdot 2^B$ will have the effect of increasing n_1 by 2^B, while leaving n_2 unaltered. It follows that

$$P[n + K \cdot 2^B] = P[n] + \left(F_0 K + \frac{(2^B + 1 + 2n_1)}{2} K\Delta F + n_2 \Delta F \right) 2^B. \tag{2.91}$$

According to our earlier reasoning, it now suffices to show that the expression between brackets is an integer. The first and last terms are clearly integers, since they are the product of integers. The middle term, however, is divided by 2, so it is necessary to check that $(2^B + 1 + 2n_1)K\Delta F$ is an even number.

Recall that K is usually a small power of 2, for example $K = 4$ for the AD9910 and $K = 8$ for the AD9858, and therefore an even number. Further, $(2^B + 1 + 2n_1)$ is clearly an odd number. Therefore, the product $K(2^B + 1 + 2n_1)$ is an even number, and it follows that the total product $(2^B + 1 + 2n_1)K\Delta F$ is an even number, regardless of whether ΔF is even or odd.

This concludes the proof that $\epsilon_{P,t}$ is periodic with a maximum period of $K \cdot 2^B$. In fact, it can be shown that the actual period is smaller if ΔF contains factors of 2. Our purpose here, however, is only to show periodicity to validate the application of the theory described in Section 3.2.

3.5 An upper bound for the effect of digital phase errors on the beat signal spectrum

We conclude this chapter by combining our previous results to obtain our main result: an upper bound for the spurious-to-peak level (SPL) of spurious signals in the beat signal spectrum of our model FMCW-Doppler transceiver, due to phase errors attributable to the 'staircase approximation' and phase truncation effects in the digital chirp synthesis.

3.5.1 The amplitude of the worst-case "ghost" target

In Section 3.4.3, we showed that these effects result in a periodic phase error sequence with maximum amplitude

$$\theta_{max} = \frac{2\pi}{2^L} 2^B = \frac{2\pi}{2^W} \tag{2.92}$$

where L is the total number of bits in the phase accumulator, B the number of truncated bits, and $W = L - B$ the number of bits used for phase-to-amplitude conversion.

Inserting this value into the upper bound, obtained in Section 3.3, for the spurious-to-peak level (SPL) due to digital phase errors,

$$SPL \leq 6.02 + 20 \log_{10}(\theta_{max}), \tag{2.93}$$

we obtain the final result applied to DDSs

$$SPL \leq 23.0 - 6.02W \tag{2.94}$$

where as stated earlier, W is the number of bits used for phase-to-amplitude conversion. The upper bound (2.94) holds in the small-angle approximation, $\theta_{max} \ll 1$.

As an example, for the Analog Devices AD9910 direct digital synthesizer, $W = 19$, corresponding to a maximum phase error of is $\theta_{max} = 2\pi/2^{19} = 1.2 \times 10^{-5}$ radian. Therefore, according to (2.94) we expect to the worst-case spurious or "ghost" target to be at 92 dB down from the real target.

3.5.2 Comparison to ADC quantization noise

In a practical application, this level should be compared to the signal-to-quantization noise ratio (SQNR) of the analog-to-digital converter (ADC) used to sample in the beat signal. For a Q-bit ADC, the SQNR is given by

$$SQNR = 20\log_{10}(2^{Q}) \approx 6.02Q. \tag{2.95}$$

Hence, for the 16-bit ADC employed in our model system (as described in Section 2.1), the $SQNR$ is $16 \times 6.02 \approx 96$ dB. Therefore, for our model system, the worst-case spurious is only about 4 dB above the quantization noise floor of the ADC.

3.5.3 Concluding remarks

In short, we have constructed a mathematical model of the 'staircase' approximation and phase truncation, in which the combined effect of the two is replaced by an effective periodic digital phase error. This periodic phase error was shown to lead to the appearance of 'replicas' of the desired chirp in the output spectrum of the direct digital chirp synthesizer. The effect of these 'replicas' on the beat signal spectrum of our model FMCW-Doppler transceiver was calculated, and the results were confirmed by simulation. An application of our results show that the worst-case spurious sidelobe is 92 dB down from the desired 'point' target response; this is only 4 dB above the quantization noise floor of the ADC.

4 The effect of phase errors on Doppler processing

In the previous chapter, we derived the effect of digital phase errors on *range* processing. It was shown that a periodic phase error with fundamental frequency f_{sl} leads to spurious sidelobes or 'paired echoes' offset by multiples of f_{sl} from the desired target beat signal. In this chapter, we investigate the effect of periodic phase errors on *Doppler* processing.

It is shown that if the phase errors are *coherent* with the transmitted frequency sweep – that is, if the period of the phase errors is commensurate with the sweep period – then the spurious sidelobes will not be displaced from the target signal in Doppler. Thus in this case, the target still be appears to be moving as a rigid body (albeit one whose shape is distorted in the direction of the radar's line of sight). This is a desirable property, since in radar tracking algorithms Doppler shifts play an important role in distinguishing targets from unwanted echoes (or "clutter" in the parlance of radar literature).

4.1 The effect of sinusoidal phase errors in the beat signal

To the best of the author's knowledge, the effect of *deterministic* phase errors in the transmitted signal of a FMCW radar on Doppler processing has not been discussed in the literature. The work of Adamski et al. (Adamski, Kulpa et al. 2000) on the effect of phase *noise* does, however, contain an intermediate result that we have found useful. In this section, we recapitulate Adamski's result.

Adamski et al. (Adamski, Kulpa et al. 2000) discuss the effect of phase *noise* on the two-dimensional spectrum of the beat signal in homodyne radar. To this end, they define the *differential phase error*

$$\Delta\phi(t) \equiv \delta\phi(t) - \delta\phi(t-\tau), \tag{3.1}$$

where $\delta\phi(t)$ is the phase error of the transmitted signal. They then analyze the effect of a differential phase error component of the following form:

$$\Delta\phi(t) = \bar{\beta}\cos\left[2\pi\left(\Delta R + \frac{\Delta v}{M}\right)\frac{t}{T}\right], \qquad \bar{\beta} \ll 1, \tag{3.2}$$

where $\bar{\beta}$ is a modulation parameter[28], M is the number of processed sweeps, and ΔR and Δv determine the frequency of the sinusoidal phase error. It is understood in (3.2) that $\Delta v/M$ is a proper fraction. It is then shown that this differential phase error generates two spurious sidelobes or 'paired echoes' shifted ΔR range cells and Δv velocity cells from the main target lobe, as illustrated in Figure 36.

[28] In (Adamski, Kulpa et al. 2000), the modulation parameter $\bar{\beta}$ is written without an overbar; here, we add the overbar to distinguish it from the dimensionless velocity parameter β defined in (1.19).

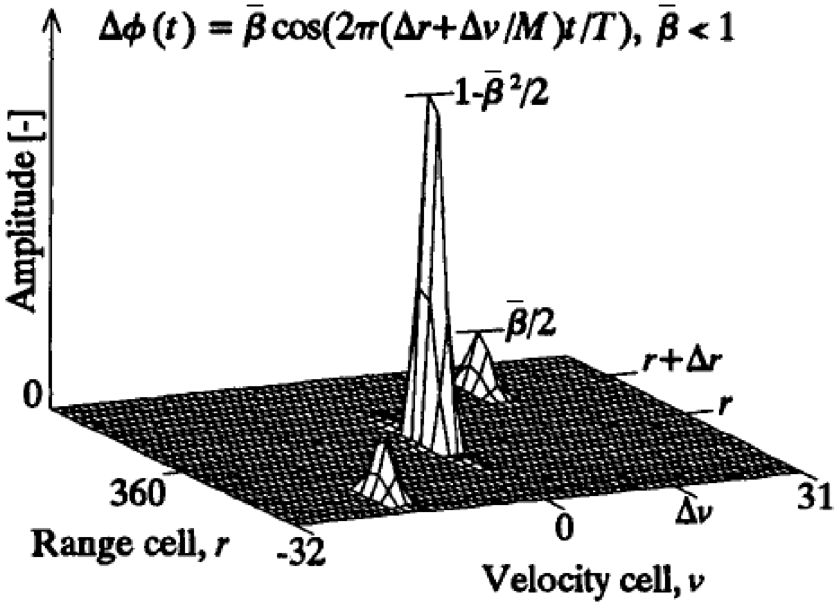

Figure 36 Two-dimensional amplitude spectrum of an ideal stationary point object for a single-tone small-index differential phase modulation, as simulated by Adamski et al. (Adamski, Kulpa et al. 2000). According to that reference, the sweep period is T = 1 ms, the target delay τ = 100 µs, and the target beat frequency f_b = 360.45 kHz. (This corresponds to a chirp rate of α = 3.60 GHz/s and a chirp bandwidth of 3.60 MHz). The total number of samples per sweep is N = 2048, and the number of processed sweeps is M = 64. The first N_0 = 432 fast-time samples within each sweep are set to zero, and a Hanning window is used for the range FFT; the Doppler FFT is performed after weighting with a Hamming window. (After (Adamski, Kulpa et al. 2000)).

The result stated above implies that if the sinusoidal differential phase error is *coherent* with the transmitted chirp – that is, if the number of periods within one sweep, $\Delta R + \Delta v/M$, is an integer (this implies that $\Delta v = 0$) – then the 'paired echoes' will be offset from the desired target signal in range only, not in Doppler.

This result is not directly applicable to our case, however, because we wish to investigate the effects of deterministic phase errors $\delta\phi(t)$ in the transmit signal, and in view of (3.1) cannot posit the form of the differential phase error $\Delta\phi(t)$ directly, since it will depend on $\delta\phi(t)$. The result we derive below, however, is quite similar to Adamski's.

Our simulation results show, however, that essentially the same result holds if (3.2) represents the transmitted phase error. Moreover, this remains the case if the wavelength of the phase errors is not long compared to the target delay time τ.

4.2 The effect of sinusoidal phase errors in the transmitted signal

Here we study periodic phase errors in the transmitted signal which are coherent with the transmitted sweep. Such phase errors are a function of time, t, through the internal time per sweep or fast-time t_m:

$$\delta\phi(t) = \delta\phi(t_m), \tag{3.3}$$

where t_m is the fast-time variable within the mth pulse given by (1.6). We maintain that phase errors of the form (3.3) do not cause any shifts from the target Doppler frequency after Doppler processing.

To show this, we consider the form of the differential phase error $\Delta\phi(t)$. During the portion of the mth sweep in which the 'lower' beat signal is observed, the differential phase error is given by

$$\Delta\phi(t) = \delta\phi(t_m) - \delta\phi\big(t_m - \tau(t)\big). \tag{3.4}$$

As shown in Section 2.2.3, the two-way propagation delay $\tau(t)$, which is referenced to the range R_0 at $t = 0$, is given by equation (1.19):

$$\tau(t) = \tau_0 + \beta t_m + \beta m T, \tag{3.5}$$

where $\tau_0 = 2R_0/c$ is the initial delay, $\beta = 2v/c$ is the dimensionless radial velocity, t_m is the fast-time variable within the mth pulse, m the pulse number or slow-time variable, and T the sweep period. Inserting (3.5) into (3.4) yields

$$\Delta\phi(t) = \delta\phi(t_m) - \delta\phi(t_m - \tau_0 - \beta t_m - \beta m T). \tag{3.6}$$

Expanding the second term as a Taylor series about $t_m - \tau_0 - \beta t_m$, we find

$$\begin{aligned}\Delta\phi(t) = \delta\phi(t_m) - \delta\phi(t_m - \tau_0 - \beta t_m) + \beta m T \delta\phi^{'}(t_m - \tau_0 - \beta t_m) \\ -\frac{1}{2}\beta^2 m^2 T^2 \delta\phi^{''}(t_m) + \cdots.\end{aligned} \tag{3.7}$$

The first two terms depend on time t through the fast time t_m only, and hence do not cause any Doppler error according to the results of Section 4.1. The subsequent terms, however, contain a depend on the slow time variable m, and could affect Doppler processing. We show below, however, that their effect is negligible for the model system considered in this thesis.

Consider a harmonic phase error $\delta\phi(t_m)$ of the form

$$\delta\phi(t_m) = A_{sl}\sin(2\pi f_{sl} t_m + \varphi_{sl}), \tag{3.8}$$

where A_{sl} is the peak phase error, f_{sl} the phase error frequency, and φ_{sl} a constant phase term. This represents the worst-case scenario in which all the energy of the phase error is concentrated into a single harmonic. The maximum absolute value of the derivative of (3.8) is

$$\max|\delta\phi^{'}(t_m)| = 2\pi f_{sl} A_{sl}. \tag{3.9}$$

Now, for an error caused by phase truncation, we expect the maximum amplitude of the phase error to be $A_{sl} = \theta_{max} = 2\pi/2^W$, where W is the number of used bits in the phase accumulator. Further, the maximum frequency expected at the output is Nyquist frequency of the DDS clock, $f_{clk}/2$. For an AD9910 direct digital synthesizer with W = 19 and f_{clk} = 1 GHz, we obtain $\max|\delta\phi^{'}(t_m)| \approx$ 38 kHz.

Now, consider the third term in (3.7), which is linear in $\beta m T$. With $\beta \cong 10^{-7}$, $m \cong 100$, and T = 500 µs, the maximum value of this term is

$$\max|2\pi\beta m T A_{sl} f_{sl}| \cong 2 \times 10^{-4} \ll 1.$$

Thus, the linear term in m in (3.7) is negligible for the example considered here. By similar reasoning, it is easily seen that the higher-order terms in m are negligible, too.

Thus, to an excellent approximation, the differential phase error resulting from phase errors which are coherent with the transmitted sweep has negligible slow-time dependence. It follows that such phase errors have a negligible effect on Doppler processing.

4.3 Verification by simulation

We have verified the analytical result of Section 4.2 by simulation in MATLAB. The simulation is a straightforward implementation of the theory of Chapter 2. A listing of the MATLAB script used for the simulation is given in the Appendix. Below, we present results of our simulation for a number of cases of interest.

4.3.1 Phase-coherent error function

The simulation below shows a range-Doppler profile for the parameters of chapter 2 for a phase error with amplitude of 0.1 radian and a periodicity of 3 cycles per sweep. Thus, the sinusoidal phase error is coherent with the transmitted frequency sweep.

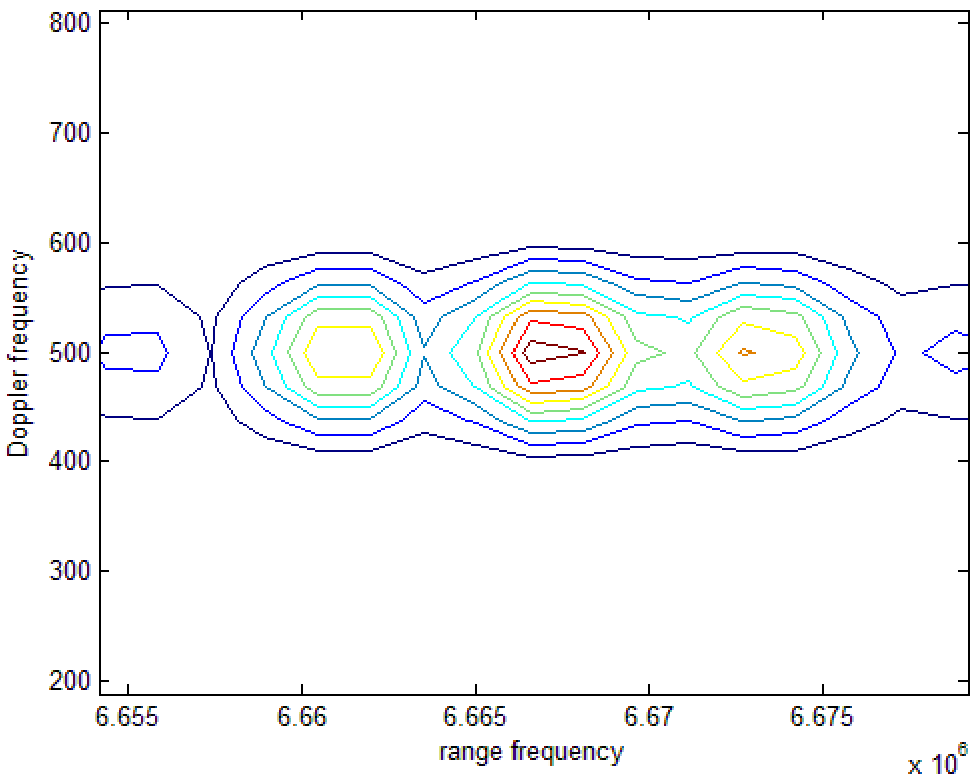

Figure 37 Range-Doppler profile of a target at 7.5 km range with 7.5 m/s velocity, where the transmitted signal is affected by a sinusoidal phase error with periodicity of 3 cycles per sweep and amplitude 0.1 radian.

As seen from Figure 37, the spurious sidelobes resulting from the coherent phase error are offset in range only.

4.3.2 Phase-incoherent error function

In Figure 38, we show the results of a simulation which is the same as in the previous section, except that the number of phase error cycles per sweep has been increased from 3 to 3.1. Thus, the phase error is incoherent with the transmitted chirp, and accumulates at rate of 0.1 cycles per sweep. This leads to spurious sidelobes which are also offset in Doppler, similar to those found by Adamski et al. (Adamski, Kulpa et al. 2000)

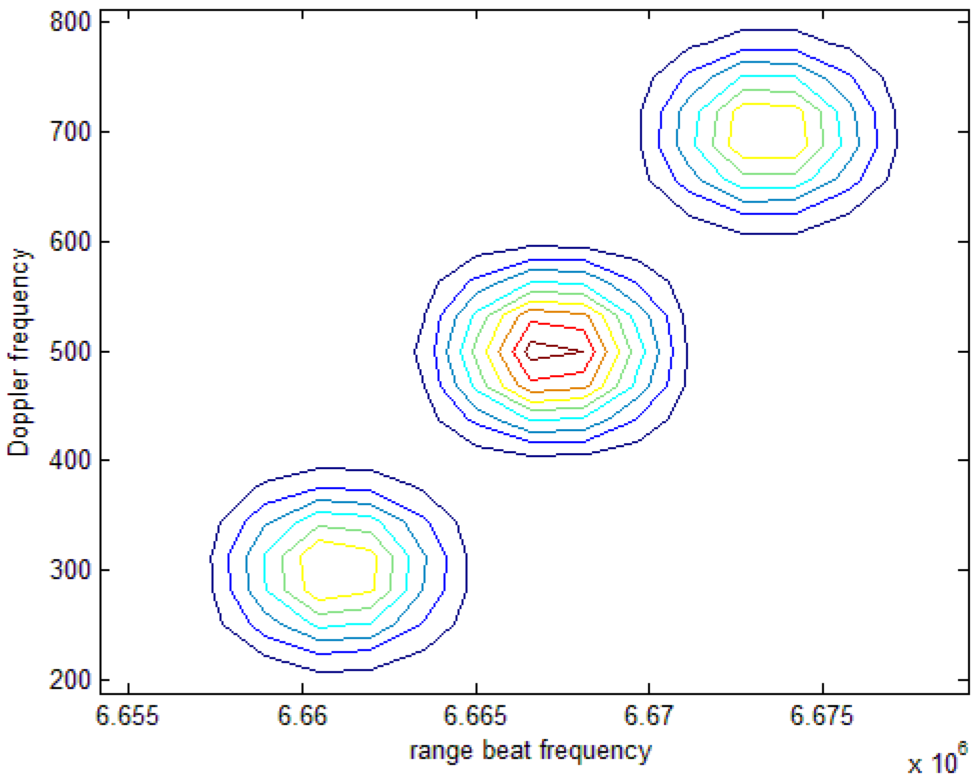

Figure 38 The same as the previous figure, except the periodicity of the phase error is now 3.1 cycles per sweep. The spurious sidelobes are now shifted in Doppler as well as in range.

4.4 Conclusion

In short, we have shown analytically and confirmed by a simulation that phase errors which are *coherent* with the transmitted frequency sweep – that is, whose period is commensurate with the sweep period – have no effect on Doppler processing. By this we mean that the spurious sidelobes which appear after range processing are not offset in Doppler from the main target signal in the range-Doppler profile of the target. This is a desirable property for target tracking and classification, where Doppler processing plays an important role in distinguishing targets from unwanted echoes or 'clutter'.

5 Implementing periodic and phase-continuous sweep transitions

In this chapter, we discuss a method to implement a *periodic* FMCW signal using a direct digital chirp synthesizer (DDCS).

In Section 5.1, we introduce the problem and explain why such sweep transitions are desirable. In Section 5.2, we describe the discrete constraints on the parameters of a chirp generated by a DDCS. In Section 5.3, we show how chirp parameters can be chosen such that they simultaneously satisfy the conditions for phase-coherent and phase-continuous sweep transitions and the discrete constraints for a DDCS.

5.1 Introduction

As explained in Section 2.2.2, a coherent FMCW radar requires *phase-coherent* frequency sweeps. In practice, it can be advantageous to use a *periodic* FMCW signal as assumed in our discussion in 2.2, for a number of reasons:

- With a periodic FMCW signal, a zero Doppler shift also shows up at zero frequency after the second step of double-FFT digital processing, which is physically intuitive.
- As discussed in Chapter 3, chirp generation by a DDS results in a deterministic sequence of phase errors. This sequence depends on the phase at which the sweep starts. Hence, if each sweep starts at the same phase, then the phase error sequence will be periodic with the sweep period. In Chapter 4, we show that in this case, the phase errors do not affect Doppler processing.
- There exist signal processing methods to compensate for *systematic* phase errors in the FMCW transmit signal (Burgos-Garcia, Castillo et al. 2003; Meta, Hoogeboom et al. 2006). If these are to be applied, they will only work if the phase errors are the same for each sweep.
- Finally, if the sweeps transitions all occur at the same phase, then they can be chosen to take place at a portion of the sweep where

In a DDS, changes in output frequency are by default not necessarily phase-*coherent*, but phase-*continuous*. Phase continuity at sweep transitions in a chirp DDS may be achieved by allowing the phase accumulator to 'run on'[29]. The phase continuity ensures lower spectral leakage into adjacent user bands than phase discontinuous waveforms. In general, however, the phase at the beginning of each sweep transition will change from sweep to sweep, as illustrated in Figure 39.

[29] In a practical application using the Analog Devices AD9858 or AD9910 DDS, phase-continuous sweeping is implemented in the "continuous ramping" mode of operation, which is invoked by setting both the "no-dwell high" and "no-dwell low" control bits equal to Logic 1, according to the Analog Devices AD9910 user manual. In continuous ramping mode, the output of the AD9910's frequency accumulator (or "digital ramp generator" (DRG), in the parlance of the manual) automatically oscillates between its upper and lower limits using the programmed slope parameters.

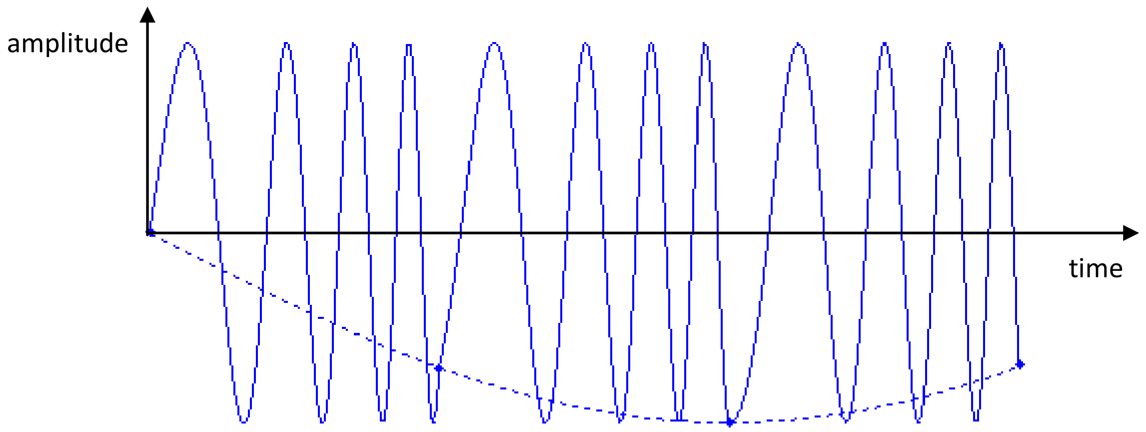

Figure 39 A linear FMCW signal (solid line) of which the sweep transitions (dots) are phase-continuous, but not periodic. The dashed line represents the baseband alias of the chirp's center frequency sampled at the sweep repetition frequency (SRF).

Numerically controlled oscillators (NCOs) usually feature a 'clear' control going to the phase register, which resets the value in the phase register to zero (or any other desired value). The 'clear' control provides a means to ensure that frequency sweeps are periodic by resetting the phase to zero at the beginning of each sweep, as illustrated in Figure 40.

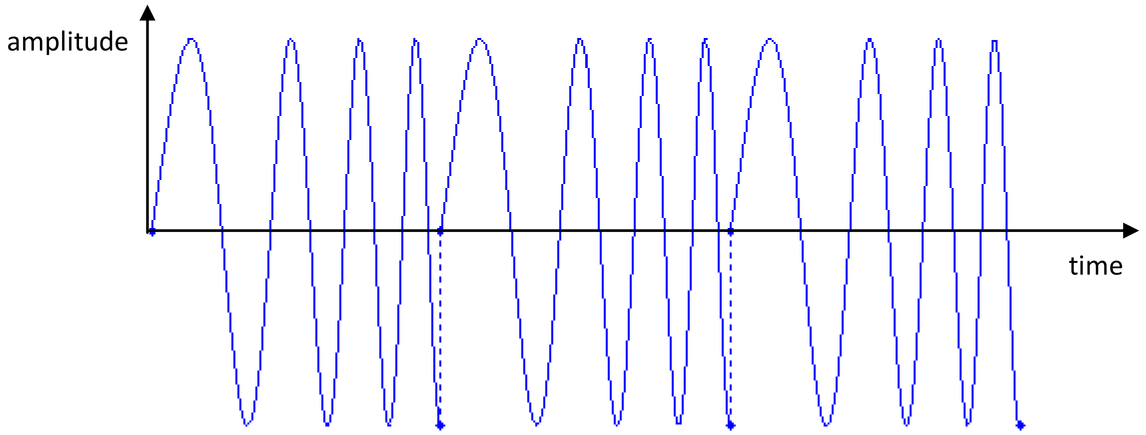

Figure 40 A linear FMCW signal (solid line) which is periodic, but not phase-continuous. The dashed lines indicate 'jumps' in the DDS output made upon resetting its phase accumulator value to zero.

A disadvantage of this approach, however, is that abruptly resetting the phase to zero will generally cause an instantaneous change in the amplitude of the DDS output signal. This leads to spurious emissions in the frequency domain called *spectral splatter* (or *switch noise*). Further, if the DDS is programmed for sine output, resetting the phase to zero effectively switches the synthesizer off, which – without fast programming of the phase – causes amplitude modulation of the output (Salous 1992).

The need for resetting the phase accumulator to zero at each sweep can be avoided by choosing the DDS parameters such that the output is both phase-continuous and phase-coherent from sweep to sweep. This means that if the sweep starts at zero phase, it must oscillate an integer number of cycles and return to zero at the end of each sweep, as illustrated in Figure 41.

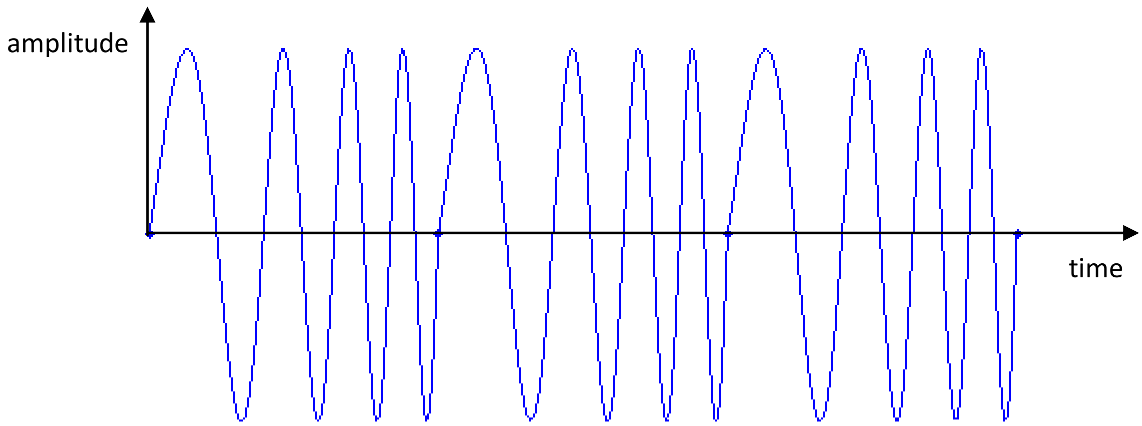

Figure 41 Periodic FMCW signal with phase-continuous sweep transitions.

Mathematically, the condition for periodic sweeping can be expressed as (Durbridge and Warne 1991)

$$f_c = \frac{k}{T}, \quad k \in \mathbb{N} \tag{3.10}$$

where k represents the number of cycles per sweep, T is the sweep period and f_c is the chirp's center frequency given by

$$f_c = \frac{f_0 + f_1}{2} \tag{3.11}$$

with f_0 and f_1 representing the chirp's start and stop frequencies, respectively. Although here we consider only frequency sweeps with instantaneous fly-backs, equations (3.10) and (3.11) also guarantee CP sweep transitions for FMCW waveforms with linearly chirped fly-backs (Brunson, Sole et al. 2007).

The effect of switch noise can be visualized by the spectrogram of the FMCW signal. Figure 42 compares the spectrograms of two cosine linear FMCW waveforms which both have a sweep period of 1 second, center frequency of 200 Hz, and bandwidth of 100 Hz, but slightly different center frequencies of 200 Hz (Figure 42(a)) and 200.5 Hz (Figure 42(a)). As result, the waveform in (a) has a discontinuity of twice the amplitude at the sweep transitions, whereas the waveform in (b) is continuous there both in value and first derivative. This manifests itself in a lower content of frequencies outside the nominal bandwidth of the chirp at the sweep transitions.

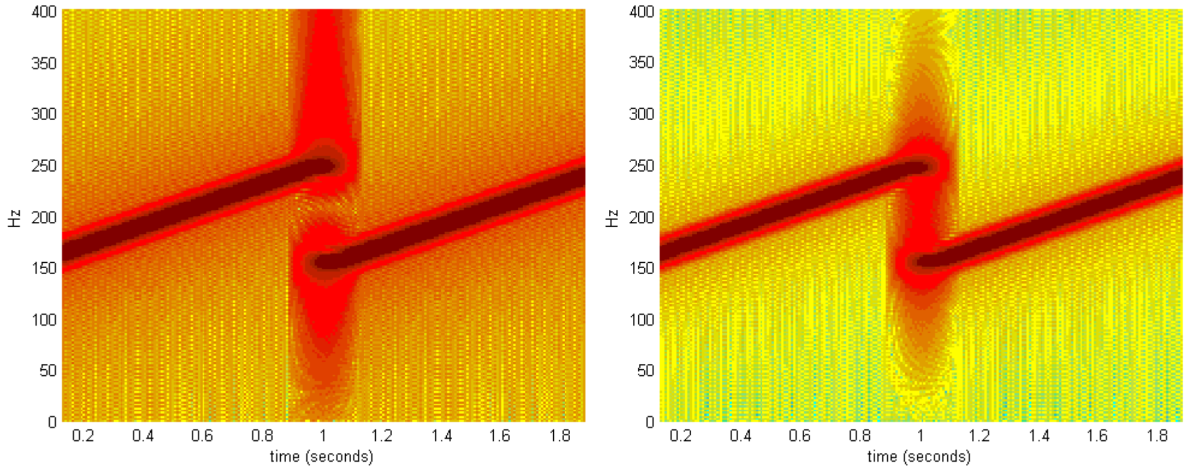

Figure 42 Spectrograms of a coherent, cosine FMCW waveform with sweep repetition interval 1 second, peak-to-peak frequency deviation 100 Hz, and center frequencies of (a) 200.5 Hz and (b) 200 Hz. The sampling frequency was taken at 8,192 Hz, and 16,384 samples were calculated over two sweep repetition intervals. A Hamming window of length 256 samples was used with overlaps of 248 samples, and an FFT length of 512 samples.

It should be noted that in applications in which the output of the DDCS is up-converted by mixing, the center frequency $f_{c,RF}$ of the final output at RF is given by

$$f_{c,RF} = f_{c,IF} + f_{LO} \tag{3.12}$$

where $f_{c,IF}$ is the center frequency of the chirp at intermediate frequency (IF) generated by the DDS, and f_{LO} is the local oscillator (LO) frequency. Thus in principle, with a 'free-running' (as opposed to a 'phase-locked') LO, f_{LO} could be adjusted such that $f_{c,RF}$ would satisfy (3.10), even though the separate terms $f_{c,IF}$ and f_{LO} might not do so individually. In practical FMCW radars operating above 10 GHz, however, coherency is usually achieved by locking all transmit chain sources and the and the ADC sampling clock to a common reference oscillator (Beasley 2006). This requires that the local oscillator frequency f_{LO} must be commensurate with the sweep repetition interval: $f_{LO} = k/T$ for some integer k; hence in this case, $f_{c,IF}$ must also be commensurate with T in order for their sum to satisfy (3.10). In any case, the generation of phase-continuous periodic chirps by DDS is directly useful for HF radar applications in which the DDS signal is transmitted directly (Gurgel, Antonischki et al. 1999).

Thus, it is desirable and in many cases necessary that the DDCS generate an output at an intermediate center frequency $f_{c,IF}$ which itself satisfies (3.10). Equation (3.10) was stated by Durbridge (Durbridge and Warne 1991) as a condition for ensuring perfect periodicity as well as phase continuity in the sweep transitions of a DDS. However, no attempt was made to translate this *continuous* criterion to an algorithm for choosing the *discrete* chirp DDS parameters; it was simply stated that "in general it is necessary to modify these conditions by scaling factors to account for quantization of values and the limited precision of the fixed-point arithmetic" (Durbridge and Warne 1991). To the best of our knowledge, a detailed description of how exactly to achieve these modifications has also not been given elsewhere in the literature.

5.2 Chirp DDS discretization constraints

In order to devise an algorithm for choosing chirp DDDS parameters so as to ensure periodic, phase-continuous sweep transitions, we first need to formulate mathematically the discrete constraints which any chirp generated by a DDS must satisfy. In order to apply our results to practical DDSs such as the AD9858 and the AD9910, we construct a model of a DDS which operates by the dual-clock principle explained in Section 2.3.2.

Figure 43 shows a time-frequency plot of a 'staircase' or 'stepped CW' approximation of a linear chirp as generated by a dual-clock chirp DDS. As explained in Section 2.3, the phase accumulator of the DDCS is updated at the master clock frequency f_{clk} , whereas the frequency accumulator is updated at a lower rate, namely, a sub-multiple K of f_{clk} , which results in the 'staircase' time-frequency characteristic (the solid line in Figure 43, in which K = 4). As shown in Chapter 3, the resulting signal phase can be represented as the sampled values of an ideal linear chirp (dashed line) perturbed by a periodic phase error. Here, however, we focus on the discrete constraints that must be satisfied by the DDCS parameters, several of which can be directly inferred from Figure 43.

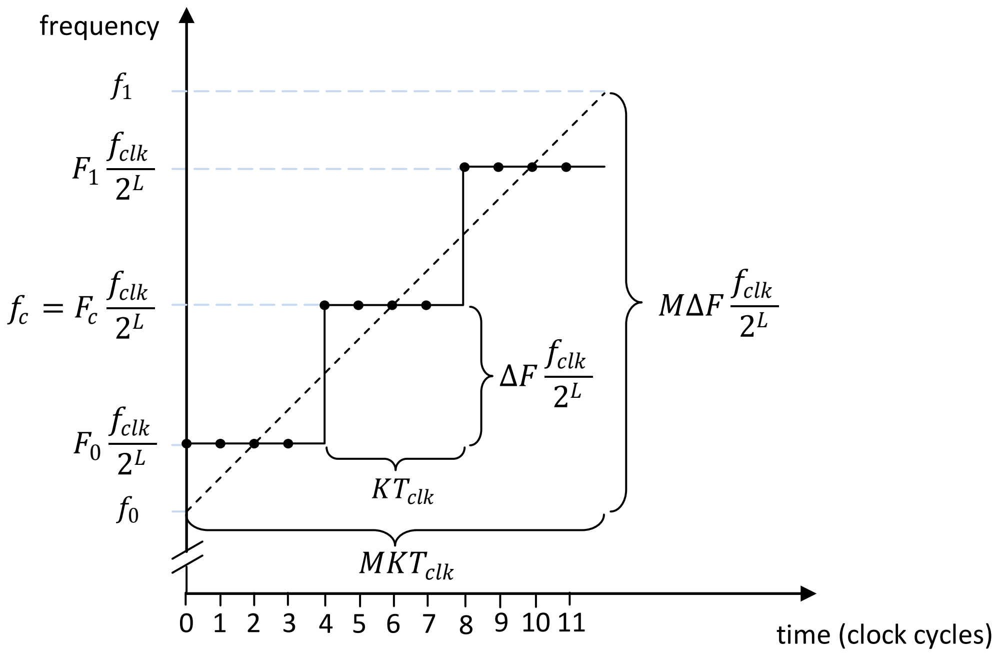

f_{clk}	=	system clock frequency (= 1 GHz)
T_{clk}	=	system clock period (= 1 ns)
L	=	number of bits of the frequency and phase accumulators (= 32)
F_0	=	start frequency tuning word
F_c	=	center frequency tuning word
F_1	=	stop frequency tuning word
ΔF	=	frequency increment
f_0	=	ideal start frequency
f_1	=	ideal stop frequency
K	=	frequency accumulator clock division ratio (= 4 for AD9910, 8 for AD9858)
M	=	number of frequency levels per sweep

Figure 43 Discrete time vs. frequency plot of a staircase approximation (solid line) to an ideal chirp (dashed line), the former of which represents the frequency register values (dots) generated by the DDCS with L-bit frequency and phase accumulators and clock frequency $f_{clk} = 1/T_{clk}$. The frequency register has start and stop values F_0 and F_1, respectively, a frequency increment ΔF, and updates every K clock cycles during a total of $N = MK$ clock cycles each sweep.

Firstly, we constrain the sweep period to equal an integral number of frequency accumulator clock periods. Since one frequency accumulator clock period is K master clock periods T_{clk}, we have

$$T = MKT_{clk} \equiv NT_{clk}, \qquad M, K, N \in \mathbb{Z}_+, \tag{3.13}$$

where T_{clk} is the system clock period, K is the number of system clock periods per frequency accumulator update, M the number of frequency levels per sweep.

As detailed in the data sheets for the DDCSs of interest, the Analog Devices AD9910 and AD9858, the frequency accumulator update rate K can be chosen in increments of 4 in the AD9910 (2010) and in increments of 8 in the AD9858 (2009). Henceforth, however, we assume that K is chosen at its lowest possible value in order to minimize the phase error due to the staircase approximation. Thus, we assume that

$$K = 2^n \tag{3.14}$$

For the AD9910, we take $n = 2$, and for the AD9858 $n = 3$.

The second fundamental parameter of a chirp is its peak-to-peak frequency deviation, or bandwidth. We distinguish the 'continuous' bandwidth corresponding to the difference $f_1 - f_0$ between the start and stop frequencies of the ideal linear chirp (the dashed line in Figure 43), and the 'discrete' bandwidth corresponding to the difference $(F_1 - F_0)(f_{clk}/2^L)$ between the start and stop frequencies generated by the DDCS staircase approximation (the solid lines in Figure 43). Since the staircase approximation slightly 'leads' the ideal linear chirp at the beginning of the sweep and 'lags' it at the end, the 'discrete' bandwidth is slightly less than the 'continuous' bandwidth. The latter is seen from Figure 43 to equal

$$f_1 - f_0 = M\Delta F \frac{f_{clk}}{2^L}, \tag{3.15}$$

where M represents the number of frequency *levels* (not steps) in each sweep as given by Eq. (3.13), ΔF denotes the frequency increment, f_{clk} the system clock frequency, and L the number of bits of the phase accumulator. Equation (3.15) simply expresses the fact that upon each update of the frequency accumulator, the output frequency increases by ΔF times the frequency resolution $f_{clk}/2^L$, and that there are M such updates in each sweep.

The 'discrete' peak-to-peak frequency deviation corresponding to the difference between the start and stop frequency tuning words F_0 and F_1 is slightly less than the expression given in (3.15), however. In units of the frequency resolution $f_{clk}/2^L$, it is given by

$$F_1 - F_0 = (M-1)\Delta F, \qquad F_0, F_1 \in \mathbb{Z}^+_{2^{L-1}} \tag{3.16}$$

where $(M-1)$ corresponds to the number of frequency *steps* (not levels) within each sweep. The symobol $\mathbb{Z}^+_{2^{L-1}}$ denotes the set of all non-negative integers modulo 2^{L-1}, to which all frequency tuning words must belong in order to satisfy the Nyquist sampling criterion (see Section 2.3).

5.3 Selecting chirp parameters for CP frequency sweeping

In this section, we devise an algorithm for selecting the DDCS parameters in such a way as to ensure phase-coherent and phase-continuous sweep transitions. In Section 5.3.1, we show that in order to ensure this, the product of the number of system clock periods per sweep N and the tuning word F_c corresponding to the chirp's center frequency must contain at least L factors of 2 in its prime factorization. In Section 5.3.2, we show how the sweep period constraint (3.13) with assumption (3.14) can be satisfied simply by requiring N itself to contain n factors of 2. Finally, in Section

5.3.1 Relationship between the discretized sweep period and center frequency

The discretization constraints in Eqs. (3.13) and (3.16) ensure that the chirp's duration and frequency levels are such that it can actually be generated by a chirp DDS. They do not, however, ensure that the sweep transitions are CP. To satisfy this additional requirement, we must also satisfy the constraint (3.10), which we write below in a slightly different form:

$$f_c T = k, \qquad k \in \mathbb{N}. \tag{3.17}$$

where k is the number of cycles per sweep.

At this point, we make the assumption that F_0 and F_1 are either both even or both odd[30], so that we may define an integer-valued 'center frequency tuning word' as

$$F_c = \frac{F_0 + F_1}{2}, \qquad F_c \in \mathbb{Z}^+_{2^{L-1}}. \tag{3.18}$$

As illustrated in Figure 43, the 'discrete' center frequency $F_c(f_{clk}/2^L)$ is equal to the 'continuous' center frequency of the ideal linear chirp:

$$f_c = F_c \frac{f_{clk}}{2^L}. \tag{3.19}$$

Inserting (3.19) and (3.13) into (3.17), we find

$$\frac{F_c N}{2^L} = k, \qquad k \in \mathbb{N}. \tag{3.20}$$

In order to satisfy this equation, the product F_c and N must have a combined total of at least L prime factors of 2.

Concretely, let us define the number of prime factors 2 contained in N as p, so that we can write a 'partial prime factorization' of N as follows:

$$N = 2^p q \tag{3.21}$$

with q an odd integer. This corresponds to a sweep duration of

$$T = 2^p q T_{clk} \equiv q\Delta T, \tag{3.22}$$

where $\Delta T = 2^p T_{clk}$ is a discretization step which represents the 'fineness' with which the sweep interval can be chosen while preserving coherent and continuous sweep transitions.

Next, we consider the choice of the center frequency tuning word F_c. If N is given by (3.21), then in order to satisfy (3.20), the center frequency tuning word F_c must have the form

$$F_c = 2^{L-p} r, \tag{3.23}$$

where r is an integer. Inserting (3.23) into (3.19) we find that the center frequency is given by

$$f_c = \frac{r}{2^p} f_{clk} \equiv r\Delta f_c, \tag{3.24}$$

where $\Delta f_c = f_{clk}/2^p$ represents the 'fineness' with which the chirp's center frequency can be discretized while preserving coherent and continuous sweep transitions.

Equations (3.22) and (3.24) show that there is a trade-off between the sweep period discretization step ΔT and the center frequency discretization step Δf_c. If p is a small number, then the permissible sweep periods T are closely spaced, but the permissible center frequencies f_c are few and far apart; the situation is vice versa if p is large. Table 6 illustrates this effect for a DDCS operating at a master clock frequency of f_{clk} = 1 GHz.

[30] In the chirp parameter selection algorithm to be derived, we first determine F_c and then obtain F_0 and F_1 by subtracting and adding a fixed number, which justifies this assumption.

p	2	3	4	5	6	7	8	9
ΔT (ns)	8	16	32	64	128	256	512	1,024
Δf_c (MHz)	125	62.5	31.25	15.625	7.8125	3.90625	1.953125	0.9765625

Table 6 Discretization steps ΔT and Δf_c as a function of p, for a master clock frequency of f_{clk} = 1 GHz.

5.3.2 Discretization of the sweep period in multiples of frequency accumulator updates

According to Eq. (3.13), the total number of master clock periods per sweep N must be a multiple of the frequency accumulator update rate K. With the assumption in Eq. (3.14) that $K = 2^n$, this amounts to requiring that N itself contain at least n factors of 2. With N represented as in Eq. (3.21), this requirement is expressed as

$$p \geq n. \tag{3.25}$$

Further, recall from Section 2.3 that F_c is chosen such that $F_c < 2^{L-1}$ in accordance with the Nyquist theorem. According to Eq. (3.23), this implies that

$$p \geq 2. \tag{3.26}$$

It follows that for the AD9910 with $n = 2$, Eqs. (3.25) and (3.26) are the same, and commensurability of the sweep period with the frequency accumulator clock period is automatically guaranteed.

5.3.3 Discretization of frequency levels

It remains to include the integer frequency increment constraint (3.16) in our analysis. Firstly, however, we combine Eqs. (3.18) and (3.23) and multiply by 2 to obtain

$$F_0 + F_1 = 2^{p+1} r. \tag{3.27}$$

Equations (3.16) and (3.27) constitute a pair of simultaneous linear equations for F_0 and F_1, which can be added and subtracted to yield

$$\begin{aligned} 2F_0 &= 2^{p+1} r - (M-1)\Delta F, \\ 2F_1 &= 2^{p+1} r + (M-1)\Delta F. \end{aligned} \tag{3.28}$$

If we choose at least one of $(M-1)$ and ΔF to be an even number (so that their product $(M-1)\Delta F$ is even), then Eq. (3.28) can be divided throughout by 2 to obtain

$$\begin{aligned} F_0 &= F_c - \frac{(M-1)\Delta F}{2}, \\ F_1 &= F_c + \frac{(M-1)\Delta F}{2}. \end{aligned} \tag{3.29}$$

This gives the start and stop frequency tuning words for the CP chirp.

5.4 Algorithm for selecting DDCS parameters

In this section, we employ the results of the previous section in an algorithm to select the parameters for a DDCS with phase-coherent and phase-continuous sweep transitions, which we illustrate by an example.

As posited in Chapter 2, we wish to generate a chirp with sweep period T = 400 µs and peak-to-peak frequency deviation B = 38.14 MHz. In order to allow a sufficient width for the bandpass filter following upconversion by mixing, we would like the chirp's start frequency f_0 to be at leat 50 MHz. We assume that the chirp is generated by an AD9910 DDCS employing a phase accumulator with L = 32 bits and operating at a clock frequency of f_{clk} = 1 GHz.

Firstly, we determine the number of factors 2 in N:

$$N = \frac{T}{T_{clk}} = \frac{400\ \mu\text{s}}{1\ \text{ns}} = 400{,}000 = 2^7 \times 3{,}125, \tag{3.30}$$

where the last equality is the result of a 'partial' prime factorization of N. This corresponds, by comparison with (3.21), with p = 7. It follows that the center frequency discretization step Δf_c is

$$\Delta f_c = \frac{f_{clk}}{2^p} = \frac{1\ \text{GHz}}{2^7} = 7.8125\ \text{MHz}. \tag{3.31}$$

Thus, in order to ensure phase-coherent and phase-continuous sweep transitions, we must choose the center frequency f_c a multiple of 7.8125 MHz. In order to ensure that chirp starting frequency f_0 is above 50 MHz with a chirp bandwidth of B, we choose

$$f_c = \Delta f_c \left\lceil \frac{f_0 + B/2}{\Delta f_c} \right\rceil = 9 \times 7.8125\ \text{MHz} = 70.3125\ \text{MHz}. \tag{3.32}$$

The corresponding center frequency word is

$$F_c = r \times 2^{L-p} = 9 \times 2^{32-7} = 301{,}989{,}888. \tag{3.33}$$

Next, we choose the frequency increment ΔF. If we assume that K = 4, then $M = N/K = 2^5 \times 3{,}125$ is an even number, so $M - 1$ is an odd number. Since the product of $M - 1$ and ΔF should be even, it follows that ΔF should be even.

As seen in Figure 39, the DDCS output frequency increases by $\Delta F(f_{clk}/2^L)$ every KT_{clk} seconds. This corresponds to a chirp rate of $(\Delta F/K2^L)f_{clk}^2$, which we wish to be as close as possible to the 'design value' for the chirp rate B/T, with B = 38.14 MHz and T = 400 µs. This can be effectuated by choosing

$$\begin{aligned} \Delta F &= 2 \times \text{round}\left(\frac{BK2^L}{2f_{clk}^2 T}\right) \\ &= 2 \times \text{round}\left(\frac{38.14\ \text{MHz} \times 4 \times 2^{32}}{2 \times (1\ \text{GHz})^2 \times (400\ \mu\text{s})}\right) = 1{,}638. \end{aligned} \tag{3.34}$$

This value for the frequency increment leads to a chirp rate of

$$\alpha = \frac{\Delta F}{K2^L} f_{clk}^2 = \frac{1{,}638}{4 \times 2^{32}} \times (1\ \text{GHz})^2 \approx 95.344\ \text{GHz/s}, \tag{3.35}$$

which is slightly less than the design value of $\alpha = 95.367$ GHz/s. According to Eq. (3.15), the swept bandwidth is of

$$B = f_1 - f_0 = M\Delta F \frac{f_{clk}}{2^L} = 100{,}000 \times 1{,}638 \times \frac{(1\ \text{GHz})}{2^{32}} \approx 38.138\ \text{MHz}. \tag{3.36}$$

The required initial and final frequency tuning words are obtained from Eq. (3.29):

$$F_0 = F_c - \frac{(M-1)\Delta F}{2} = 9 \times 2^{25} - \frac{99{,}999 \times 1{,}638}{2} = 220{,}090{,}707,$$
$$F_1 = F_c + \frac{(M-1)\Delta F}{2} = 9 \times 2^{25} + \frac{99{,}999 \times 1{,}638}{2} = 383{,}889{,}069. \tag{3.37}$$

We have validated these values in a simulation. Figure 44 shows a zoomed-in view of the output samples generated by a chirp DDS using the values derived above. At the end of the sweep, at $T = 400$ µs, the phase (and, since this DDS generates a sine output, the amplitude) returns exactly to zero as required.

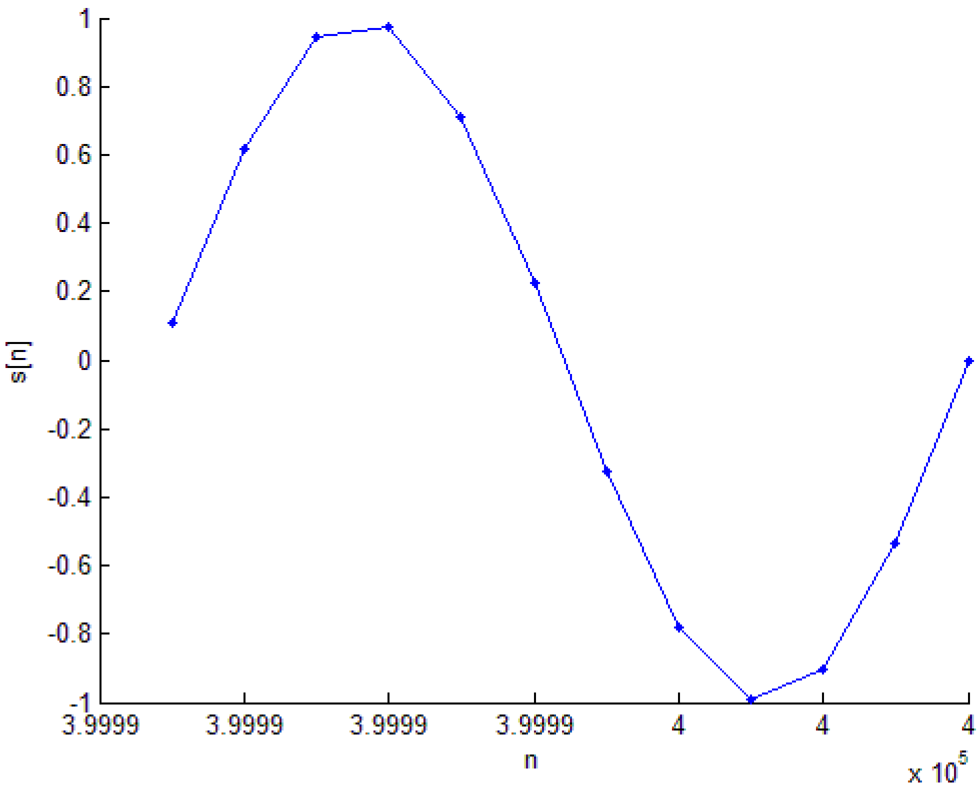

Figure 44 Zoomed-in view of the DDS output sequence $s[n]$ at the end of the sweep.

Figure 45 shows the spectrum output spectrum of the DDS. The chirp sweeps from f_0 = 51.24 MHz to f_1 = 89.38 MHz.

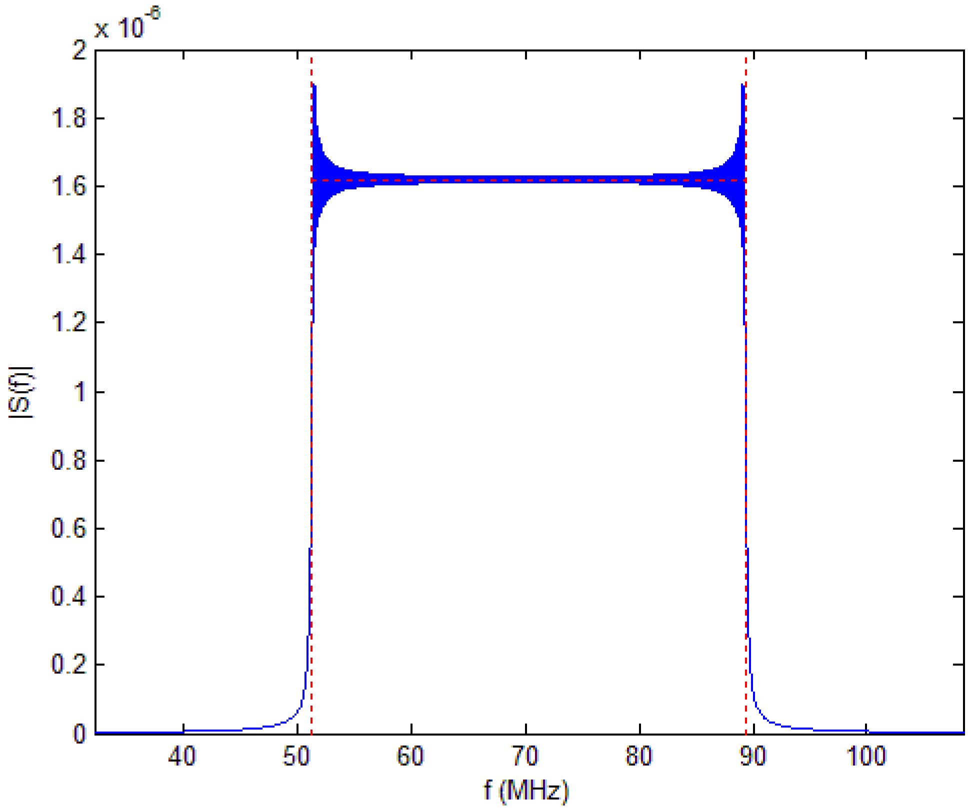

Figure 45 Digital output spectrum of a chirp DDS generating a signal with unity amplitude (solid line) juxtaposed to the nominal bandwidth and power of the ideal chirp spectrum (dashed line).

5.5 Concluding remarks

To summarize, we have devised an algorithm for choosing DDS parameters such that the FMCW waveform is perfectly periodic, eliminating the need to reset the phase to zero at the beginning of each sweep using the phase accumulator 'clear' control. The application of this algorithm eliminates the need for discontinuities and the associated 'switch noise' at the sweep transitions, and allows for the digital phase errors to be perfectly periodic so that they have no effect on Doppler processing, as explained in Chapter 4.

6 Conclusions and discussion

We first sum up the contributions of this thesis to the current level of knowledge (Section 6.1), describe their implications for technological development (Section 6.2) and finally give recommendations for further research (Section 6.3).

6.1 Summary of contributions to knowledge

The purpose of this thesis is to model the effects of digital phase errors on the performance of a FMCW-Doppler radar.

- For a direct digital chirp synthesizer (DDCS) which operates by the look-up table method with the phase generated by a pair of cascaded accumulators, we have shown that combined hardware effects of

  (1) clocking the frequency accumulator at a lower rate than the phase accumulator, and
  (2) truncating the output of the phase accumulator prior

  can be modeled by an effective periodic phase error.

- By applying the method of Salis (Riera Salis 1994) to the digital synthesis of chirps, we have shown that the spectrum of the output of a DDCS contains 'replicas' of the desired chirp which have the same chirp rate, but are at different center frequencies, as well as 'replicas' of its image, which are also at different center frequencies, but which have the opposite chirp rate. This in itself is a valuable result, since spurious 'replicas' can partially be removed by bandpass-filtering the DDS output signal.

- We have characterized the effect of the replicas on the FMCW beat signal spectrum. We showed that amplitudes of the spurious "ghost" targets can be expressed in terms of the discrete Fourier transform of the complex exponential of the phase error sequence. Using Parseval's theorem, we derived an upper bound for the worst-case spurious target for a digital phase error of a given maximum amplitude.

- We have shown that phase errors which are coherent with the periodic sweep have no effect on Doppler processing. This is a useful for practical applications of FMCW-Doppler radar, because Doppler shifts play an important role in distinguishing targets from clutter.

- We have devised a method to program a direct digital chirp synthesizer in such a way, that it generates perfectly periodic sweep signals with no discontinuities at the phase transitions. Such waveforms have attractive properties in FMCW Doppler applications.

The theoretical results enumerated above were applied to a practical model FMCW-Doppler radar in order to determine how its performance is affected by the digital phase errors. We discuss the results, as well as other implications for technological development, below.

6.2 Implications for technological development

We first recapitulate our evaluation of the impact of digital phase errors on the performance of the model FMCW-Doppler transceiver (Section 6.2.1). Subsequently, we comment on hybrid systems which have been developed to mitigate the effects of spurii in DDCS, and argue that the spurii resulting from phase truncation do not mandate the need for such systems.

6.2.1 Performance of the model system

This thesis investigates a model FMCW-Doppler transceiver architecture in which a transmitted chirp is generated at intermediate frequency (IF) by an Analog Devices AD9910 direct digital chirp synthesizer and upconverted to radio frequency (RF) by single-sideband upconversion using the filter method. It shown that the spurious signals due to clocking the frequency accumulator at a lower rate than the phase accumulator (the 'staircase' approximation) and truncation of the output of the phase accumulator prior to addressing a sine look-up table leads to spurious targets in the beat spectrum which are at most **92 dB** below the target signal. This is only 4 dB above signal-to-quantization noise ratio (SQNR) of 96 dB for a 16-bit analog-to-digital converter which could realistically be used in such a transceiver. It is highly likely that the effect of the phase truncation errors is negligible in the presence of other sources of error, such as timing jitter, DAC nonlinearity, filter group delay etc.

6.2.2 Comparison to hybrid techniques

In order to reduce the effect of spurii, Salous (Salous 1992) has recommended a hybrid technique in which the direct digital chirp synthesizer is phase-locked, using a phase-locked loop (PLL) with a frequency scaling factor of one, to a voltage-controlled oscillator (VCO). It is well known (Gardner 2005) that the phase-lock technique suppresses rapid variations in the frequency of its input "reference" signal, which could be caused by the spurii. The flipside of this property, however, is that a PLL is slow to respond to the sudden changes in its output frequency which occur when the synthesizer 'flies back' to its starting frequency at the sweep transitions[31]. Although the fly-back can be 'speeded up' using feed-forward techniques, the model system described in this thesis still performs better in this respect, since a DDCS can change its output frequency in a single clock cycle, and its settling time is limited only by the transient response of the low-pass interpolating filter.

The results of this thesis show that as far as 'staircase' approximation and phase truncation errors are concerned, there is no need for spectral 'clean-up' by phase-lock techniques. (Of course, such techniques could still be necessary to eliminate spurious from other techniques such as DAC nonlinearity). This knowledge is useful for simplifying the design of future chirp synthesizers.

6.2.3 Possibility of frequency multiplication

The upconversion method employed in the model system *translates* the DDS output frequency by the local oscillator frequency. This technique does not result in an increase of the chirp bandwidth and hence requires a wideband signal at intermediate frequency (IF). Hybrid frequency synthesizers using a DDCS in phase-locked loop with a voltage-controlled oscillator (VCO) have the capability of providing frequency *multiplication* by a factor of N (Gardner 2005). An advantage of relying on frequency multiplication to provide chirp bandwidth is that the DDCS can be used at frequencies which are low compared to its Nyquist frequency, in which case the effects of DAC nonlinearity are

[31] In fact, there are two conflicting requirements here: a smaller bandwidth of the phase-locked loop leads to better rejection of close-in spurious signals, but causes a longer transient response (Gardner 2005).

less severe (Goldberg 1999). A disadvantage, however, is that the phase errors due to spurii are multiplied by the same factor N. Our results show, however, that as far as phase truncation spurii are concerned, the chirp generated by a DDCS can be multiplied by significant factors without causing unacceptable degradation of the signal integrity. The possibility of frequency multiplication could be useful for the design of ultra-wideband (UWB) radar systems which are currently of much technological interest.

6.3 Recommendations for further research

This thesis considers just one source of errors in the model system, namely, errors in the digital phase value used to address a sine look-up table. However, as discussed in Section 2.3.3, there are many other sources of error to be contended with, which probably have more detrimental effects on system performance than the digital phase errors considered here. In our recommendations for further research, however, we focus on a few of these errors which could be modeled using the theoretical framework developed in this thesis.

6.3.1 Including the effect of amplitude quantization in the model

In Chapter 3, we assumed the angle-to-amplitude conversion in the DDCS was ideal. In practice, however, the digital-to-analog converter outputs a quantized amplitude signal. Thus, each output sample is affected by a deterministic amplitude quantization error as well as phase truncation error.

We propose to model the additional effect of the amplitude quantization errors as follows. Firstly, the amplitude quantization error for each sample is determined by simulation. These amplitudes errors can then be mapped to an equivalent phase error, and this equivalent phase error added to the original digital phase error sequence to produce a new 'total' phase error sequence. In general, the period of the 'total' phase error sequence will be different from that of the original digital phase errors; however, if the DDCS is programmed to produce periodic sweeps as described in Chapter 5, then the period of the 'total' phase error is at most equal to the number of clock cycles per sweep, N. In the latter case, we would expect spurious beat frequencies to occur at multiples of the sweep repetition frequency, $1/T$, from the target signal.

Our main point here is that, though amplitude-to-phase mapping, the amplitude quantization error can *also* be modeled as an 'effective' periodic phase error. After this has been done, the theory developed in Section 3.3 can be brought to bear to calculate the effects of the amplitude errors on the beat signal spectrum.

6.3.2 Closed-form calculation of the amplitudes of the spurii

In chapter 3, we showed that the amplitudes of the "ghost targets" in the beat signal spectrum can be calculated, within the small phase-error approximation, from discrete Fourier transform $A[k]$ of the complex exponential $\exp(-j\theta_m)$ of the phase error sequence, θ_m. We then used the upper bound for θ_m and assumed the phase error energy was concentrated in a single harmonic to evaluate the worst-case "ghost target" amplitude. Our simulations show, however, that in fact $A[k]$ is 'noise-like' and spread over many harmonics, and suggest that the upper bound obtained here is unduly pessimistic.

A tighter bound could be obtained by calculating $A[k]$ in closed form. Such a calculation could proceed along the lines of Nicholas and Samueli (Nicholas and Samueli 1987), who evaluated the discrete Fourier transform of a sampled *linear* sawtooth phase error which occurs in a conventional *carrier* DDS generating a single output frequency. Our case is slightly different, however, since the quadratic phase of a *chirp* DDS is affected by the sampled values of a *quadratic* sawtooth phase error. Judging from the complexity of (Nicholas and Samueli 1987), such a calculation would be a formidable exercise in number theory, which to the best of our knowledge has not yet been undertaken.

References

Adamski, M. E., K. S. Kulpa, et al. (2000). Effects of Transmitter Phase Noise on Signal Processing in FMCW Radar. Proc. International Conf. on Microwaves, Radar & Wireless Communications MIKON-2000, Wroclaw, Poland.

Adler, E. D., E. A. Viveiros, et al. (1995). Direct digital synthesis applications for radar development. Radar Conference, 1995., Record of the IEEE 1995 International.

Analog Devices (2009). AD9858 Direct Digital Synthesizer Data Sheet (Rev. C), Analog Devices.

Analog Devices (2010). AD9910 Direct Digital Synthesizer Data Sheet (Rev. C), Analog Devices.

Andrews, V., C. T. M. Chang, et al. (1992). A Monolithic Digital Chirp Synthesizer Chip with I-Channel and Q-Channel, Ieee-Inst Electrical Electronics Engineers Inc.

Barrick, D. E. (1973). FM/CW Radar Signals and Digital Processing. NOAA Technical Report ERL 283-WPL 26.

Barrick, D. E., B. J. Lipa, et al. (1994). Gated FMCW DF Radar and Signal Processing for Range/Doppler/Angle Determination. U. S. P. Office, Codar Ocean Sensors, Ltd., Los Altos, Calif.

Barry, G. H. and R. B. Fenwick (1967). "Extraterrestrial and Ionospheric Sounding with Synthesized Frequency Sweeps." Hewlett-Packard Journal **16**(7): 8-12.

Beasley, P. and D. Lawrence (2006). Frequency Modulated Continuous Wave (FMCW) Radar Having Improved Frequency Sweep Linearity. Q. Ltd.

Beasley, P., T. Leonard, et al. (2010). High Resolution Surveillance Radar.

Beasley, P. D. L. (2006). The Influence of Transmitter Phase Noise on FMCW Radar Performance. Microwave Conference, 2006. 36th European.

Boashash, B. (1992). "Estimating and interpreting the instantaneous frequency of a signal. I. Fundamentals." Proceedings of the IEEE **80**(4): 520-538.

Brooker, G. M. (2005). Understanding Millimetre-Wave FMCW Radars. 1st International Conference on Sensing Technology. Palmerston North, New Zealand**:** 152-157.

Brunson, L., R. Sole, et al. (2007). JRG-70: Theory of FMCW Radar Waveforms. Joint Regulator's Group (JRG). Mainz, Germany.

Burgos-Garcia, M., C. Castillo, et al. (2003). "Digital on-line compensation of errors induced by linear distortion in broadband LFM radars." Electronics Letters **39**(1): 116-118.

Carson, J. R. (1922). "Notes on the Theory of Modulation." Proceedings of the IRE **10**(1): 57-64.

Castetter, D. (2011). "An Introduction to YIG Tuned Oscillators." from http://www.microsource-inc.com/yigintro.pdf.

Cooley, J., P. Lewis, et al. (1967). "Application of the fast Fourier transform to computation of Fourier integrals, Fourier series, and convolution integrals." Audio and Electroacoustics, IEEE Transactions on **15**(2): 79-84.

Cushing, R. (2000). "Single-Sideband Upconversion of Quadrature DDS Signals to the 800-to-2500-MHz Band." Analog Dialogue **34**(3): 1-5.

Durbridge, L. J. and G. M. Warne (1991). A frequency ramp generator for an HF skywave radar implemented with direct digital synthesis techniques. HF Radio Systems and Techniques, 1991., Fifth International Conference on.

Durrant, R. J. and S. M. Parkes (1991). The implementation of high time bandwidth chirp pulses using digital techniques. High Time-Bandwidth Product Waveforms in Radar and Sonar, IEE Colloquium on.

Fig, M. (2005). "gaussquad." Matlab Central. from http://www.mathworks.com/matlabcentral/fileexchange/8679-gaussquad.

Fuller, K. L. (1990). "To see and not be seen [radar]." Radar and Signal Processing, IEE Proceedings F **137**(1): 1-10.

Gardner, F. M. (2005). Phaselock Techniques, John Wiley & Sons, Inc.

Goldberg, B. G. (1999). Digital frequency synthesis demystified: DDS and fractional-N PLLs, LLH Technology Publishing.

Gori, F. (1994). Why is the Fresnel Transform So Little Known? Current Trends in Optics. J. C. Dainty, Academic Press.

Griffiths, H. D. (1990). "New ideas in FM radar." Electronics & Communication Engineering Journal **2**(5): 185-194.

Griffiths, H. D. (1991). The effect of phase and amplitude errors in FM radar. High Time-Bandwidth Product Waveforms in Radar and Sonar, IEE Colloquium on.

Gurgel, K. W., G. Antonischki, et al. (1999). "Wellen Radar (WERA): a new ground-wave HF radar for ocean remote sensing." Coastal Engineering **37**(3-4): 219-234.

Harris, F. J. (1978). "On the use of windows for harmonic analysis with the discrete Fourier transform." Proceedings of the IEEE **66**(1): 51-83.

Hymans, A. J., Lait, J. (1960). "Analysis of a frequency-modulated continuous-wave ranging system." Proc. Inst. Elect. Eng. **107B**: 365-372.

Jakowatz, C. V., D. E. Wahl, et al. (1996). Spotlight-Mode Synthetic Aperture Radar: A Signal Processing Approach, Kluwer Academic Publishers.

Jenq, Y. C. (1988). "Digital spectra of nonuniformly sampled signals: fundamentals and high-speed waveform digitizers." Instrumentation and Measurement, IEEE Transactions on **37**(2): 245-251.

Jenq, Y. C. (1997). "Perfect Reconstruction of Digital Spectrum from Nonuniformly Sampled Signals." Instrumentation and Measurement, IEEE Transactions on **46**(3): 649-652.

Kelly, E. J. and R. P. Wishner (1965). "Matched-Filter Theory for High-Velocity, Accelerating Targets." IEEE Trans. Military Electronics **9**: 56-69.

Kester, W. (2002). High Speed DACs and DDS Systems, Analog Devices.

Kester, W. A. (2005). Data Conversion Handbook. Oxford, UK, Newnes.

Klauder, J. R., Price, A.C., Darlington, S., and Albersheim, W.J. (1960). "The Theory and Design of Chirp Radars." Bell. Syst. Tech. J. **39**(4): 745-809.

Laakso, T. I., V. Valimaki, et al. (1996). "Splitting the unit delay [FIR/all pass filters design]." Signal Processing Magazine, IEEE **13**(1): 30-60.

Marple, L., Jr. (1999). "Computing the discrete-time “analytic” signal via FFT." Signal Processing, IEEE Transactions on **47**(9): 2600-2603.

Mehrgardt, S. (1983). "Noise spectra of digital sine-generators using the table-lookup method." Acoustics, Speech and Signal Processing, IEEE Transactions on **31**(4): 1037-1039.

Meta, A., P. Hoogeboom, et al. (2006). Range Non-linearities Correction in FMCW SAR. Geoscience and Remote Sensing Symposium, 2006. IGARSS 2006. IEEE International Conference on.

Mielenz, K. D. (2000). "Computation of Fresnel Integrals. II." Journal of Research of the National Institute of Standards and Technology **105**: 589.

Morgan, G. D., P. D. Beasley, et al. (2006). Design considerations for a millimetric front-end for FMCW radar. MM-Wave Products and Technologies, 2006. The Institution of Engineering and Technology Seminar on.

Murphy, E. and C. Slattery (2004). "All About Direct Digital Synthesis." Analog Dialogue **38**.

Musa, M. and S. Salous (2000). "Ambiguity elimination in HF FMCW radar systems." Radar, Sonar and Navigation, IEE Proceedings - **147**(4): 182-188.

Nicholas, H. T. and H. Samueli (1987). An Analysis of the Output Spectrum of Direct Digital Frequency Synthesizers in the Presence of Phase-Accumulator Truncation. Proc. 41st Annu. Frequency Contr. Symp.

Nuttall, A. H. and E. Bedrosian (1966). "On the quadrature approximation to the Hilbert transform of modulated signals." Proceedings of the IEEE **54**(10): 1458-1459.

Oppenheim, A. V., R. W. Schafer, et al. (1999). Discrete-time signal processing, Prentice-Hall.

Pace, P. E. (2004). Detecting and classifying low probability of intercept radar, Artech House.

Papoulis, A. (1994). "Pulse compression, fiber communications, and diffraction: a unified approach." J. Opt. Soc. Am. A **11**(1): 11.

Perez-Martinez, F., M. Burgos-Garcia, et al. (2001). "Group delay effects on the performance of wideband CW-LFM radars." Radar, Sonar and Navigation, IEE Proceedings - **148**(2): 95-100.

Piper, S. O. (1995). Homodyne FMCW radar range resolution effects with sinusoidal nonlinearities in the frequency sweep. Radar Conference, 1995., Record of the IEEE 1995 International.

Pozar, D. M. (2005). Microwave Engineering, John Wiley & Sons, Inc.

Riera Salis, J. M. (1994). Spurious performance of direct digital synthesizers generating modulated signals. Electrotechnical Conference, 1994. Proceedings., 7th Mediterranean.

Salous, S. (1992). "IF digital generation of FMCW waveforms for wideband channel characterisation." Communications, Speech and Vision, IEE Proceedings I **139**(3): 281-288.

Salous, S. and P. R. Green (1994). A novel digital chirp generator using a dual clock field programmable gate array architecture. HF Radio Systems and Techniques, 1994., Sixth International Conference on.

Sheehan, D. V. and H. D. Griffiths (1992). "The effect of pulse phase distortion on the height estimation of a radar altimeter." International Journal of Remote Sensing **13**(17): 3303-3310.

Skolnik, M. (2008). Radar Handbook, McGraw-Hill.

Slepian, D. (1983). "Some Comments on Fourier Analysis, Uncertainty and Modeling." SIAM Review **25**(3): 379-393.

Smith, D. (1998). Signals, Samples, and Stuff: a DSP Tutorial, ARRL.

Smith, S. W. (2003). Digital Signal Processing: A Practical Guide for Engineers and Scientists, Elsevier Science.

Soumekh, M. (1999). Synthetic Aperture Radar Signal Processing with MATLAB Algorithms, John Wiley & Sons.

Stove, A. G. (1992). "Linear Fmcw Radar Techniques." Iee Proceedings-F Radar and Signal Processing **139**(5): 343-350.

Stove, A. G. (2004). Modern FMCW radar - techniques and applications. Radar Conference, 2004. EURAD. First European.

Teledyne Ferretec (2011). from http://www.teledynewireless.com/products/Oscillators/Ultra_Low_Phase_Noise_YIG_Oscillators.aspx.

Thales Nederland (2010). "Surface Scout." from www.thalesgroup.com/scout.

Tierney, J., C. Rader, et al. (1971). "A digital frequency synthesizer." Audio and Electroacoustics, IEEE Transactions on **19**(1): 48-57.

van Rooyen, G. J. and J. G. Lourens (2000). "A quadrature baseband approach to direct digital FM synthesis." Broadcasting, IEEE Transactions on **46**(3): 227-230.

Vankka, J. (2000). Direct Digital Synthesizers: Theory, Design, and Applications. Department of Electrical and Communications Engineering. Helsinki, Helsinki University of Technology. **Ph.D.**

Volegov, P. (2004). "Fresnel Integrals." Matlab Central File Exchange. from http://www.mathworks.com/matlabcentral/fileexchange/6580.

Willis, N. J. and H. D. Griffiths (2007). Advances in Bistatic Radar, SciTech Publishing, Inc.

Wojtkiewicz, A., J. Misiurewicz, et al. (1997). Two-Dimensional Signal Processing in FMCW Radars. Proc. XX KKTOiUE, Kolobrzeg, Poland.

Appendix: FMCW-Doppler simulation

In this section, we describe a simulation of a FMCW-Doppler radar. The MATLAB code used is listed below.

```
% FMCW radar parameters
fc=10e9;        % center frequency (10 GHz)
B=50e6;         % chirp bandwidth (50 MHz)
f0=fc-B/2;      % starting frequency (9.975 GHz)
T=500e-6;       % chirp period (500 us)
alpha=B/T;      % chirp rate (100 GHz/s)

% Target parameters
v=7.5;                  % target speed (7.5 m/s)
c=3e8;                  % speed of light (3*10^8 m/s)
R0=10e3;                % initial target range (10 km)
tau0=2*R0/c;            % initial target delay (50 us)
R=@(t) R0+v*t;          % target range
tau=@(t) 2/c*R(t);      % target transit time (assuming v<<c)
fD=2*v/c*fc;            % Doppler frequency 500 Hz

% Instrumented range
Rmax=15e3;              % instrumented range 15 km
taumax=2*Rmax/c;        % maximum target transit time 100 us
fbmax=alpha*2*Rmax/c;   % maximum beat frequency 10 MHz

% ADC and signal processing parameters
fs=20e6;                % sampling frequency 25 MHz
Ts=1/fs;                % sampling period (40 ns)
N=round(T/Ts);          % number of samples per sweep repetition interval
(SRI)
Nmax=round(fs*taumax);  % number of samples affected by the 'fly-back' of
the local oscillato to f0
Np=N-Nmax;              % number of processed samples per interval
M=64;                   % number of processed intervals

% Sinusoidal error function
dR=100;                                 % offset of spurious sidelobes in
ideal range bins (2 kHz, or 3 m)
dv=20;                                  % offset of spurious sidelobes in
Dopper bins (31.25 Hz, or 0.47 m/s)
fsl=(dR+dv/M)/T;                        % sidelobe ripple frequency
Asl=0.1;                                % phase error amplitude 0.1 radians
dphi=@(t) Asl*sin(2*pi*fsl*t);          % phase error function

% Beat signal function
tf=@(t) mod(t,T);                                       % fast time variable
phiTX=@(t) 2*pi*(f0*tf(t)+1/2*alpha*tf(t).^2+dphi(t)); % transmit signal
phase
phib=@(t) phiTX(t)-phiTX(t-tau(t));                     % beat signal phase
r=@(t) heaviside(t-taumax)-heaviside(t-T);              % observation window
% sb=@(t) r(tf(t)).*cos(phib(t));                       % real beat signal
sb=@(t) r(tf(t)).*exp(1j*phib(t));                      % I/Q demodulated
beat signal

% Generate input data
t=(0:M*N-1)*Ts;                         % time axis
x=sb(t);                                % sampled beat signal
X=transpose(reshape(x,N,M));            % arrange beat signal in fast-
                                        and slow-time matrix
```

```
X=X(:,Nmax+1:N);                          % discard points sampled within
maximum target transit time

% Range FFT
X=X.*repmat(hamming(Np,'periodic')',M,1);   % weight rows of X by a "DFT-
even" Hamming window
NFFT=2^nextpow2(Np);                        % number of range FFT points
(6,384)
f1=(0:NFFT/2-1)/NFFT*fs;                    % frequency axis for range FFT
X2=Ts/N*fft(X,NFFT,2);                      % perform range FFT over the
rows of X to obtain X2
X3=X2(:,1:NFFT/2);                          % maintain only those points
corresponding to positive frequencies

% Doppler FFT
MFFT=2^nextpow2(M);                             % number of processed
intervals (64)
f2=(-MFFT/2:MFFT/2-1)/MFFT*1/T;                 % frequency axis for
Doppler FFT
X3=X3.*repmat(hamming(M,'periodic'),1,NFFT/2);  % weight columns of X3 by
"DFT-even" Hamming window
X4=T*fftshift(fft(X3,MFFT),1);                    % to obtain a symmetric
spectrum, apply fftshift to the columns

% Plot results
figure
contour(f1/1e6,f2,abs(X4))
xlabel('range beat frequency (MHz)'); ylabel('Doppler frequency (Hz)')
grid on
```

The code is a straightforward implementation of the theory described in Chapter 2, and the comments provided within the code describe its operation to sufficient detail. Note that we have chosen to define the beat signal as a composite function, using in-line functions. This simplifies considerably the expressions involved when compared to Chapter 2.